

Spring 2015

Estimation and Thermodynamic Modeling of Solid Iron Species in the Berkeley Pit Water

Rajesh Srivastava

Montana Tech of the University of Montana

Follow this and additional works at: http://digitalcommons.mtech.edu/grad_rsch



Part of the [Metallurgy Commons](#)

Recommended Citation

Srivastava, Rajesh, "Estimation and Thermodynamic Modeling of Solid Iron Species in the Berkeley Pit Water" (2015). *Graduate Theses & Non-Theses*. 28.

http://digitalcommons.mtech.edu/grad_rsch/28

This Thesis is brought to you for free and open access by the Student Scholarship at Digital Commons @ Montana Tech. It has been accepted for inclusion in Graduate Theses & Non-Theses by an authorized administrator of Digital Commons @ Montana Tech. For more information, please contact sjuskiewicz@mtech.edu.

ESTIMATION AND THERMODYNAMIC MODELING OF SOLID IRON
SPECIES IN THE BERKELEY PIT WATER

by
Rajesh Srivastava

A thesis submitted in partial fulfillment of the
requirements for the degree of

Master of Science in Metallurgical Engineering

Montana Tech

2015



Abstract

Since the cessation of open-pit mining activities from the Berkeley Pit located in Butte, MT in 1982, the pit had gradually filled with metal-laden acidic mine water. The purpose of this investigation was to estimate and apply thermodynamic theory to a group of iron-sulfate solids that might equilibrate with the Berkeley Pit water. Thermodynamic data was incomplete for acid mine affected water, and the effects of Cu cementation on the formation of iron oxide and sulfate solids had not been analyzed. Ferric iron compounds such as Ferrihydrite, Goethite, Schwertmannite, Potassium Jarosite and Potassium Hydronium Jarosite were modelled in Stabcal using variables such as temperature, Eh from field records or from a redox couple, pH and chemical composition. Water quality records were analyzed from field data collected by the MBMG since 1987. Computation of saturation indices using log Q data showed that the Berkeley pit water was under-saturated with Ferrihydrite and over-saturated with Goethite and K-Jarosite. In addition, commonly expressed variables for thermodynamic data, such as dG_{25C} , S_{25C} , C_p using the Maier Kelley equation, were estimated by using a weighted multiple regression model for Schwertmannite, KH-Jarosite, and K-Jarosite. Schwertmannite had a $dG_{25C} = -978$ kcal, $S_{25C} = -6049$ cal, $H_{25C} = -2964$ kcal and C_p values of [$a = 161273488$, $b = -378690560$, $c = -43316576$]. Schwertmannite also had a dG_{rex} at $25^\circ\text{C} = -95.794$ kcal. KH-Jarosite had a $dG_{25C} = -786$ kcal, $S_{25C} = 5118$ cal, $H_{25C} = 586$ kcal and C_p values of [$a = -145717088$, $b = 342660160$, $c = 39022976$]. K-Jarosite had a $dG_{25C} = -765$ kcal/mol, S_{25C} of -1139 cal, $H_{25C} = -1249$ kcal and C_p values of [$a = -46482960$, $b = 107543872$, $c = 112836016$]. Thermodynamic quantities such as $dG_{\text{formation}}$ of the species, dG_{rex} and log K from reactions involving Fe^{3+} and Fe^{2+} ions were also tabulated. Based on the tabulated data, Eh-pH diagrams were constructed and a titration simulation was performed to determine the acidities of selected samples. An analysis of the effect of copper cementation on water chemistry over the last decade was also conducted.

Keywords: Berkeley Pit, Schwertmannite, Jarosite, Ferrihydrite, Goethite

Dedication

To my parents Dr. and Mrs. T.B. Srivastava and family for their love and support

and to all the hard-working miners that helped make
Butte, MT the “Greatest Hill on Earth”

Acknowledgements

I would like to thank and acknowledge many people for their help in making this work possible.

First, I would like to sincerely thank my advisor, Professor Hsin H. Huang for his dedication and generosity in making this work possible. In particular, his guidance, intellectual vision, wisdom and insightful interpretations have caused this project to evolve into a work that will undoubtedly be welcomed by the academic community.

Secondly, I would like to thank Terence Duaine at the Montana Bureau of Mines and Geology for his expert management and recordkeeping of the Berkeley pit water quality records over the last twenty-five years, without which this work would not be possible.

In addition, I would also like to thank Steve McGrath also from the Montana Bureau of Mines and Geology who spent many hours over the past several decades analyzing the water quality samples and providing the quantitative data upon which this work is based.

The overall guidance provided by Margaret Delaney, Professional Scientist at the Montana Bureau of Mines and Geology was invaluable, and in this regard, a particular note of thanks must be given.

I would like to kindly acknowledge Dr. Chris Gammons and Nick Tucci for their contributions to the academic literature and increasing my understanding of acid rock drainage, geochemistry and hydrogeology of the Berkeley pit.

I would also like to thank my additional committee members Dr. Larry Twidwell and Dr. Gary Icopini for their help in reviewing this manuscript and in making suggestions for improvement.

I must also give special thanks to the entire faculty of the Metallurgical and Materials Engineering department who have been so influential in teaching me the key concepts in metallurgical engineering such as process control, thermodynamics, and physical metallurgy.

And finally, I would like to thank the head of my department, Dr. Courtney Young for his academic leadership and financial support.

Table of Contents

ABSTRACT	I
DEDICATION	II
ACKNOWLEDGEMENTS	III
TABLE OF CONTENTS.....	IV
LIST OF TABLES.....	VI
LIST OF FIGURES.....	IX
LIST OF EQUATIONS	XII
GLOSSARY OF TERMS	XIV
1. INTRODUCTION	1
1.1. <i>Background</i>	1
1.2. <i>Purpose of Research</i>	2
1.3. <i>Scope of Work</i>	3
2. LITERATURE REVIEW.....	4
2.1. <i>Acid Rock Drainage</i>	4
3. THERMODYNAMIC THEORY	13
3.1. <i>Fundamental Databases, Thermodynamics, Calculations</i>	13
3.2. <i>Speciation of the Berkeley pit water, and log Q of Investigated Solids</i>	24
3.3. <i>Regression Analysis for Thermodynamic data of Schwertmannite and other Fe-SO₄ solids</i>	30
3.4. <i>Using Estimated Thermodynamic Data</i>	43
3.5. <i>Analysis of Iron Species Concentration over Time</i>	53
3.6. <i>Computer Simulation & Fe²⁺/Fe³⁺ Results</i>	55
4. RESULTS.....	58
4.1. <i>Matlab Output (3D Stem Plot)</i>	58

4.2.	<i>Log Q Matlab Output for Schwertmannite</i>	59
4.3.	<i>Log Q Matlab Output for Potassium Hydronium Jarosite</i>	61
4.4.	<i>Log Q Matlab Output for Potassium Jarosite</i>	64
4.5.	<i>Log Q Matlab Output for Ferrihydrite</i>	66
4.6.	<i>Log Q Matlab Output for Goethite</i>	69
5.	DISCUSSION	72
5.1.	<i>Ferrihydrite, Goethite & K-Jarosite Saturation Indices</i>	72
5.2.	<i>Thermodynamic Output for Schwertmannite</i>	73
5.3.	<i>Thermodynamic Output for KH-Jarosite & K-Jarosite</i>	76
5.4.	<i>Copper Cementation Effect on Solid Iron Species Formation</i>	79
6.	CONCLUSION	80
6.1.	<i>Recommendations</i>	81
7.	REFERENCES	82
	APPENDIX	86
1.	COMPUTER SPECIATION PROCEDURE IN STBCAL	86
1.1.	<i>Data Source</i>	86

List of Tables

Table I: Common Acid Generating Minerals (GARDGUIDE).....	4
Table II: Berkeley Pit Water Quality for June 10, 2011	9
Table III: Free Energy of Formation and Free Energy of Individual Species for Fe(OH) ₃	15
Table IV: Formation with Master and Non Master Species	19
Table V: Master and Non-master Species for Combined Fe ²⁺ /Fe ³⁺ Redox Couple Equilibrium Calculation.....	21
Table VI: Activity of Master Species and Log Q for Goethite and Ferrihydrite.....	23
Table VII: Computed SI Index for Goethite and Ferrihydrite	23
Table VIII: MBMG Water Analysis of Berkeley Pit At Three Important Times.....	25
Table IX: Activities for Component Species at 6°C for Measured Eh and Fe ²⁺ /Fe ³⁺ Couple.....	27
Table X: Log Q Eh vs Log Q Fe ²⁺ /Fe ³⁺ for Various Iron Sulfate Mineral Species for Records 195 & 502	28
Table XI: Saturation Indices for Goethite, Ferrihydrite, and K-Jarosite	30
Table XII: Schwertmannite Input Matrix in Excel	35
Table XIII: Calculated G values from Schwertmannite Log Q Values in Excel.....	36
Table XIV: Non-coded and Coded Matrix X Values for Schwertmannite	37
Table XV: Summary of Formulas for Independent Regressor Variables and Values at 6°C.....	38
Table XVI: Regression Coefficients for Schwertmannite calculated between 2°C & 14°C.....	38

Table XVII: Thermodynamic Properties for Schwertmannite.....	39
Table XVIII: Regression Output of Schwertmannite for NBS Database	40
Table XIX: Regression Output for KH Jarosite and K-Jarosite	40
Table XX: Reestimate of Schwertmannite for pH greater than 2.4.....	42
Table XXI: Energy values for Schwertmannite from 4°C to 8°C	43
Table XXII: Calculation of G_{rex} , Log K and dH_{rex} for Schwertmannite from Fe^{3+} and Fe^{2+} between 4°C and 8°C.....	44
Table XXIII: Energy Values for KH-Jarosite from 4°C to 8°C	44
Table XXIV: Calculation of G_{rex} , Log K, dH_{rex} for KH-Jarosite for Fe^{3+} and Fe^{2+} between 4°C to 8°C	45
Table XXV: Energy Values for K-Jarosite from 4°C to 8°C	45
Table XXVI: Calculation of G_{rex} , Log K, dH_{rex} for K-Jarosite for Fe^{3+} and Fe^{2+} between 4°C to 8°C	46
Table XXVII: Elemental Components used to Construct Eh-pH diagrams in Stabcal ...	46
Table XXVIII: MBMG Sample Data Before, During, and After Cu Cementation Process	50
Table XXIX: Cu Cementation Acidity Calculation Results for Berkeley Pit	52
Table XXX: Selected Water Quality Info Adapted from MBMG Analytical Report Related to Cu Cementation	54
Table XXXI: Titration Simulation of Samples with Aqueous O_2 for Cu Recovery Process	56
Table XXXII: Avg Log Q for Schwertmannite by Temperature.....	61

Table XXXIII: Avg. Log Q for KH-Jarosite by Temperature	63
Table XXXIV: Avg. Log Q for Potassium Jarosite by Temperature	66
Table XXXV: Avg. Log Q for Ferrihydrite by Temperature	68
Table XXXVI: Avg. Log Q for Goethite by Temperature	71
Table XXXVII: MBMG Water Quality Records for Total Iron Speciation.....	88
Table XXXVIII: MBMG Water Quality Records for Fe ²⁺ /Fe ³⁺ Speciation.....	91

List of Figures

Figure 1: Schematic Illustration of Mineral Formation due to Cementation (Gammons & Tucci 2015)	2
Figure 2: Schematic of Pyrite Oxidation with Reactions (after Stumm & Morgan 1981)	5
Figure 3: Eh-pH diagram of Ferrihydrite produced in Stabcal	9
Figure 4: Picture of Schwertmannite with XRD Scan	11
Figure 5: Schwertmannite and Jarosite Crystals under SEM (Gammons & Tucci 2015)	12
Figure 6: Stabcal Eh-pH Diagram for KH-Jarosite, Schwertmannite, K-Jarosite at 6°C.....	42
Figure 7: Eh-pH Diagram at 4°C showing Schwertmannite and Various Jarosite Species	47
Figure 8: Eh-pH Diagram at 6°C showing Schwertmannite and Various Jarosite Species	48
Figure 9: Eh-pH Diagram at 7°C showing Schwertmannite and Various Jarosite Species	48
Figure 10: Eh-pH Diagram at 8°C showing Schwertmannite and Various Jarosite Species	49
Figure 11: Stabcal Initial Titration Screen for ID#195	51
Figure 12: Stabcal Final Titration Screen for ID#195	51
Figure 13: Concentration of Fe ²⁺ and Fe ³⁺ during Cementation Process 2002-2012 (Duaimé & Tucci 2012)	53

Figure 14: Aqueous Titration Simulation with O ₂ for Fe ²⁺ /Fe ³⁺ during Cementation	
Process	57
Figure 15: Schwertmannite 4° C Matlab Output	59
Figure 16: Schwertmannite 6° C Matlab Output	59
Figure 17: Schwertmannite 7° C Matlab Output.....	60
Figure 18: Schwertmannite 8° C Matlab Output.....	60
Figure 19: Potassium Hydronium Jarosite 4° C Matlab Output	61
Figure 20: Potassium Hydronium Jarosite 6° C Matlab Output	62
Figure 21: Potassium Hydronium Jarosite 7° C Matlab Output	62
Figure 22: Potassium Hydronium Jarosite 8° C Matlab Output	63
Figure 23: Potassium Jarosite 4° C Matlab Output.....	64
Figure 24: Potassium Jarosite 6° C Matlab Output.....	64
Figure 25: Potassium Jarosite 7° C Matlab Output.....	65
Figure 26: Potassium Jarosite 8° C Matlab Output.....	65
Figure 27: Ferrihydrite 4° C Matlab Output	66
Figure 28: Ferrihydrite 6° C Matlab Output	67
Figure 29: Ferrihydrite 7° C Matlab Output	67
Figure 30: Ferrihydrite 8° C Matlab Output	68
Figure 31: Goethite 4° C Matlab Output.....	69
Figure 32: Goethite 6° C Matlab Output.....	69
Figure 33: Goethite 7° C Matlab Output.....	70
Figure 34: Goethite 8° C Matlab Output.....	70

Figure 35: Temperature vs Saturation Index for Goethite, Ferrihydrite, K-Jarosite	73
Figure 36: Temperature vs Log Q Schwertmannite.....	75
Figure 37: Temperature vs G & dG values for Schwertmannite	75
Figure 38: Temperature vs Average Log Q for KH-Jarosite & K-Jarosite.....	77
Figure 39: Temperature vs Predicted G(kcal) for KH & K Jarosite	78
Figure 40: Temperature vs Predicted dG for KH & K-Jarosites	78
Figure 41: Fe Speciation Flowsheet Summary	95

List of Equations

Equation 1: Relation between K and dG.....	14
Equation 2: Relationship between Free Energy of a Species and Free Energy of Formation for a Reaction	16
Equation 3: Gibbs Free Energy Function.....	17
Equation 4: Gibbs Free Energy of Formation Function.....	17
Equation 5: Enthalpy and Entropy Equations for a Given Temperature	17
Equation 6: Enthalpy and Entropy Equations after Integration	17
Equation 7: Equilibrium Mass Action Law	18
Equation 8: Calculation of Equilibrium Constant K using Mass Action Law.....	20
Equation 9: Equilibrium Constant as a Function of Activity.....	20
Equation 10: Calculation of Equilibrium Constant K using Redox Couple	22
Equation 11: Alternate Form of Nernst Equation for One Electron Process	22
Equation 12: Equation to Calculate Activity for a species	26
Equation 13: Calculation of Ionic Strength for a Solution	26
Equation 14: Davies Equation for Ionic Strength.....	26
Equation 15: Combined Regression Equation for Free Energy.....	31
Equation 16: General Multiple Linear Regression Model.....	31
Equation 17: Regression Coefficients for Multiple Linear Regression Model.....	32
Equation 18: General Identity Matrix W used for Weighting Factor	33
Equation 19: Matrix Form of Weighted Least Squares Estimation for Regression Coefficients.....	33

Equation 20: Regressor Variable Transformation	34
Equation 21: Reconversion of Estimated Regression Intercept to Noncoded Form	34
Equation 22: Standard Equation to Calculate Acidity	49
Equation 23: Enthalpy Equation for Schwertmannite between 4°C and 8°C based on Multiple Linear Regression Model	74
Equation 24: Entropy Equation for Schwertmannite between 4°C and 8°C based on Multiple Linear Regression Model	74
Equation 25: Enthalpy Equation for KH-Jarosite between 4°C and 8°C based on Multiple Linear Regression Model	76
Equation 26: Entropy Equation for KH-Jarosite between 4°C and 8°C based on Multiple Linear Regression Model	76
Equation 27: Enthalpy Equation for K-Jarosite between 4°C and 8°C based on Multiple Linear Regression Model	77
Equation 28: Entropy Equation for K-Jarosite between 4°C and 8°C based on Multiple Linear Regression Model	77

Glossary of Terms

Symbols and Definition

G, S, H, Cp	Energy (Free energy, Entropy, Enthalpy and heat capacity) of a species.
Solids	Species presumed to equilibrate with the Berkeley pit water. They are Schwertmannite, Jarosite, H-Jarosite, KH-Jarosite, Ferrihydrite and Goethite.
dG, dS, dH	Change in free energy of formation, entropy, enthalpy of a species produced from the most stable elements. Formation reaction for Schwertmannite: $8\text{Fe} + 1.6\text{S} + 19.2\text{O}_2 + 4.8\text{H}_2 \rightarrow \text{Fe}_8\text{O}_8(\text{OH})_{4.8}(\text{SO}_4)_{1.6}$
T or (T)	Temperature in C, but must change T to K (Kelvins) for all thermodynamic calculations
rm or (rm)	Represents room temperature of 25°C or 298.15K
Rex, M, v _M	Reaction to produce solids, Master species to balance the reaction and their stoichiometric coefficients. Master species chosen are: H ⁺ , H ₂ O(l), SO ₄ ²⁻ , K ⁺ , and Fe ³⁺ . The reaction of Schwertmannite would be $12.8\text{H}_2\text{O} + 1.6\text{SO}_4^{2-} + 8\text{Fe}^{3+} \leftrightarrow \text{Fe}_8\text{O}_8(\text{OH})_{4.8}(\text{SO}_4)_{1.6} + 20.8\text{H}^+$
C _p	Heat capacity as a function of Temperature. Maier-Kelly function, $C_p = a + b \times 10^{-3} T + c \times 10^5 T^{-2}$
C or [Species]	Concentration of a dissolved species, moles/L unless specified
a or {species}	Activity of a species = Activity coefficient × Concentration, $a = \gamma \times C$.
γ	Activity coefficient computed from selected model: Davis or Extended Debye or SIT
K	Equilibrium Constant, K, derived from Le Chatelier's Principle.
Q	Reaction quotient, Q, is the activity of master species at non-equilibrium (but equilibrated with the Berkeley pit water.)
SI	Saturation index $SI = \text{Log } K - \text{Log } Q$. If $SI > 0$, the solution water is over-saturated with the solid, < 0 under-saturated, = 0 equilibrium. If the solid is assumed to be equilibrated the solution, K will be equal to Q.
Matrices	See Part 3.3.3 Regression

1. Introduction

1.1. Background

Butte, Montana has a rich history of mining dating from the late 1800's. Originally, gold placer mining started in 1864 followed by silver mining in 1866¹. After several decades, the mining industry turned its focus towards copper because of the presence of high grade copper deposits around the Butte area. Underground copper mining took place and between the 1870's and 1975, approximately 49 miles of vertical shafts and 56 miles of horizontal drifts were created². In 1955, open pit mining commenced to extract lower grade ores from the Berkeley Pit. Mining continued until 1983 when the Anaconda Company discontinued operations. Montana Resources restarted operations in 1986 and presently continue operations in 2015. When open pit mining ceased, the Berkeley pit started filling with water from surrounding bedrock and also maybe more importantly from the underground horseshoe bend tunnels from which ore had been extracted. As of February 2015, water is flowing into the Berkeley at a rate of 2,400 gallons per minute³. As of December 2013, an estimate of the volume of the Berkeley pit lake was approximated at 43.6 billion gallons⁴. This mine water is highly acidic due to the presence of iron minerals and must be treated prior to discharge.

1.2. Purpose of Research

The purpose of the current research is to analyze water quality data from the Berkeley pit provided by the Montana Bureau of Mines and Geology which were collected over a period of 25 years from 1987 to 2012. In particular, formation of solid minerals within the Berkeley pit such as Schwertmannite— $\text{Fe}_8\text{O}_8(\text{OH})_{4.8}(\text{SO}_4)_{1.6}$, Hydronium Jarosite— $\text{H}_3\text{OFe}_3(\text{SO}_4)(\text{OH})_6$, Potassium-Hydronium Jarosite— $\text{K}_{0.51}(\text{H}_3\text{O})_{0.49}\text{Fe}_3(\text{SO}_4)_2(\text{OH})_6$, Potassium-Jarosite— $\text{KFe}_3(\text{SO}_4)_2(\text{OH})_6$, Ferrihydrite— $\text{Fe}(\text{OH})_3$, and Goethite— FeOOH have been considered in this thesis. From January 2004 to February 2013, Montana Resources operated a circuit to recover copper from the Berkeley Pit water. Gammons and Tucci⁵ explain that,

Approximately 50 million L/day of deep Berkeley Pit water containing more than 100 mg/L dissolved copper were pumped into bins containing scrap iron where the copper was precipitated as the native element through the “cementation process: $\text{Cu}^{2+} + \text{Fe}_{(s)} \rightarrow \text{Cu}_{(s)} + \text{Fe}^{2+}$

Iron rich water was returned back to the pit lake, and the ferrous iron combined with sulfate ions to produce a variety of FeSO_4 and hydroxide minerals. In their recently published paper, Gammons and Tucci⁶ provide an illustration of the Cu cementation process shown in Figure 1.

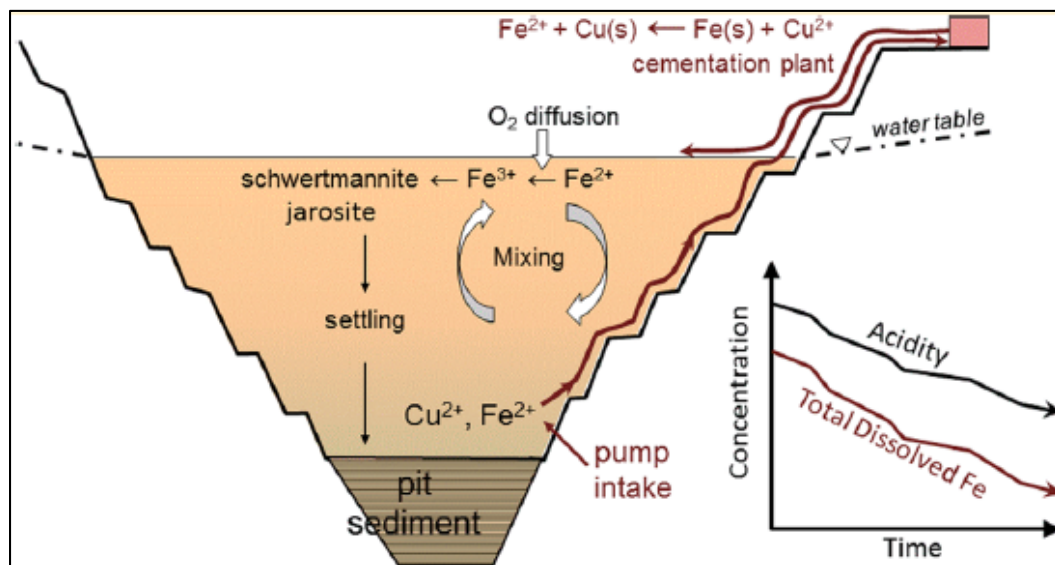


Figure 1: Schematic Illustration of Mineral Formation due to Cementation (Gammons & Tucci 2015)

Because of the extensive water-quality data recorded over 25 years, an analysis using computer modeling and thermodynamic tools to confirm previous findings and perhaps gain some insight into the properties of iron hydroxysulfate minerals, particularly Schwertmannite and Jarosite is possible. This analysis will be useful to predict thermodynamic quantities such as free energy of reaction which will be modelled from empirical water-quality data.

1.3. Scope of Work

The scope of the work involved using computer simulation with the Stabcal program created by Dr. Hsin H. Huang of Montana Tech⁷ to examine the water quality records to gain an understanding of the chemistry of solids forming in the Berkeley pit. Studies on the Berkeley pit water as well as similar acid mine drainage around the world have indicated that the acid mine water were saturated with precipitated Schwertmannite and/or various forms of Jarosite. For our modeling investigation the MBMG supplied the iron concentration for 127 samples that had reported total iron as Fe. Of those samples 99 supplied characterization data for Fe²⁺ and Fe³⁺ concentrations. Speciation calculations were performed with both total iron and the iron redox couple. Once these values were input, log Q values could be generated to calculate the saturation index. A multiple linear regression model was also used to calculate thermodynamic constants for Schwertmannite.

2. Literature Review

2.1. Acid Rock Drainage

2.1.1. Background

One of the main sources of acidic water formation is sulfide mineralization in the earth's crust. When sulfide minerals react with water and oxygen, acid is produced which lowers the pH of the water. Sulfide minerals are an important source of many metallic ores without which modern civilization could not exist. Mining of these minerals can expose the sulfides to oxygen and when rainfall or groundwater infiltration takes place, acid is formed which can change the water chemistry of the surrounding environment. Table I which is adapted from the GARD Guide⁸ shows a list of the important acid generating minerals present in the earth's crust.

Table I: Common Acid Generating Minerals (GARDGUIDE)

Mineral	Formula
Common Sulfides that generate acid w/ oxygen as oxidant	
Pyrite, Marcasite	FeS ₂
Pyrrhotite	Fe _{1-x} S
Bornite	Cu ₅ FeS ₄
Arsenopyrite	FeAsS
Enargite/Famatinite	Cu ₃ AsS ₄ /Cu ₃ SbS ₄
Tennantite/Tetrahedrite	(Cu,Fe,Zn) ₁₂ As ₄ S ₁₃ /(Cu,Fe,Zn) ₁₂ Sb ₄ S ₁₃
Realgar/Orpiment	AsS
Orpiment	As ₂ S ₃
Stibnite	Sb ₂ S ₃
Common Sulfides that generate acid w/ ferric iron as oxidant	
All of the above and:	
Sphalerite	ZnS
Galena	PbS
Chalcopyrite	CuFeS ₂
Covellite	CuS
Cinnabar	HgS
Millerite	NiS
Pentlandite	(Fe,Ni) ₉ S ₈
Greenockite	CdS

2.1.2. Schematic of Pyrite Oxidation

The Gard Guide also describes pyrite oxidation in a schematic taken from (Stumm and Morgan 1981)⁹. Figure 2 is an illustration and the bracketed numbers represent separate reactions which are explained in further detail:

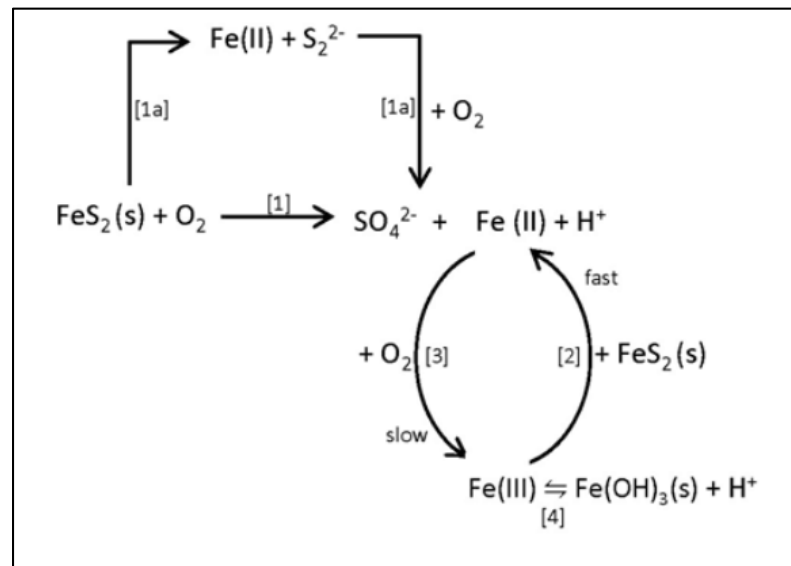


Figure 2: Schematic of Pyrite Oxidation with Reactions (after Stumm & Morgan 1981)

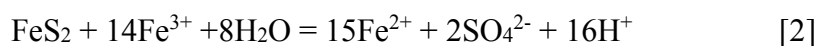
2.1.2.1. Detailed Pyrite Oxidation Reactions (GARDGUIDE)¹⁰

The pyrite oxidation reaction requires pyrite, air and water and the first reaction shown in Figure 2 is labeled [1]: The overall pyrite oxidation reaction is written,



Reaction [1] can occur with or without the presence of bacteria and is known as direct oxidation. In Figure 2, a variant process can occur labeled [1a]. In this reaction, the solid pyrite can be dissolved and then oxidized with O_2 . Under most circumstances, atmospheric oxygen acts as the oxidant. Oxygen dissolved in water, such as in underground conditions, can also cause pyrite oxidation, but due to its limited solubility in water, this process is much less

prominent¹¹. Reaction [2] shows how aqueous ferric iron Fe^{3+} can oxidize pyrite. The reaction is,



This reaction occurs at a considerably higher rate (2 to 3 orders of magnitude) greater than the reaction with oxygen [1] and produces a greater amount of acidity per mole of pyrite oxidized, but is limited to situations where significant amounts of dissolved ferric iron (Fe^{3+}) occur (i.e. acidic conditions). As a result, pyrite oxidation is generally initiated by reaction [1] at circumneutral ($6.5 < \text{pH} < 7.5$) or higher pH followed by reaction [2] when conditions have become sufficiently acidic ($\text{pH} < 4.5$ and lower). A third reaction [3] is required to generate and replenish ferric iron, through oxidation of ferrous iron by oxygen as follows,



A common misunderstanding is that ferric iron can oxidize pyrite indefinitely in the absence of oxygen. As shown in reaction [3], oxygen is required to generate ferric iron from ferrous iron. Also, acid generating bacteria may catalyze this reaction and require oxygen for cellular respiration. Therefore, some nominal amount of oxygen is needed for this process to be effective even when catalyzed by bacteria, although the oxygen requirement is less than for oxidation without bacteria. This reaction is the rate limiting step for pyrite oxidation in acidic environments¹².

A process of environmental importance related to pyrite oxidation concerns the fate of ferrous iron generated through reaction [1]. Ferrous iron can be removed from solution under slightly acidic to alkaline conditions through oxidation and subsequent hydrolysis and the formation of a relatively insoluble iron hydroxide, known as Ferrihydrite. Ferrihydrite has been formulated by Paktunc, et al¹³ as $5\text{Fe}_2\text{O}_3 \cdot 9\text{H}_2\text{O}$. However, for purposes of this thesis Ferrihydrite

will be represented as $\text{Fe}(\text{OH})_3$. Assuming the nominal composition of Ferrihydrite $\text{Fe}(\text{OH})_3$ for the product phase, the reaction [4] is given by,



When reactions [1] and [4] are combined, which generally is the case when the conditions are not acidic (i.e. $\text{pH} > 4.5$), it can be seen that oxidation of pyrite generates twice the amount of acidity relative to reaction [1] as,



2.1.2.2. Aqueous Fe Geochemistry

Some additional information is useful and was provided by Dr. Chris Gammons of Montana Tech.

Ferric iron (Fe^{3+}) is the dominant valence state in waters that contain dissolved oxygen. It exists in dissolved form as Fe^{3+} at $\text{pH} < 2$, but undergoes hydrolysis to form aqueous complexes of the type $\text{Fe}(\text{OH})_x^{3-x}$ at $\text{pH} > 2$.¹⁴

Ferrous iron (Fe^{2+}) is the dominant valence state in waters that do not contain oxygen. It exists in dissolved form mainly as Fe^{2+} over a wide range of pH. Ferrous iron is soluble over a much wider pH range than ferric iron. Concentrations > 10 mg/L (ppm) are possible even at neutral pH.¹⁵

Ferric iron is soluble at low pH, but forms insoluble Ferrihydrite at $\text{pH} > 3.5$. The Ferrihydrite reaction is fast and occurs by pH acidification in acidic, oxidized waters rich in ferric iron and is given by,



Ferrihydrite can also be produced by the reaction that was mentioned as reaction [4] where oxidation of reduced waters rich in ferrous iron gives,



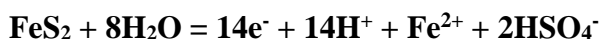
This reaction is a redox reaction and takes longer than reaction [6]. Reaction [4] is reasonably fast at pH 7, but decreases exponentially as the pH decreases. At low pH, iron oxidizing bacteria can increase the rate of conversion of Fe^{2+} to $\text{Fe}(\text{OH})_3$.¹⁶

The rate of oxidation of pyrite by Fe^{3+} increases as the $\text{Fe}^{3+}/\text{Fe}^{2+}$ ratio increases. Since the Eh of acid mine waters is typically controlled by the $\text{Fe}^{3+}/\text{Fe}^{2+}$ couple, the higher the Eh, the faster the rate of pyrite oxidation¹⁷.

2.1.3. Eh-pH Diagram for Ferrihydrite Formation

A summary of the relationship between Eh and pH is best presented graphically. Figure 3 shows an Eh-pH diagram¹⁸ for the formation of Ferrihydrite to show the relationship between Eh and pH for pyrite and the ferrous and ferric iron species. The steps to form Ferrihydrite are numbered 1 to 3 and are labelled in Figure 3. The following chemical reactions are given.

1. Pyrite oxidation



2. Fe^{2+} oxidation to Fe^{3+}



3. Fe^{3+} acidification



As discussed in the previous section, pyrite is converted into ferrous iron at low pH and higher Eh values. This is represented by arrow 1. At low pH and higher Eh, the ferrous iron is converted into ferric iron represented by arrow 2. When pH increases, ferric iron is converted into Ferrihydrite, shown in reaction [6] and represented by arrow 3.

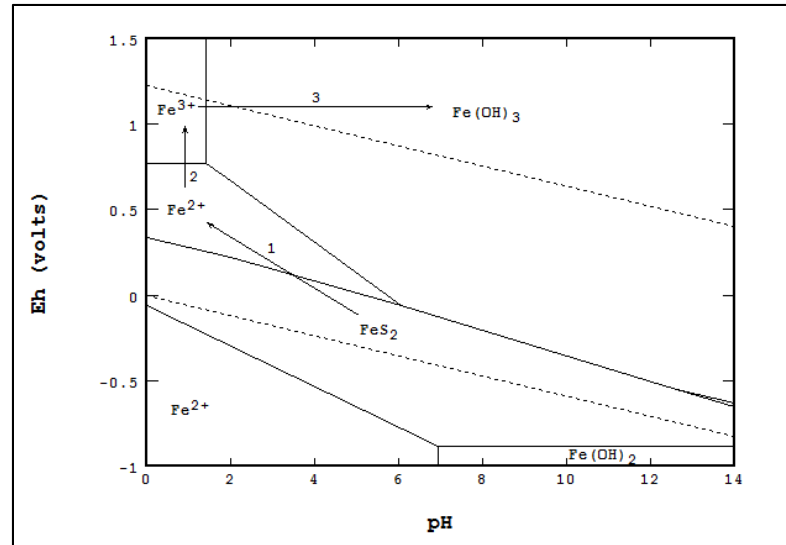


Figure 3: Eh-pH diagram of Ferrihydrite produced in Stabcal

2.1.4. Typical Water Quality from the Berkeley Pit

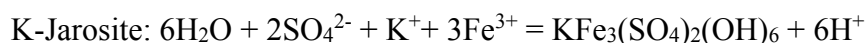
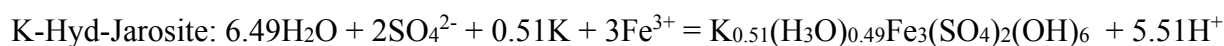
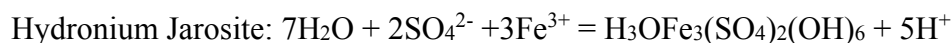
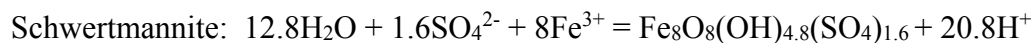
Table II shows some water quality values from a sample from the Berkeley Pit taken on June 10, 2011.¹⁹

Table II: Berkeley Pit Water Quality for June 10, 2011

	Milligram/Liter	Molality
Iron (total)	185.000	0.004
Copper	57.617	0.001
Zinc	565.262	0.010
Sodium	70.500	0.004
Potassium	8.710	0.0003
Calcium	462.700	0.014
Magnesium	547.730	0.026
Aluminum	281.928	0.012
Silica	111.600	0.002
Sulfate	10674.000	0.111
pH (units)	2.600	
Temperature (°C)	4.470	

As shown in Table II, sulfate values are quite high. As a consequence of ferric iron production at low pH (< 2) in the Berkeley Pit, a group of iron (oxy)hydroxysulfate species form. The

following reactions illustrate the formation of the iron (oxy)hydroxysulfate species of interest. However, using Eh-pH diagrams and Stabcal, Dr. H.H. Huang of Montana Tech²⁰ determined that Hydronium Jarosite does not form as a separate species in the Berkeley pit water. Although its chemical equation is shown below, its thermodynamic properties were not included as part of the modeling.



2.1.4.1. Schwertmannite and Jarosite

Schwertmannite is a mineral that was discovered in 1994 at the Pyhasalmi Mine in Finland and named after U. Schwertmann. Its physical properties are semi-transparent, brownish-yellow tetragonal crystals and it is associated with Goethite, Jarosite, Natrojarosite, Ferrihydrite, and sulfides²¹. It also forms a buffered complex with Jarosite in acidic waters. A paper published by Bigham²² in 1990 suggested that the solid composition and the Fe/S ratio can be used to determine x for Schwertmannite according to:



A picture of Schwertmannite²³ from Australia is shown in Figure 4 along with an XRD scan:

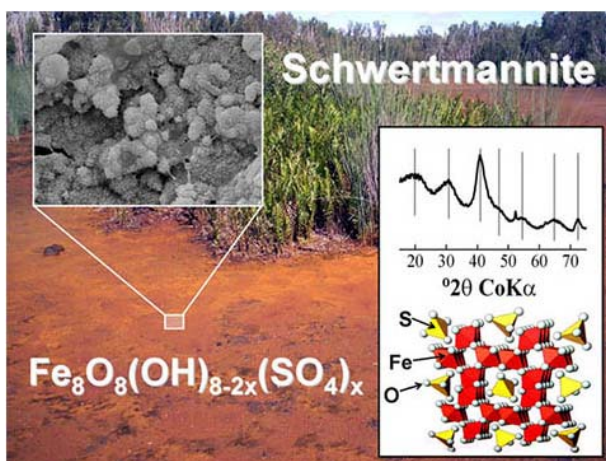


Figure 4: Picture of Schwertmannite with XRD Scan

A Virginia Tech world survey published in *Chemical Geology*²⁴ (2013) published the Fe/S molar ratios for Schwertmannite using samples from 30 locations. The mean SO₄ molar composition for the Schwertmannite samples was 1.56. For the speciation study of the Berkeley Pit, a value of 1.6 was used. The OH molar composition came out to be 4.8. This gave a Schwertmannite formula of Fe₈O₈(OH)_{4.8}(SO₄)_{1.6}. Potassium Hydronium Jarosite was another mineral that formed in iron and sulfate rich acid mine waters. The formula for Jarosite given by Dutrizac²⁵ (1983) is:

$K_{0.51}(H_3O)_{0.49}Fe_3(SO_4)_2(OH)_6$ and the reaction is given in section 2.1.4

Figure 5 was taken by Dr. Chris Gammons²⁶ on November 18, 2008 and shows Schwertmannite and euhedral crystals of Jarosite in the center of the photo at high magnification. On that day, water quality samples that were taken indicated a pH of 2.66, a temperature of 6°C, and an Eh of 666.8 mV. Figure 9 on page 62 shows an Eh-pH diagram at 6°C. Using the values from November 18th, 2008 in conjunction with Figure 9 likely indicates that the Jarosite species shown in figure 5 is KH-Jarosite ($K_{0.51}(H_3O)_{0.49}Fe_3(SO_4)_2(OH)_6$.)

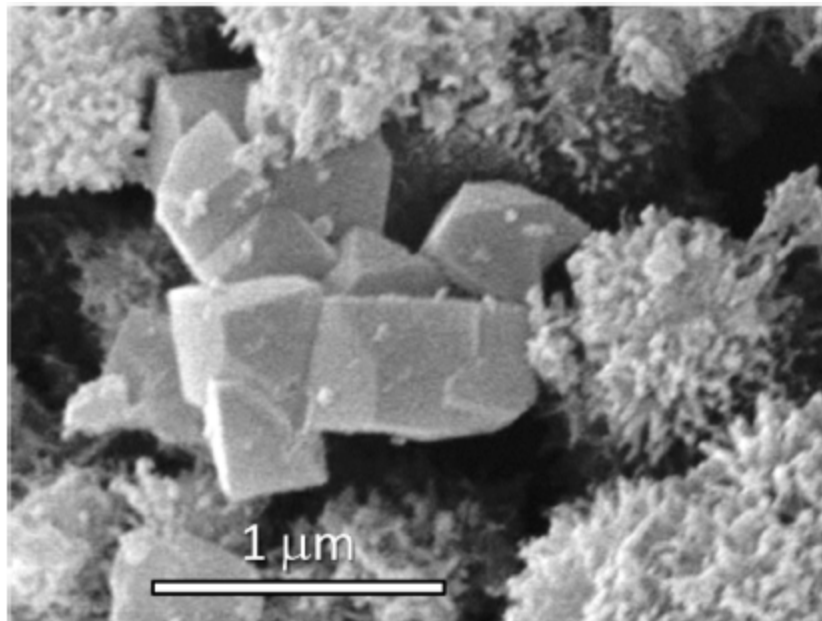


Figure 5: Schwertmannite and Jarosite Crystals under SEM (Gammons & Tucci 2015)

3. Thermodynamic Theory

According to the Water Quality report, the Montana Bureau of Mine and Geology has constantly sampled and analyzed Berkeley pit water since the beginning of flooding the pit in 1987. There were 127 samples which were used in the analysis. Ninety-nine of those samples also reported Fe^{2+} and Fe^{3+} separately producing a total of 226 samples for analysis. (Section 8 of the appendix lists all records which were used.) Since the $\text{Fe}^{2+}/\text{Fe}^{3+}$ redox couple as well as the dissolved oxygen yielded their own Eh's, additional study was performed.

Studies on the Berkeley pit water as well as the similar acid mine drainage around the world have indicated that the acid mine waters were either saturated with or precipitated out Schwertmannite and various forms of Jarosite. This study will examine the chemistry of possible solid formation including iron hydroxides for their thermodynamic properties as a function of temperature associated with the Berkeley pit water.

In order to analyze the chemical properties of the Berkeley pit water, it is necessary to discuss some of the relevant thermodynamic principles.

3.1. Fundamental Databases, Thermodynamics, Calculations

3.1.1. Thermodynamic data in Stabcal

The versatility of Stabcal lies in the fact that many different thermodynamic databases can be used for evaluation of chemical reactions. There are several databases in Stabcal that can be directly accessed: These are: 1. NBS²⁷ with C_p from Helgeson²⁸, 2. Naumov²⁹, 3. NIST Critical database (46)³⁰, 4. SuperCrit 92 and later³¹, 5. Win-MINTEQA2³², 6. LLnL³³ and 7. WATEQ4F.³⁴ Since temperature was a critical factor in this research work, it was determined that the NBS (National Bureau of Standards) database with C_p data from Helgeson would give the best results because of the extensive database size. The dG values of $\text{AsO}_3\text{F}^{2-}$ and HAsO_3F^-

in the database were deleted because their thermodynamic data would have caused errors to occur in the modeling. The reason for this was that the species $\text{AsO}_3\text{F}^{2-}$ and HAsO_3F^- had log K values that were much too large and caused the program to fail to converge. This was probably due to a sign error when calculating the free energy of formation in the original database³⁵.

The popular databases (items #5 through 7) that were linked to PHREEQC were not selected because most of their data pertained to non-Master dissolved species which were calculated using the Van't Hoff Equation³⁶. This equation assumed ΔC_p for the reaction was zero which was not a good assumption for analyzing the temperature effect. If one wanted to use these databases, the parameters of log K and ΔH_{rex} for each equilibrated solid would have had to be changed.

3.1.2. Equilibrium Calculation and Equilibrium Constants

The equilibrium calculation for a system at any temperature, involves (1) equilibrium constants among species, and (2) mass input to each component. A common method to obtain equilibrium constants is by using the free energy of formation, dG, of the species. For a chemical reaction $aA + bB = cC + dD$, the dG of reaction ($dG_{\text{rex}} = c \times dG(C) + d \times dG(D) - (a \times dG(A) + b \times dG(B)$) where a, b, c, d are the number of moles. The relation between the equilibrium constant K and dG_{rex} is expressed in Equation 1.

Equation 1: Relation between K and dG

$$\log K = \frac{-dG_{\text{rex}}}{RT \ln(10)} \text{ where } R = 1.98720650096 \text{ cal/K mole (Codata 2006)}$$

3.1.3. Calculating Free energy for a given Temperature

3.1.3.1. Calculating Free Energy of Formation from Stable Elements

There are several fundamental concepts and steps in order to estimate $dG_{(T)}$ for room temperature. Free Energy, G , is the energy of individual species and the free Energy of formation, dG , is the energy of reaction from the stable elements.

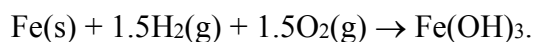
Free energy of formation can be calculated by two methods. The first method involves calculating dG° for a compound from the stable elements using the free energy of the species G . Free energy G° in the standard state is the free energy of the individual species at standard state conditions of 298.15K, 1M concentration, and 1 atm pressure. Table III lists the free energies of related species at 25°C and 50°C.

Table III: Free Energy of Formation and Free Energy of Individual Species for Fe(OH)₃

Species, Charge, State	dH(kcal)	dS(cal)	dG(kcal)	H(kcal)	S(cal)	G(kcal)
25°C						
Fe ⁰ S	0	0	0	0	6.520000	-1.943938
H ₂ ⁰ G	0	0	0	0	31.234000	-9.312417
O ₂ ⁰ G	0	0	0	0	49.029	-14.617996
H ⁺ A	0	0	0	0	0	0
Fe ³⁺ A	-11.609234	-35.171000	-1.123000	-11.609234	-75.502000	10.901688
H ₂ O ⁰ A	-68.314627	-39.039500	-56.675000	-68.314627	16.709000	-73.296415
Fe(OH) ₃ ⁰ S ppt	-196.703137	-101.412500	-166.467000	-196.703137	25.502000	-204.306558
50°C						
Species, Charge, State	dH(kcal)	dS(cal)	dG(kcal)	H(kcal)	S(cal)	G(kcal)
Fe ⁰ S	0	0	0	0.149975	7.003039	-2.113057
H ₂ ⁰ G	0	0	0	0.172228	31.788710	-10.100294
O ₂ ⁰ G	0	0	0	0.175400	49.593928	-15.850878
H ⁺ A	0	0	0	0	0	0
Fe ³⁺ A	-11.929103	-36.204451	-0.229635	-12.037469	-76.884477	12.807749
H ₂ O ⁰ A	-68.131659	-38.450335	-55.706434	-67.871732	18.135339	-73.732166
Fe(OH) ₃ ⁰ S ppt	-196.753004	-101.573751	-163.929446	-196.081588	27.503244	-204.969261
S = solid, A = aqueous						
G = gas						

Here is an example calculation:

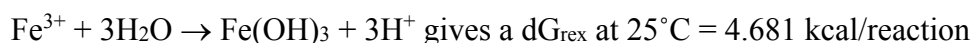
For Ferrihydrite Using Stable Elements at 25°C:



$dG_{\text{Fe(OH)}_3} = G_{\text{Fe(OH)}_3} - [G_{\text{Fe}} + 1.5G_{\text{H}_2(\text{g})} + 1.5G_{\text{O}_2(\text{g})}] = -166.467 \text{ kcal/mol}$. This value is the free energy of formation, dG for Fe(OH)_3 shown in the third column of Table III.

3.1.3.2. Calculating Free Energy of Reaction from Master Species

Another method involves calculating dG_{rex} for a reaction from various “master species.” These master species are H^+ , $\text{H}_2\text{O}(\text{l})$, SO_4^{2-} , K^+ , and Fe^{3+} . If dG_{rex} from the master species for a reaction is known, dG can be calculated without having to calculate the G value from the constituent elements. For example,



The calculation at 25°C is: $[-166.467+3*(0)]-[-1.123]+3*(-56.675)] = \mathbf{4.681 \text{ kcal}}$

If one used the G values in Table III, column 6, for the constituent elements, the chemical equation would still be the same given by $\text{Fe}^{3+} + 3\text{H}_2\text{O} \rightarrow \text{Fe(OH)}_3 + 3\text{H}^+$, but the dG_{rex} calculation at 25°C would be:

$[-204.306558+3*(0)]-[10.901668+3*(-73.296415)] = \mathbf{4.681 \text{ kcal}}$ which is identical.

Therefore, dG_{rex} will be identical calculated either from Free Energy of the individual species or from Free Energy of formation and can be expressed by the general equation 2:

Equation 2: Relationship between Free Energy of a Species and Free Energy of Formation for a Reaction

$$dG_{\text{rex}} = G(\text{Fe(OH)}_3) + \Sigma(\nu_M \times G_M) = dG(\text{Fe(OH)}_3) + \Sigma(\nu_M \times dG_M)$$

3.1.3.2.1. Using Gibbs relationship for Entropy and Enthalpy

Estimation of the energy change due to temperature is more understandable using Entropy (S) and Enthalpy (H). These values can be obtained from Free Energy using the Gibbs Relationship given in Equation 3:

Equation 3: Gibbs Free Energy Function

$$G(T) = H(T) - T \times S(T)$$

The same relationship holds for the Free Energy of formation by taking the derivative and is shown in Equation 4:

Equation 4: Gibbs Free Energy of Formation Function

$$dG(T) = dH(T) - T \times dS(T)$$

3.1.3.2.2. Entropy and Enthalpy Change from changing Temperature

For a temperature other than standard state of 298.15K, enthalpy and entropy can be expressed by Equation 5:

Equation 5: Enthalpy and Entropy Equations for a Given Temperature

$$H_T = H_{rm} + \int_{T_{rm}}^T C_p dT, \quad S_T = S_{rm} + \int_{T_{rm}}^T \frac{C_p}{T} dT$$

When Maier – Kelly C_p is used, the expressions after integration are illustrated in Equation 6:

Equation 6: Enthalpy and Entropy Equations after Integration

$$H_T = H_{rm} + a \times (T - T_{rm}) + b \times 10^{-3} \frac{(T^2 - T_{rm}^2)}{2} - c \times 10^5 \left(\frac{1}{T} - \frac{1}{T_{rm}} \right)$$

and

$$S_T = S_{rm} + a \times \ln\left(\frac{T}{T_{rm}}\right) + b \times 10^{-3}(T - T_{rm}) - \frac{c \times 10^5}{2} \left(\frac{1}{T^2} - \frac{1}{T_{rm}^2}\right)$$

Where a, b, c are the regression coefficients³⁷ of the polynomial series for the specific heat capacity at constant pressure: $c_p = a + b \times 10^{-3} T - c \times 10^5 T^{-2}$

3.1.3.2.3. Accounting for Species Charge

The charge of a species is balanced out by the formation of H^+ . For instance, the formation of Fe^{3+} comes from



Using Table III, at 50°C,

$$dG(Fe^{3+}) = G(Fe^{3+}) + 1.5G(H_2(g)) - [(G(Fe) + 3G(H^+))] = -0.2296347 \text{ kcal/mole}$$

3.1.3.3. Equilibrium calculation using Mass Action Law.

The mass action law to calculate the equilibrium constant K is usually presented as follows. For a chemical reaction in equilibrium consisting of $aA + bB \rightleftharpoons cC + dD$, where the reactants are A and B and the products are C and D, and where a, b, c, d are the molar coefficients, the mass action law³⁸ is represented in Equation 7.

Equation 7: Equilibrium Mass Action Law

$$K_{eq} = \frac{\{C\}^c \{D\}^d}{\{A\}^a \{B\}^b}$$

{ } = activity of species

When the system is not at equilibrium, then the K value is changed to Q which is termed the reaction quotient. The reaction quotient is based on Le Chatelier's Principle³⁹, which states that

If a chemical system is at equilibrium and we add a substance (either a reactant or a product), the reaction will shift so as to reestablish equilibrium by consuming part of the added substance. Conversely, removal of a substance will result in the reaction moving the direction that forms more of the substance.

An example of the equilibrium calculation using the mass action law is best illustrated with a hypothetical case. For this example, the solution contains sulfur with a valence of 6 indicated by, S(6), and with a redox couple for the iron species, Fe(2) and Fe(3). The system is at 25°C, Eh = 0.660 V, pH = 3.00, $\Sigma[S(6)] = 0.01$ moles/liter, and $\Sigma[Fe(2,3)] = 0.008$ moles/liter. Two cases are shown for the purpose of illustration.

3.1.3.3.1. Fe²⁺ and Fe³⁺ components behave independently

Case 1: We will assume that Fe(2) and Fe(3) components behave independently, with $\Sigma[Fe(2)] = 0.005$ moles/liter and $\Sigma[Fe(3)] = 0.003$ moles/liter.

In addition to the S(6), Fe(2) and Fe(3) components, there are also H(1) and O(2) components, and a total of 18 aqueous species according to the NBS database which are used by Stabcal. To be able to setup and compute equilibrium constants, a master species is chosen for each component and is listed in Table IV. It should be noted that there is no electron transfer between Fe(2) and Fe(3) species, so an additional electron component e(-1) will not be necessary.

Table IV: Formation with Master and Non Master Species

Compt	Master	Non-Master						
H(1)	H ⁺ A							
O(2)	H ₂ O ⁰ A	OH ⁻						
S(6)	SO ₄ ²⁻ A	HSO ₄ ⁻	FeSO ₄ ⁺ A*	Fe(SO ₄) ₂ ⁻ A*				
Fe(2)	Fe ²⁺ A	FeOH ⁺ A	Fe(OH) ₂ ⁰ A	Fe(OH) ₃ ⁻ A	Fe(OH) ₄ ²⁻ A			
Fe(3)	Fe ³⁺ A	FeOH ²⁺ A	Fe(OH) ₂ ⁺ A	Fe(OH) ₃ ⁰ A	Fe ₂ (OH) ₂ ⁴⁺ A	Fe(OH) ₄ ⁻ A	FeSO ₄ ⁺ A	Fe(SO ₄) ₂ ⁻ A

A = aqueous

* Species are listed both in S(6) and Fe(3) components

There will be a total of 18 (5 masters and 13 non-masters) species, and their unknown concentrations requiring 18 known equations or data.

Solving these equations given the data are shown by two examples:

- a. Calculating the equilibrium constant for each of 13 non-master species from 5 master species.

For instance, to form $\text{Fe}(\text{SO}_4)_2^-$ which is a non-master species from the master species Fe^{3+} and 2SO_4^{2-} shown in Table IV, the following reaction takes place:

$\text{Fe}^{3+} + 2\text{SO}_4^{2-} \leftrightarrow \text{Fe}(\text{SO}_4)_2^-$ The equilibrium constant is computed from Equation 8.

Equation 8: Calculation of Equilibrium Constant K using Mass Action Law

$$\log K = 5.385382 = \log\left(\frac{\{\text{Fe}(\text{SO}_4)_2^-\}}{\{\text{Fe}^{3+}\}\{\text{SO}_4^{2-}\}^2}\right)$$

Since Activity = [Concentration] x Activity coefficient (γ), by rearranging Equation 7 which is the equilibrium equation, the concentration of non-master species can be expressed by concentrations of master species shown in Equation 9:

Equation 9: Equilibrium Constant as a Function of Activity

$$\frac{[C]^c [D]^d}{[A]^a [B]^b} \cdot \frac{[\gamma]^c [\gamma]^d}{[\gamma]^a [B\gamma]^b} = K_{eq}$$

- b.) Another method involves using mass balance equations from 3 inputs as shown below.

Using Table IV, we can write the following equations where the sum of the component species equals the sum of the master and non-master species,

- 1.) $\Sigma[S(6)] = [SO_4^{2-}] + [HSO_4^-] + [FeSO_4^+] + 2*[Fe(SO_4)_2^-] = 0.01$ moles/liter
- 2.) $\Sigma[Fe(2)] = [Fe_2^+] + [FeOH^+] + 2*[Fe(OH)_2^0] + 3*[Fe(OH)_3^-] + 4*[Fe(OH)_4^{2-}] = 0.005$ moles/liter
- 3.) $\Sigma[Fe(3)] = [Fe_3^+] + [Fe(OH)^{2+}] + 2*[Fe(OH)_2^+] + 3*[Fe(OH)_3^0] + 2*[Fe_2(OH)_2^{4+}] + 4*[Fe(OH)_4^-] + [FeSO_4^+] + 2*[Fe(SO_4)_2^-] = 0.003$ moles/liter

where the concentrations of H(1) and O(2) are normally unknown, and an assumption of two additional conditions are given by (i) and (ii).

- i. $[H_2O(l)] = 1$
- ii. $[H^+] = 10^{-pH} = 0.001$

With this information, we can use the Law of Mass Action is to solve all the unknown concentrations with the known equations simultaneously. This is normally done by using Newton's method⁴⁰. The Stabcal program uses the same principles but by solving the concentrations of master species first.

3.1.3.3.2. Fe²⁺/Fe³⁺ Redox Couple

Case 2: We will assume that Fe(2) and Fe(3) components are grouped together so that we can combine Fe(2) and Fe(3) to 0.008 moles/L which is then is redistributed using measured Eh. The same principles are applied for the distribution of the Fe²⁺/Fe³⁺ redox couple by the measured Eh. There will only be one Fe component and one master species. The rearranged listing is presented in Table V:

Table V: Master and Non-master Species for Combined Fe²⁺/Fe³⁺ Redox Couple Equilibrium Calculation

Compt () = charge	Master	Non-Master						
Electron(-1)		e ⁻						
H(1)	H ⁺ A							
O(2)	H ₂ O ⁰ A	OH ⁻						
S(6)	SO ₄ ²⁻ A	HSO ₄ ⁻	FeSO ₄ ⁺ A*	Fe(SO ₄) ₂ ⁻ A*				
Fe(2+3)	Fe ²⁺ A	FeOH ⁺ A	Fe(OH) ₂ ⁰ A	Fe(OH) ₃ ⁻ A	Fe(OH) ₄ ²⁻ A			Fe ³⁺ A
		FeOH ²⁺ A	Fe(OH) ₂ ⁺ A	Fe(OH) ₃ ⁰ A	Fe ₂ (OH) ₂ ⁴⁺ A	Fe(OH) ₄ ⁻ A	FeSO ₄ ⁺ A	Fe(SO ₄) ₂ ⁻ A

* Species are listed both in S(6) and Fe(3) components

Some differences from Case 1 are that:

The equilibrium equations of Fe(3) species will be expressed by the master of Fe(2).

For instance, the equation is represented by the following reaction,



and the log K calculation is shown in Equation 10.

Equation 10: Calculation of Equilibrium Constant K using Redox Couple

$$\log K = 5.385382 = \log\left(\frac{\{\text{Fe}(\text{SO}_4)_2^-\}\{\text{e}^-\}}{\{\text{Fe}^{3+}\}\{\text{SO}_4^{2-}\}^2}\right)$$

In addition, there will only be one mass input for total Fe which is given by,

$$\Sigma\text{Fe}(2+3) = 0.008 \text{ mole/L}$$

One of the missing mass inputs will be replaced by the activity of $\{\text{e}^-\}$ as shown in Equation 11.

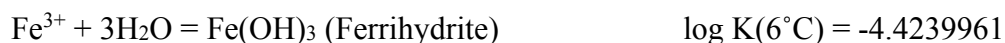
Equation 11: Alternate Form of Nernst Equation for One Electron Process

$$\log\{\text{e}^-\} = -Eh \times \frac{F}{\ln(10) \cdot RT}$$

3.1.3.4. Formation Reaction of Solid (Reaction Quotient and Direction, and Saturation Index)

In order to illustrate the formation reactions for some of the mineral species present in the Berkeley Pit, the reaction quotient and saturation index will be looked at. Goethite and Ferrihydrite will be used as an example. In addition Record 195 at 6°C from May 4, 2005 in the MBMG data set will be used.

The formation reactions from master species and Equilibrium constants based on the National Bureau of Standards database (NBS) at 6°C are:



From record 195, the activities of the master species, and log Q for the formation of both solids are given in Table VI.

Table VI: Activity of Master Species and Log Q for Goethite and Ferrihydrite

Master	H ⁺	H ₂ O(l)	Fe ³⁺		Solids	FeOOH	Fe(OH) ₃
Activity	3.548134E-03	1	2.539274E-05		Log Q	-2.7547095	-2.7547095

Le Châtelier's Principle was presented in section 3.1.3.3, and the saturation index, $SI = \log K - \log Q$. As explained earlier, the K value is the equilibrium constant, and the Q value is the reaction quotient. The difference measured as "SI" is called the saturation index, and is commonly used to show the status of the solid. A positive SI means the solid is over-saturated and has the potential to precipitate until equilibrium is returned to 0 where the $SI = 0$. A negative SI indicates that there is an under-saturated solid present which will not precipitate out of solution.

An examination of the FeOOH solid (Goethite) shows that $\log Q < \log K$ (e.g. $-2.7547095 < -1.0808495$ from Table VII). Therefore, the reaction will favor the forward direction. In other words, the solution will be oversaturated with FeOOH. As shown in Table VII, the saturation index (SI) is 1.673860, so Goethite will precipitate out. For Ferrihydrite Fe(OH)₃ species, however, $\log Q > \log K$, and the saturation index is negative, so the reaction will favor the reverse direction. As a result, the solid Ferrihydrite Fe(OH)₃ will not precipitate from solution because it is under-saturated.

Table VII: Computed SI Index for Goethite and Ferrihydrite

Solid	Log Q (B-pit)	Log K(NBS)	Direction	Saturation index $SI = \log K - \log Q$	
FeOOH	-2.754710	-1.080850	K > Q forward	1.673860	Over-Saturated Solution
Fe(OH) ₃	-2.754710	-4.423996	Q > K reversed	-1.669287	Under-saturated Solution

3.1.4. Thermodynamic Data for Temperatures other than 25°C

The $dG_{(T)}$ of a species (dG value for a given temperature) may not always be available. It is best to estimate this quantity from thermodynamic data. The data should include the following two groups of values.

Group 1 refers to the heat capacity function, C_p of the species. As shown in section 3.1.3.2.2 (Equation 6), it is also known as the Maier-Kelly function, where $C_p = a + b \times 10^{-3} T + c \times 10^5 T^{-2}$. As mentioned earlier, the values for a , b , c are the regression coefficients of the polynomial series for the specific heat capacity C_p at constant pressure.

Group 2 refers to the free energy and the entropy at room temperature: dG_{rm} and S_{rm} . Although many databases report enthalpy of formation values, $dH_{rm} = H_{rm}$, these numbers may not be as accurate because of approximation by the van't Hoff equation. For consistency purposes, it is best to recalculate the values from dG_{rm} and S_{rm} using Equation 4 given in Section 3.1.3.2.1. For instance, given Ferrihydrite, $Fe(OH)_3$, recalculating dH_{rm} using dG_{rm} and S_{rm} values gives $dH_{rm} = -823.0$ kJ/mole which agrees perfectly with values from the NBS database. However, looking at a different species, Fe^{3+} and recalculating $dH_{rm} = -49.91$ kJ/mole. This quantity does not agree with -48.5 kJ/mole for dH_{rm} reported in the NBS database.

3.2. Speciation of the Berkeley pit water, and log Q of Investigated Solids

3.2.1. Speciation of the Berkeley pit water

There were 260 samples which were individually investigated. Temperatures ranged from 2°C to 23°C (truncated to 0 decimal places), and depth from the Berkeley Pit surface to 700ft below. Excluding H(1), O(2) and e(-1), there were 27 elements including Fe(2) and Fe(3).

Table VIII lists important conditions, components and their analytical results taken from 05/04/05 at 100 ft below the surface. ID #195 used the measured ORP for Eh (shown

in green), and ID # 502 used Eh of $\text{Fe}^{2+}/\text{Fe}^{3+}$ redox couple for Eh (shown in yellow).

Temperature was truncated to zero decimal places for the analysis.

The table also includes ID #98 just before MR started to pump the water from depth to recover Cu (12/99) as part of the cementation process, and also includes ID #291 which is one of the last samples before the pit wall failure on 11/3/2012. These water quality records are included to illustrate changes in water chemistry over time due to the cementation process and are presented below.

Table VIII: MBMG Water Analysis of Berkeley Pit At Three Important Times

Sample ID	DATE	DEPTH	pH	Temp	ORP	DO	pH(lab)	Ca	Mg
	mm/dd/yy	(Feet)		(C)	(MV)	(mg/l)		(mg/l)	(mg/l)
195/502	05/04/05	100	2.45	5.56	667	0.43	2.89	466	471
98	11/19/99	200	2.2	4.9	637		2.9	423	532
291	06/14/12	250	2.58	2.67	679	0.2	2.84	470.63	567.38
Na	K	Fe	Mn	SiO ₂	Cl	SO ₄	F	Al	As
(mg/l)	(mg/l)	(mg/l)	(mg/l)	(mg/l)	(mg/l)	(mg/l)	(mg/l)	(ug/l)	(ug/l)
78.3	10.57	499	233	103.0	<50	9,010	17.0	230,138	88
75.2	7.2	942	216	108	58.3	8,778	33.6	226,000	749
74.36	9.08	259,596	240.152	116.01	17.81	7,964	32.98	293,858	73.01
B	Cd	Co	Cu	Li	Ni	Sr	U	Zn	Ce
(ug/l)	(ug/l)	(ug/l)	(ug/l)	(ug/l)	(ug/l)	(ug/l)	(ug/l)	(ug/l)	(ug/l)
<300	1,676	1,185	67,712	321	1,189	1,551	563	527,315	
<300	2,220	1,480	184,000	340	1,330	1,220		609,000	
45.30	2033.3	1,496	54134.38	285.51	1203.39	1,097	724.75	632,926	857.22
La	Nd	Pr	Th	Fe(2)	Fe(3)				
(ug/l)	(ug/l)	(ug/l)	(ug/l)	mg/l	mg/l				
				185	435				
248.07	425.16	86.53	81.71						

Based on the NBS database, excluding H^+ , $\text{H}_2\text{O}_{(l)}$, OH^- , $\text{O}_{2(a)}$ and $\text{O}_{2(g)}$ there are 507 species, and 175 of them are aqueous and distributed in 27 additional components. The results of the speciation calculation assuming no precipitate and measured Eh are listed below. Ionic strength of the Berkeley pit water is normally around 0.25. A value of 0.25 is considered to be a

higher ionic strength solution. In concentrated solutions or higher ionic strength solutions, ion-ion interactions reduce the chemical strength of the species, so the concentration has to be corrected for activity according to Equation 12.

Equation 12: Equation to Calculate Activity for a species

$$a = \gamma \cdot C$$

Where a is activity, γ is activity coefficient, and C is the species concentration

The ionic strength is needed to calculate the activity coefficient and is presented in Equation 13.

Equation 13: Calculation of Ionic Strength for a Solution

$$I = \frac{1}{2} \sum C z^2$$

Where I is ionic strength, C is the species concentration, and z is the species charge

Although Stabcal has three different methods to calculate activity coefficients of the charged species, the Davies Equation was used for the speciation procedure and is shown in Equation 14.

Equation 14: Davies Equation for Ionic Strength

$$\log \gamma = -Az^2 \frac{\sqrt{I}}{1 + \sqrt{I}} - 0.24I$$

Where A is a constant with a value of 0.5 for water at 25°C where I usually has a value between 0.2 and 0.3

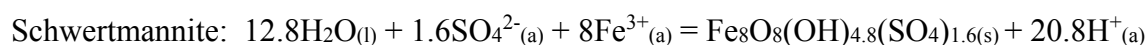
Although all species contribute to determine the precipitation/dissolution of Schwertmannite and other solids, certain master species and their equilibrium activities are arbitrarily selected for the reaction. These are H^+ , $H_2O(l)$, SO_4^{2-} , K^+ , and Fe^{3+} .

Results from the measured Eh (ID 502, Fe^{2+}/Fe^{3+}) and from dissolved O_2 are listed in Table XI. The Eh determined from Fe^{2+}/Fe^{3+} couple seems to reasonably agree with the measured one. However, the Eh calculated from dissolved O_2 is much higher than calculation from the other two methods as shown in Table IX. As a result, Eh results from dissolved O_2 will no longer be considered for determining the equilibrium constants of Schwertmannite.

Table IX: Activities for Component Species at 6°C for Measured Eh and Fe^{2+}/Fe^{3+} Couple

Temp 6	dG kcal	Measured Eh		Eh from Fe^{2+}/Fe^{3+} Couple		Eh from Dissolved O_2	
Eh(V)		0.667		0.667791275		1.079253705	
pH		2.45		2.45		2.45	
		Moles/L	Activity	Moles/L	Activity	Moles/L	Activity
H^+ A	0	4.953506E-03	3.548134E-03	4.953879E-03	3.548134E-03	4.944383E-03	3.548134E-03
H_2O^0 L	-57.4210	55.50825019	1	55.50825019	1	55.50825019	1
SO_4^{2-} A	-180.3500	6.541092E-02	1.721867E-02	6.408760E-02	1.686524E-02	6.111331E-02	1.620644E-02
K^+ A	-67.2290	2.466106E-04	1.766441E-04	2.470554E-04	1.769493E-04	2.478887E-04	1.778872E-04
Fe^{3+} A	-1.7790	5.115917E-04	2.539274E-05	6.524838E-04	3.236395E-05	9.573252E-04	4.831154E-05
A = aqueous, L = liquid							

The reaction for the formation of Schwertmannite from master species is given by:



Using the stoichiometric coefficients, ν_M , activity, and dG_M from master species, the calculation for Log Q is as follows:

$$\text{Log Q} = \sum \nu_M \times \log(\text{activity}_M).$$

For example, calculation of the log Q value for Schwertmannite using the measured Eh is as follows (where the activity of Schwertmannite is 1):

$$[1 \cdot \log(1) + 20.8 \cdot (\log(3.548134 \times 10^{-3}))] - [8 \cdot (\log(2.539274 \times 10^{-5})) + 1.6 \cdot (\log(1.721867 \times 10^{-2}))] = -11.3752756173902$$

which is the same result given by Stabcal shown in Table X.

The same calculation using the Eh from the $\text{Fe}^{2+}/\text{Fe}^{3+}$ couple is calculated as follows:

$$1 \cdot \log(1) + 20.8 \cdot (\log(3.548134 \times 10^{-3})) - [8 \cdot (\log(3.236395 \times 10^{-5})) + 1.6 \cdot (\log(1.686524 \times 10^{-2}))] = -12.2$$

and is shown in column 3 of Table X.

Table X: Log Q Eh vs Log Q $\text{Fe}^{2+}/\text{Fe}^{3+}$ for Various Iron Sulfate Mineral Species for Records 195 & 502

Solid species	Log Q(Eh)	Log Q($\text{Fe}^{2+}/\text{Fe}^{3+}$)	Chemical reactions
Schwertmannite	-11.4	-12.2	$12.8\text{H}_2\text{O} + 1.6\text{SO}_4^{(2-)} + 8\text{Fe}^{(3+)} = \text{Fe}_8\text{O}_8(\text{OH})_{4.8}(\text{SO}_4)_{1.6} + 20.8\text{H}^{(+)}$
K-Jarosite	6.37	6.07	$6\text{H}_2\text{O} + 2\text{SO}_4^{(2-)} + \text{K}^{(+)} + 3\text{Fe}^{(3+)} = \text{KFe}_3(\text{SO}_4)_2(\text{OH})_6 + 6\text{H}^{(+)}$
H-Jarosite	5.06	4.77	$7\text{H}_2\text{O} + 2\text{SO}_4^{(2-)} + 3\text{Fe}^{(3+)} = \text{H}_3\text{OFe}_3(\text{SO}_4)_2(\text{OH})_6 + 5\text{H}^{(+)}$
Ferrihydrite	-2.75	-2.86	$3\text{H}_2\text{O} + \text{Fe}^{(3+)} = \text{Fe}(\text{OH})_3 + 3\text{H}^{(+)}$
Goethite	-2.75	-2.86	$2\text{H}_2\text{O} + \text{Fe}^{(3+)} = \text{FeOOH} + 3\text{H}^{(+)}$
KH-Jarosite	5.73	5.43	$6.49\text{H}_2\text{O} + 2\text{SO}_4^{(2-)} + 0.51\text{K} + 3\text{Fe}^{(3+)} = \text{K}_{.51}(\text{H}_3\text{O})_{.49}\text{Fe}_3(\text{SO}_4)_2(\text{OH})_6 + 5.51\text{H}^{(+)}$

After analyzing the estimated log Q for the investigated solids, there were a total of 248 samples used for Schwertmannite (out of the original 260 samples). Twelve of the original samples had missing record information. Out of the remaining 248 samples, 16 samples were excluded within the temperature range of 15°C to 23°C because only a total of one or two samples were recorded at each of those temperatures. This left 232 samples within the temperature range of 2°C to 14°C. Six additional samples were excluded because they were considered to be outliers (outside of 3 standard deviations of the average log Q) leaving a total of 226 samples for analysis.

3.2.2. Outlier Determination Procedure

The procedure for determining the number of outliers involved taking an average of the log Q values within each temperature interval measured in 1°C increments. The standard deviation (S.D.) for log Q was also calculated for each temperature increment. Multiplying 3 x

S.D. and subtracting from the average log Q as well as adding 3 x S.D. to the average log Q produced a range of log Q values from low to high for each temperature. Any values which did not fall within the range of 3 standard deviations below and 3 standard deviations above the average log Q value was rejected. The remaining set of values produced a 99.9% confidence interval for estimated log Q values. These log Q values were the estimated output result from Stabcal based on the MBMG water quality records which were the input source. The resulting log Q frequencies from 2°C to 14°C were used as weights in a matrix for the multiple regression analysis.

3.2.3. Comparison of Log Q to Log K for Goethite, Ferrihydrite, and K-Jarosite

This section is included to identify the saturation status of Goethite, (FeOOH), Ferrihydrite, $\text{Fe}(\text{OH})_3$ and K-Jarosite, $\text{KFe}_3(\text{SO}_4)_2(\text{OH})_6$ in the Berkeley pit water. The evaluation was performed by comparing the computed log Q value to the equilibrium constant, log K for these two solids. The comparison uses the averages of log Q (based on measured Eh) from all temperatures versus log K(T) calculated from the NBS database. The numerical values are listed in Table XI where the weight column represents the number of samples at each temperature.

The calculated log Q values for Goethite, Ferrihydrite, and K-Jarosite were computed based on their chemical formulas shown for the equilibrium reactions in Table X. In addition, using the measured Eh and Eh values from the $\text{Fe}^{2+}/\text{Fe}^{3+}$ redox couple shown in Table IX, results were calculated which are presented in columns 3 and 10 of Table XI:

Table XI: Saturation Indices for Goethite, Ferrihydrite, and K-Jarosite

Temp	Weight	FeOOH/Fe(OH)3			Fe(OH)3		K-Jarosite		
		Log Q	Log K	SI	Log K	SI	Log Q	Log K	SI
2	3	-3.2789	-1.2061	2.0728	-4.6506	-1.3717	5.4287	7.3570	1.9284
3	5	-3.0981	-1.1744	1.9237	-4.5934	-1.4953	7.4571	7.4492	-0.0078
4	41	-3.0068	-1.1429	1.8638	-4.5365	-1.5297	6.0980	7.5409	1.4429
5	19	-2.6307	-1.1117	1.5189	-4.4801	-1.8494	6.8239	7.6319	0.8080
6	48	-2.9164	-1.0808	1.8355	-4.4240	-1.5076	6.4017	7.7225	1.3208
7	45	-2.9265	-1.0502	1.8763	-4.3683	-1.4418	6.2739	7.8124	1.5385
8	17	-3.0702	-1.0199	2.0503	-4.3131	-1.2428	6.0934	7.9018	1.8085
9	11	-2.3573	-0.9898	1.3675	-4.2582	-1.9008	7.9416	7.9907	0.0491
10	8	-2.2093	-0.9600	1.2493	-4.2037	-1.9943	8.5538	8.0791	-0.4747
11	1	-2.8500	-0.9305	1.9195	-4.1496	-1.2996	6.5735	8.1669	1.5934
12	10	-3.5499	-0.9012	2.6487	-4.0959	-0.5459	5.0285	8.2542	3.2256
13	8	-3.3453	-0.8722	2.4731	-4.0425	-0.6972	5.6114	8.3410	2.7296
14	9	-3.1708	-0.8435	2.3274	-3.9896	-0.8187	6.6832	8.4272	1.7440
		Same both solids	Over Saturated		Under Saturated		Over Sat (ave SI/Fe = 0.4540)		

Based on the Saturation indices in Table XI, it can be concluded that the Berkeley pit water is over-saturated with Goethite. However, due to chemical kinetics, precipitation may not occur right away. The pit water is also under-saturated with Ferrihydrite, but is slightly over saturated with K-Jarosite which may be precipitating.

3.3. Regression Analysis for Thermodynamic data of Schwertmannite and other Fe-SO₄ solids

3.3.1. Regression analysis for thermodynamic data from Free Energy versus T.

Thermodynamic data can be regression analyzed from a set of free energy values versus Temperature. The free energy $G_{(T)}$ of the solid is obtained from the reaction quotient $\log Q$ which is assumed to be equal to $\log K$.

Depending on what type of energy quantity is used, the regression formula may vary. This study uses Free Energy, G , of the solid to estimate the thermodynamic data, G_{rm} , S_{rm} , and C_p coefficients (a, b, and c). H_{rm} is calculated indirectly using from G_{rm} and S_{rm} using Equation 3.

3.3.2. Regression formula

$G_{(T)}$ as a function of Temperature can be derived from the following procedure.

First, recall Equation 5 to calculate enthalpy and entropy which was given in Section 3.1.3.2.2, and is shown again below for convenience.

$$H_T = H_{rm} + a \times (T - T_{rm}) + b \times 10^{-3} \frac{(T^2 - T_{rm}^2)}{2} - c \times 10^5 \left(\frac{1}{T} - \frac{1}{T_{rm}} \right)$$

$$S_T = S_{rm} + a \times \ln \left(\frac{T}{T_{rm}} \right) + b \times 10^{-3} (T - T_{rm}) - \frac{c \times 10^5}{2} \left(\frac{1}{T^2} - \frac{1}{T_{rm}^2} \right)$$

Also recall Equation 3 used to calculate free energy.

$$G_T = H_T - T \times S_T, \quad \text{and } G_{rm} = H_{rm} - T_{rm} \times S_{rm}$$

By combining Equations 3 and 5, a new Equation 15 results.

Equation 15: Combined Regression Equation for Free Energy

$$\begin{aligned} G_T = G_{rm} + S_{rm}[-(T - T_{rm})] + a \times \left[(T - T_{rm}) - T \ln \left(\frac{T}{T_{rm}} \right) \right] + b \\ \times 10^{-3} \left[\frac{(T^2 - T_{rm}^2)}{2} - T(T - T_{rm}) \right] + c \\ \times 10^5 \left[- \left(\frac{1}{T} - \frac{1}{T_{rm}} \right) + \frac{T}{2} \left(\frac{1}{T^2} - \frac{1}{T_{rm}^2} \right) \right] \end{aligned}$$

If symbols are used to represent the Temperature variables, a multiple linear regression model and regression coefficients can be represented in Equations 16 and 17.

Equation 16: General Multiple Linear Regression Model

$$G_T = G_{rm} + S_{rm}X_S + aX_a + bX_b + cX_c.$$

Equation 17: Regression Coefficients for Multiple Linear Regression Model

Where,	G_{rm} = intercept
	$X_s = -(T - T_{rm})$ is for the Coefficient of S_{rm} ,
	$X_a = (T - T_{rm}) - T \ln\left(\frac{T}{T_{rm}}\right)$ is for the Coefficient of a,
	$X_b = 10^{-3} \left[\frac{(T^2 - T_{rm}^2)}{2} - T(T - T_{rm}) \right]$ is for the Coefficient of b, and
	$X_c = 10^5 \left[-\left(\frac{1}{T} - \frac{1}{T_{rm}}\right) + \frac{T}{2} \left(\frac{1}{T^2} - \frac{1}{T_{rm}^2}\right) \right]$ is for the Coefficient of c.

The variables G_{rm} , S_{rm} , and C_p values a, b and c are the regression coefficients and are explained further in the next section. X_s , X_a , X_b , and X_c are known as the independent regressor variables.

3.3.3. Matrix Notation

For this study, there are 14 temperatures where (n) represents the number of temperatures. There are also 5 coefficients to be estimated, where (p) represents the number of regression coefficients which are (G_{rm} , S_{rm} , a, b, c)

There are 4 Coefficients plus 1 intercept to be estimated. Matrix notation is used for easier presentation.

Y Observation Inputs, n x 1. Each Entry represents the average G from each temperature,

X Independent Regressor Variables, n x p, n rows of Temperature, and p column of coefficients, [1, X_s , X_a , X_b , X_c]. The equation for each entry was presented in Equation 17 of

Section 3.3.2

W Diagonal n x n matrix, each element represents the Frequency (weight) of that temperature. For example for the identity matrix shown, the values for 1 are replaced by the weighting frequencies at each temperature.

Equation 18: General Identity Matrix W used for Weighting Factor

$$\begin{bmatrix} 1 & 0 & 0 \\ 0 & 1 & 0 \\ 0 & 0 & 1 \end{bmatrix}$$

β A 5 x 1 matrix of regression coefficients [G_{rm} , S_{rm} , a, b, c]. Note that X^T refers to matrix transposition and raising to the power⁻¹, refers to matrix inversion. Equation 17 determines the regression coefficients. Equation 19 shows the weighted least squares regression used to determine β .

Equation 19: Matrix Form of Weighted Least Squares Estimation for Regression Coefficients

$$\beta = (X^T W X)^{-1} (X^T W Y),$$

Once the regression is performed, two other variables which quantitatively measure how well the regression model fits the data are given by the regression response and lack of fit.

\hat{Y} Response from Regression = $(X \beta)$,

\hat{e} Lack of fit = $(Y - \hat{Y})$

Excel Syntax: Transpose(M), Minverse(M) and MMULT(M1,M2).

Example for Schwertmannite at 6°C

X: According to the formulas for the regression coefficients given in Equation 15, at 6°C the coefficients are [1, X_s , X_a , X_b , X_c]. The T value is 279.15 K (6°C) and 298.15 (25°C) is T_{rm} .

Using Equation 16, substituting the values for T and T_{rm} give the following results for the regression coefficients which are [1, 19, -0.6187, -0.1805, -0.7274].

Table XV shows a summary of the results in graphical form.

Y: The average observation \bar{G} from 6°C is -1192441.992 cal/mole shown in Table XIII.

W: The Frequency from 6°C is 48 shown in Table XII.

3.3.3.1. Modification of X variables

For a large number of samples and large values of the regressor variables, it is suggested by Himmelblau⁴¹ to move each X variable from the origin (0) to its average (\bar{X}) given in Equation 20:

Equation 20: Regressor Variable Transformation

$$X(\text{Coded}) = (X(\text{nonCoded}) - \bar{X})$$

The reason for moving each variable from the origin to its average value is so that the regression will be shifted closer to where the data lies. Otherwise, too much error is introduced into the model. Once the coefficients are found, the estimated regression intercept from the coded variable (G_{rm}) will have to be converted back to noncoded form shown in Equation 21:

Equation 21: Reconversion of Estimated Regression Intercept to Noncoded Form

$$\text{Noncoded Intercept} = \text{Coded Intercept} - \Sigma(X_i \times \bar{X}_i)$$

For the reader's ease of understanding, Equation 21 can also be explained in a slightly different way as follows:

$$\text{Noncoded intercept} = G_{rm} - \Sigma (S \cdot S_{avg} + a \cdot a_{avg} + b \cdot b_{avg} + c \cdot c_{avg})$$

3.3.4. Thermodynamic data for Schwertmannite, Potassium Hydronium & Potassium Jarosite equilibrated with the Berkeley pit water

Thermodynamic data for Schwertmannite, KH-Jarosite and K-Jarosite will be estimated by assuming the entire set of data from Berkeley pit water is equilibrated (saturated) with these minerals (i.e. $\log K = \log Q$). Although $\log K$ values are available for Jarosite, the chemical formula for Jarosite is a subject of debate, and no $\log K$ data exists for Schwertmannite. This is the reason why thermodynamic estimation is required. After the data are obtained, an Eh-pH diagram will be created to test the validity of the results. Based on visual observation, the regression process will be rerun by selecting better input conditions.

3.3.5. Regression Procedure for Schwertmannite

The following outlines the procedure to produce results for Schwertmannite using all the data available from the speciation calculation.

Step 1: Input values for input matrices for Schwertmannite are: Name of solid and its formula, reaction with master species, stoichiometric coefficients of master species, and Frequency $W(T)$, and average $\log Q(T)$ for each temperature (Table XII).

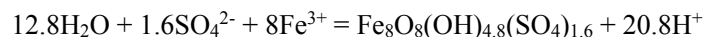
Table XII: Schwertmannite Input Matrix in Excel

Name	Schwertmannite	Formation Reaction													
Formula	$\text{Fe}_8\text{O}_8(\text{OH})_{4.8}(\text{SO}_4)_{1.6}$	$12.8\text{H}_2\text{O} + 1.6\text{SO}_4^{(2-)} + 8\text{Fe}^{(3+)} = \text{Fe}_8\text{O}_8(\text{OH})_{4.8}(\text{SO}_4)_{1.6} + 20.8\text{H}^{(+)}$													
T °C	Log Q from speciation	Weight	<table border="1"> <thead> <tr> <th>Master</th> <th>Stoichiometric</th> </tr> </thead> <tbody> <tr> <td>H⁺ A</td> <td>20.8</td> </tr> <tr> <td>H₂O⁰ L</td> <td>-12.8</td> </tr> <tr> <td>SO₄²⁻ A</td> <td>-1.6</td> </tr> <tr> <td>K⁺ A</td> <td>0</td> </tr> <tr> <td>Fe³⁺ A</td> <td>-8</td> </tr> </tbody> </table>	Master	Stoichiometric	H ⁺ A	20.8	H ₂ O ⁰ L	-12.8	SO ₄ ²⁻ A	-1.6	K ⁺ A	0	Fe ³⁺ A	-8
Master	Stoichiometric														
H ⁺ A	20.8														
H ₂ O ⁰ L	-12.8														
SO ₄ ²⁻ A	-1.6														
K ⁺ A	0														
Fe ³⁺ A	-8														
2	-14.921900	3	A = aqueous, L = liquid												
3	-12.352999	5													
4	-12.999202	41													
5	-10.457849	19													
6	-12.291827	48													
7	-12.525301	46													
8	-13.282105	17													
9	-7.830338	11													
10	-6.415385	8													
11	-11.725282	1													
12	-16.542251	10													
13	-14.770709	8													
14	-12.708048	9													

Step 2: Set up Y matrix for $G_{(T)}$ from log Q values of Schwertmannite (Table XIII).

Step 3: Computation of $G_{(T)}$ from log Q of Schwertmannite (Table XIII).

The formation reaction of Schwertmannite from selected master species is:



Step 4: The next step is to convert log K to dG_{rex} using Equation 1,

$$\text{Log K} = -dG_{\text{rex}}/(\ln(10)RT)$$

Step 5: Once dG_{rex} is calculated, the value is converted to $G_{(\text{Schwertmannite})}$ using free energy of master species with a modified form of equation 2 given by:

$$G_{(T)} = dG_{\text{rex}} - \sum \nu_M \times G_M.$$

The calculated $G_{(T)}$ from Log Q of Schwertmannite, and $G_{(T)}$ of master species calculated from the NBS database is presented in Table XIII.

G and dG at 25°C are calculated for later usage. All values are in kcal/mole.

Table XIII: Calculated G values from Schwertmannite Log Q Values in Excel

Temp	Schwertmannite	H ⁺	H ₂ O	SO ₄ ²⁻	K ⁺	Fe ³⁺
°C	G (cal) from Log Q	G (kcal) from master species				
2	-1190813.982	0	-72.928059	-218.512317	-67.055491	9.187262
3	-1193629.155	0	-72.943396	-218.530218	-67.080144	9.260704
4	-1192389.203	0	-72.958797	-218.547347	-67.104783	9.334263
5	-1195198.929	0	-72.974261	-218.563724	-67.129407	9.407938
6	-1192441.992	0	-72.989787	-218.579371	-67.154018	9.481725
7	-1191718.719	0	-73.005375	-218.594306	-67.178617	9.555621
8	-1190318.900	0	-73.021025	-218.608549	-67.203204	9.629623
9	-1196926.537	0	-73.036738	-218.622119	-67.227780	9.703730
10	-1198352.847	0	-73.052512	-218.635033	-67.252346	9.777938
11	-1191047.511	0	-73.068348	-218.647310	-67.276903	9.852245
12	-1184335.758	0	-73.084245	-218.658968	-67.301451	9.926648
13	-1186205.593	0	-73.100203	-218.670022	-67.325992	10.001145
14	-1188473.255	0	-73.116223	-218.680491	-67.350525	10.075735
25	Y-matrix	0	-73.296415	-218.761350	-67.620114	10.901688
		dG from Master species				
25		0	-56.675000	-177.947000	-67.703000	-1.123000

Step 6: Set up X matrix for regression (Table XIV).

Based on the Non-coded equation, an X matrix is first set up, and the average of each variable is calculated. The final X Coded matrix is set up by subtracting the average values shown on Table XIV(data are truncated) for Schwertmannite. These matrices are exactly the same for all equilibrated solids under study.

Table XIV: Non-coded and Coded Matrix X Values for Schwertmannite

		Non-coded matrix X					Coded Matrix X				
T°C	T K	Int	X _s	X _a	X _b	X _c	int	X _s - \bar{S}	X _a - \bar{a}	X _b - \bar{b}	X _c - \bar{c}
2	275.15	1	23	-0.9109	-0.2645	-1.0814	1	6	0.3918	-0.1130	-0.4717
3	276.15	1	22	-0.8324	-0.2420	-0.9858	1	5	0.3134	-0.0905	-0.3761
4	277.15	1	21	-0.7576	-0.2205	-0.8950	1	4	0.2385	-0.0690	-0.2853
5	278.15	1	20	-0.6863	-0.2000	-0.8089	1	3	0.1673	-0.0485	-0.1992
6	279.15	1	19	-0.6187	-0.1805	-0.7274	1	2	0.0996	-0.0290	-0.1177
7	280.15	1	18	-0.5546	-0.1620	-0.6505	1	1	0.0356	-0.0105	-0.0408
8	281.15	1	17	-0.4941	-0.1445	-0.5782	1	0	0.0249	0.0070	0.0315
9	282.15	1	16	-0.4372	-0.1280	-0.5103	1	-1	0.0818	0.0235	0.0993
10	283.15	1	15	-0.3838	-0.1125	-0.4470	1	-2	0.1352	0.0390	0.1627
11	284.15	1	14	-0.3340	-0.0980	-0.3880	1	-3	0.1851	0.0535	0.2217
12	285.15	1	13	-0.2876	-0.0845	-0.3334	1	-4	0.2314	0.0670	0.2763
13	286.15	1	12	-0.2448	-0.0720	-0.2831	1	-5	0.2742	0.0795	0.3266
14	287.15	1	11	-0.2055	-0.0605	-0.2370	1	-6	0.3136	0.0910	0.3727
			\bar{S}	\bar{a}	\bar{b}	\bar{c}					
	Average		17	-0.5190	-0.1515	-0.6097					

Example Calculation: At a temperature of 2°C, to calculate the coded matrix values for X_s, given the X_s value of 23, and the average S value of 17, $X_s - S_{avg} = 6$ which is shown in column 2 of the Coded Matrix X set of values. This process is repeated for all columns and values to get properly coded matrix values.

Table XV is a summary of the formulas based on enthalpy and entropy functions that were presented earlier for the independent regressor variables (X). The formulas are presented for the X variables and calculated at 6°C.

Table XV: Summary of Formulas for Independent Regressor Variables and Values at 6°C

T °C	T K	T _{rm}
6	279.15	298.15
Variable	Formula	Value
X _s	$= -(T - T_{rm})$	19
X _a	$= (T - T_{rm}) - T \ln\left(\frac{T}{T_{rm}}\right)$	-0.6187
X _b	$= 10^{-3} \left[\frac{(T^2 - T_{rm}^2)}{2} - T(T - T_{rm}) \right]$	-0.1805
X _c	$= 10^5 \left[-\left(\frac{1}{T} - \frac{1}{T_{rm}}\right) + \frac{T}{2} \left(\frac{1}{T^2} - \frac{1}{T_{rm}^2}\right) \right]$	-0.7274

Step 7: Regression for weight data

Although the Microsoft Excel spreadsheet does not perform least squares regression for weighted data, the regression can be done by using the matrix function in Excel for p x 1 matrix given by the following command,

=MMULT(MINVERSE(MMULT(TRANSPOSE(X),MMULT(W,X))),MMULT(TRANSPOSE(X),MMULT(W,Y))).

After converting back to the non-coded matrix form, the dG_{rm} can be calculated and is shown in the second to last column of Table XVI.

Table XVI: Regression Coefficients for Schwertmannite calculated between 2°C & 14°C

Parameter	From Coded Matrix X		To Non-coded Matrix X		Final thermodynamic data	
		G _{rm} (cal)		G _{rm} (kcal)		dG _{rm} kcal
Intercept	-1191268.956		-1296.793372		-1114.933798	
S _{rm}	32046.68359	cal	32046.68359	cal	32046.68359	S _{rm} (cal)
a	-649615328	cal	-649615328	cal	-649615328	a (cal)
b	1536372224	cal	1536372224	cal	1536372224	b (cal)
c	171980496	cal	171980496	cal	171980496	c (cal)

The first group of data comes directly from the regression results from the coded X matrix as a 5x1 column matrix output where the calculated p values are G_{rm}, S_{rm}, a, b, c. The estimated regression coefficients (S_{rm}, a, b, and c) will be the same whether a coded or noncoded matrix is used. The non-coded intercept coefficient (G_{rm}) needs to be changed from the coded intercept by using Equation 21 (shown in section 3.3.3.1) as follows.

Non-Coded intercept = Coded intercept - Σ (estimated X_i) × X_i(Avg)

The average lack of fit (LOF) from the regression is 407 calories (cal) out of the Grand Average for all G values of -1192045 cal. For most of the data that falls within the temperature range of 4°C to 8°C, and which represents a 2/3 majority of the data set, the LOF is only 115 cal.

The estimated individual G has to be converted to dG of formation which is the reverse of going from dG to G as shown at the beginning of this section. At 25°C, the dG_{rex} and $dG_{\text{Schwertmannite}}$ were calculated using the modified form of Equation 2 (described in **Step 5**).

$$dG_{\text{rex}} = G_{\text{(Schwertmannite)}} + \Sigma G_M \times v_M = -95.79459768 \text{ kcal/mole}$$

$$dG_{\text{(Schwertmannite)}} = dG_{\text{rex}} - \Sigma dG_M \times v_M = -1114.933798 \text{ kcal/mole}$$

All calculations are automatically performed including the weighted least squares matrix regression. The final answers will be presented in summary form later.

The listed numbers for 25°C are only to be used mathematically for the properties from 4°C to 8°C. They do not actually represent the real properties at 25°C. In other words, the thermodynamic values at 25°C are theoretical values that have been calculated and put into the NBS database to help model temperatures from 4°C to 8°C because there is no thermodynamic data for Schwertmannite in the NBS database. The β matrix of regression coefficients is shown in Table XVII for Schwertmannite.

Table XVII: Thermodynamic Properties for Schwertmannite

Summary		Lack of fit per Sample (cal)	
Species	Schwertmannite	All samples	407.580
Formula	$\text{Fe}_8\text{O}_8(\text{OH})_{4.8}(\text{SO}_4)_{1.6}$	4-8C 2/3 majority	115.154
dG 25°C kcal	-1114.933798	Grand average Y	-1192045.781
S 25°C	32046.68359		
a	-649615328		
b	1536372224		
c	171980496		

Table XVIII shows the formatted results that will be inserted into the NBS database.

Table XVIII: Regression Output of Schwertmannite for NBS Database

Fe ₈ O ₈ (OH) _{4.8} (SO ₄) _{1.6} S Schwertmannite	-1114.933798	32046.68359		Y	HuangRaj
	-649615328	1536372224	171980496		

3.3.6. Regression Results for Potassium Hydronium—(KH) and Potassium—(K) Jarosite

Using the identical procedure described in section 3.3.5 produced similar values for KH and K Jarosite shown in Table XIX.

Table XIX: Regression Output for KH Jarosite and K-Jarosite

Summary		Lack of fit per Sample (cal)			
Species	KH-Jarosite	All samples		184.505	
formula	K _{.51} (H ₃ O) _{.49} Fe ₃ (SO ₄) ₂ (OH) ₆	4-8C 2/3 majority		41.370	
dG 25°C kcal	-785.7218698	Grand Average Y		-924058.5785	
S 25°C	5118.473633				
a	-145717088				
b	342660160				
c	39022976				

K _{.51} (H ₃ O) _{.49} Fe ₃ (SO ₄) ₂ (OH) ₆ S	-785.7218698	5118.473633		Y	HuangRaj
	-145717088	342660160	39022976		

Summary		Lack of fit per Sample (cal)			
Species	K-Jarosite	All samples		189.199	
formula	KFe ₃ (SO ₄) ₂ (OH) ₆	4-8C 2/3 majority		45.711	
dG 25°C kcal	-765.0616715	Grand Average Y		-922031.3992	
S 25°C	-1138.888672				
	-46482960				
b	107543872				
c	12836016				

KFe ₃ (SO ₄) ₂ (OH) ₆ S K-Jarosite	-765.0616715	-1138.888672		Y	HuangRaj
	-46482960	107543872	12836016		

3.3.7. Eh-pH diagram to test the results

By inserting the regression results for these three minerals into the NBS database, an Eh-pH diagram was constructed for a temperature of 6°C. The diagram used a mass-balanced model and the average concentrations at 6°C data from the Berkeley Pit. In order to ensure the mass was

great enough to reach the saturation point and beyond, the mass was 1.5 times the average concentration and the elements are listed in Table XXVII.

The Eh-pH diagram at 6°C with all the data points from the Berkeley pit water is shown in Figure 6. The diagram shows the area of Schwertmannite which is colored yellow. Schwertmannite coexisting with either K-Jarosite or KH-Jarosite is colored orange, and K-Jarosite or KH Jarosite either forming individually or as a combination is colored light blue. The black asterisks show the Eh and pH values for the individual data points that were used.

Most of the data points shown in Figure 6 appear to fall within the Jarosite region, but some data also falls into the FeSO_4 region. This means that the assumption of using all the data from the MBMG Berkeley pit water report to estimate the thermodynamic data for Jarosite is not warranted. In addition, some data falls outside the Schwertmannite region where the pH is less than 2.4. It is, therefore, necessary to reestimate the thermodynamic data for Schwertmannite without including the data whose pH is less than 2.4. If those pH values were included, then the associated Eh and log Q values would change the input quantities for the matrix calculation and give dG values which would be inaccurate for Schwertmannite.

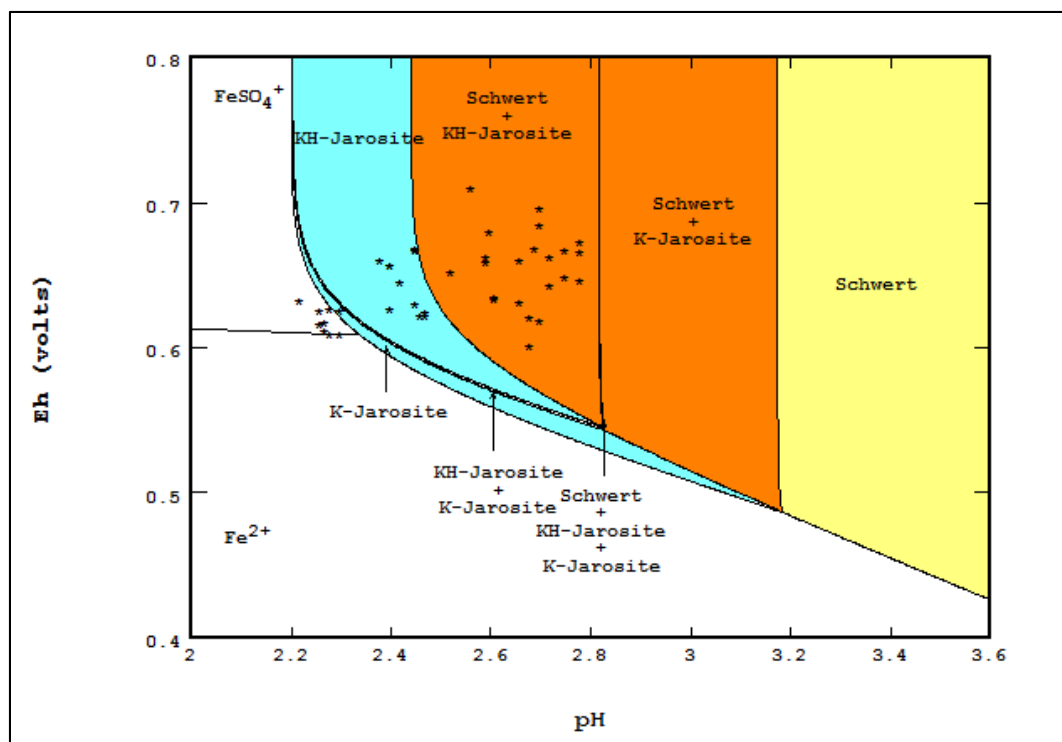


Figure 6: Stabal Eh-pH Diagram for KH-Jarosite, Schwertmannite, K-Jarosite at 6°C

3.3.8. Reestimation of thermodynamic data for Schwertmannite at pH > 2.4

The re-estimated results for Schwertmannite above pH 2.4 are shown in Table XX:

Table XX: Reestimate of Schwertmannite for pH greater than 2.4

Summary Species			Lack of fit per Sample (cal)	
Formula	$\text{Fe}_8\text{O}_8(\text{OH})_{4.8}(\text{SO}_4)_{1.6}$	$\text{Fe}_8\text{O}_8(\text{OH})_{4.8}(\text{SO}_4)_{1.6}$		
dG 25°C				
kcal	-978.5319238	-978.5319238	All samples	262.449
S 25°C	-6049.432617	-6049.432617	4-8C 2/3 majority	120.047
a	161273488	161273488	Grand Average Y	-1189968.374
b	-378690560	-378690560	Lack of fit per Sample (cal)	
c	-43316576	-43316576	All samples	262.449
	$\text{Fe}_8\text{O}_8(\text{OH})_{4.8}(\text{SO}_4)_{1.6}$	$\text{Fe}_8\text{O}_8(\text{OH})_{4.8}(\text{SO}_4)_{1.6}$	4-8C 2/3 majority	120.047
	-978.5319238	-978.5319238	Grand Average Y	-1189968.374

3.4. Using Estimated Thermodynamic Data

The various forms of Energy from Schwertmannite $\text{Fe}_8\text{O}_8(\text{OH})_{4.8}(\text{SO}_4)_{1.6}$ are used for illustration and the results are listed. As mentioned before, the calculated data represent the best fit model for the Berkeley pit water between 4°C and 8°C which represent $2/3$ of the data. The listed numbers for 25°C are only to be used mathematically to determine the corresponding thermodynamic values for Energy within the temperature range of 4°C to 8°C from which actual data was collected. The next section presents the results.

3.4.1. Energies vs. temperature for Schwertmannite— $\text{Fe}_8\text{O}_8(\text{OH})_{4.8}(\text{SO}_4)_{1.6}$

3.4.1.1. Various forms of Energy for Schwertmannite as a function of Temperature

Table XXI shows various enthalpy, entropy, and energy values for Schwertmannite from 4°C to 8°C predicted by the multiple linear regression model. As explained in section 3.3.1, the H_{rm} value was computed using G_{rm} and S_{rm} values at a temperature of 298.15K and substitution into Equation 3.

Table XXI: Energy values for Schwertmannite from 4°C to 8°C

Temp (C)	Temp (K)	dH(kcal)	dS(cal)	dG(kcal)	H(kcal)	S(cal)	G(kcal)
4	277.15	-1328.421	-1100.712	-1023.358	-1331.372	-501.017	-1192.515
5	278.15	-1388.655	-1317.683	-1022.141	-1391.466	-717.481	-1191.898
6	279.15	-1424.999	-1448.137	-1020.752	-1427.669	-847.431	-1191.109
7	280.15	-1441.765	-1508.108	-1019.269	-1444.295	-906.899	-1190.227
8	281.15	-1443.202	-1513.241	-1017.754	-1445.591	-911.531	-1189.314
25	298.15	-2964.030	-6659.393	-978.532	-2964.030	-6049.433	-1160.391

3.4.1.2. Free Energy of Reaction, Equilibrium Constant and Enthalpy of Reaction from Fe^{3+} and from Fe^{2+} and master species

The following reactions to form Schwertmannite are mentioned again as a convenience for ferric ion Fe^{3+} and ferrous ion Fe^{2+} .

The reaction to form Schwertmannite from Fe^{3+} is written,



The reaction to form Schwertmannite from Fe^{2+} and an e^- is written,



Table XXII shows a comparison of G_{rex} , $\log K$ and dH_{rex} values calculated between 4°C and 8°C for Schwertmannite using the reactions for ferric ion [1] and ferrous ion [2] shown above.

Table XXII: Calculation of G_{rex} , $\log K$ and dH_{rex} for Schwertmannite from Fe^{3+} and Fe^{2+} between 4°C and 8°C

Temp (C)	Temp (K)	From Fe^{3+}			From Fe^{2+} and e^-			
		G_{rex} (kcal)	$\log K$	dH_{rex}	G_{rex} (kcal)	$\log K$	dH_{rex}	Eh(volts)
4	277.15	16.359	-12.900	-21.446	153.737	-121.228	56.927	0.833
5	278.15	16.611	-13.051	-81.181	154.202	-121.158	-2.850	0.836
6	279.15	17.033	-13.335	-117.039	154.837	-121.221	-38.749	0.839
7	280.15	17.548	-13.689	-133.331	155.565	-121.357	-55.083	0.843
8	281.15	18.092	-14.064	-134.307	156.323	-121.514	-56.101	0.847
25	298.15	40.607	-29.765	-1649.002	182.487	-133.764	-1571.461	0.989

3.4.2. Energy vs Temperature for KH-Jarosite— $\text{K}_{.51}(\text{H}_3\text{O})_{.49}\text{Fe}_3(\text{SO}_4)_2(\text{OH})_6$

3.4.2.1. Various forms of Energy for KH-Jarosite as a function of Temperature

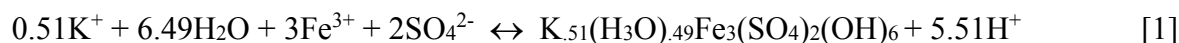
Table XXIII shows the various enthalpy, entropy, and energy values for KH-Jarosite calculated from the regression model.

Table XXIII: Energy Values for KH-Jarosite from 4°C to 8°C

Temp (C)	Temp (K)	dH (kcal)	dS (cal)	dG (kcal)	H (kcal)	S (cal)	G (kcal)
4	277.15	-933.788	-550.740	-781.150	-936.076	-44.243	-923.814
5	278.15	-875.889	-342.156	-780.718	-878.069	164.734	-923.889
6	279.15	-860.585	-287.196	-780.415	-862.656	220.085	-924.093
7	280.15	-875.440	-340.290	-780.108	-877.402	167.380	-924.294
8	281.15	-908.195	-456.988	-779.713	-910.048	51.071	-924.406

3.4.2.2. Free Energy, Equilibrium Constant and Enthalpy of Reaction from Fe^{3+} and from Fe^{2+} and other master species

The following reactions are shown for ferric ion Fe^{3+} and ferrous ion Fe^{2+} for KH-Jarosite. The reaction to form KH-Jarosite from Fe^{3+} is written as follows.



The reaction to form KH-Jarosite from Fe^{2+} and an e^- is written,

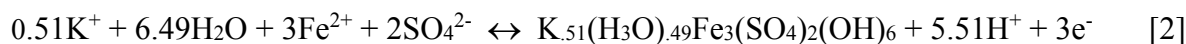


Table XXIV shows a comparison of G_{rex} , $\log K$ and dH_{rex} values calculated between 4°C and 8°C for KH-Jarosite using the reactions for ferric ion [1] and ferrous ion [2] shown above.

Table XXIV: Calculation of G_{rex} , $\log K$, dH_{rex} for KH-Jarosite for Fe^{3+} and Fe^{2+} between 4°C to 8°C

Temp (C)	Temp (K)	From Fe^{3+}			From Fe^{2+} and e^-			
		G_{rex} (kcal)	$\log K$	dH_{rex}	G_{rex} (kcal)	$\log K$	dH_{rex}	Eh(volts)
4	277.15	-6.997	5.517	1.427	44.520	-35.106	30.817	0.6435
5	278.15	-7.147	5.615	59.830	44.450	-34.925	89.204	0.6425
6	279.15	-7.427	5.815	75.626	44.250	-34.643	104.985	0.6396
7	280.15	-7.706	6.011	61.252	44.051	-34.364	90.595	0.6367
8	281.15	-7.898	6.139	28.967	43.938	-34.155	58.294	0.6351

3.4.3. Energy vs Temperature for K-Jarosite— $\text{KFe}_3(\text{SO}_4)_2(\text{OH})_6$ s

3.4.3.1. Various forms of Energy for K-Jarosite as a function of Temperature

Table XXV shows the various enthalpy, entropy, and energy values for K-Jarosite calculated from the regression model.

Table XXV: Energy Values for K-Jarosite from 4°C to 8°C

Temp (C)	Temp (K)	dH (kcal)	dS (cal)	dG (kcal)	H (kcal)	S (cal)	G (kcal)
4	277.15	-924.372	-496.618	-786.734	-926.591	-17.332	-921.787
5	278.15	-876.429	-323.901	-786.336	-878.543	155.766	-921.869
6	279.15	-865.565	-284.879	-786.041	-867.573	195.167	-922.054
7	280.15	-881.312	-341.165	-785.735	-883.214	139.259	-922.228
8	281.15	-913.350	-455.310	-785.340	-915.147	25.490	-922.313

3.4.3.2. Free Energy, Equilibrium Constant and Enthalpy of Reactions from Fe^{3+} and from Fe^{2+} and other master species

The following reactions are shown for ferric ion Fe^{3+} and ferrous ion Fe^{2+} for K-Jarosite.

The reaction to form K-Jarosite from Fe^{3+} is written,



The reaction to form K-Jarosite from Fe^{2+} and an e^- is written,



Table XXVI shows a comparison of G_{rex} , log K and dH_{rex} values calculated between 4°C and 8°C for K-Jarosite using the reactions for ferric ion [1] and ferrous ion [2] shown above.

Table XXVI: Calculation of G_{rex} , Log K, dH_{rex} for K-Jarosite for Fe^{3+} and Fe^{2+} between 4°C to 8°C

Temp (C)	Temp (K)	From Fe^{3+}			From Fe^{2+} and e^-			
		G_{rex} (kcal)	Log K	dH_{rex}	G_{rex} (kcal)	Log K	dH_{rex}	Eh(volts)
4	277.15	-7.838	6.180	6.795	43.679	-34.443	36.185	0.631
5	278.15	-7.990	6.278	55.249	43.606	-34.262	84.623	0.630
6	279.15	-8.248	6.457	66.612	43.429	-34.000	95.970	0.628
7	280.15	-8.495	6.627	51.353	43.262	-33.748	80.696	0.625
8	281.15	-8.656	6.728	19.791	43.181	-33.566	49.119	0.624

3.4.4. Eh-pH diagrams

The Eh-pH diagrams were constructed in Stabcal for the four temperatures with the highest frequencies (4°C, 6°C, 7°C, 8°C). The diagrams were constructed by using the mass-balanced model which performs equilibria and mass input calculations for the whole system at once. In addition to H(1) and O(2), 13 major components from the Berkeley pit water were included, and are shown in Table XXVII. The masses used were 1.5 times the average for 6°C samples and are listed below.

Table XXVII: Elemental Components used to Construct Eh-pH diagrams in Stabcal

Elements	S	Zn	Fe	Mg	Ca	Al	Mn	Cu	Si	Na	F	Cl	K
mg/L	4115.1	865.64	836.08	715.05	677.11	396.34	335.89	188.68	72.185	111.33	38.51	34.241	14.975

There were a total of 142 aqueous species and 46 solids. With the exception of Schwertmannite and the various Jarosites, all the complex solids as well as Fe oxides including Goethite were excluded. Individual Eh and pH values from each sample taken from each temperature and used to construct the Eh-pH diagram were plotted using the symbol *. The first

diagram labeled Figure 7 shows the region for Schwertmannite in yellow. Schwertmannite coexisting with any of the other Jarosite species is shown in orange. Finally, the region showing Jarosite by itself is shown in light blue. Notice that the region of single phase Schwertmannite diminishes as temperature increases when comparing Figure 7 with Figure 8 which shows the species at 6°C. Figure 9 and Figure 10 illustrate that at 7°C and 8°C, single phase schwertmannite no longer exists as a separate species.

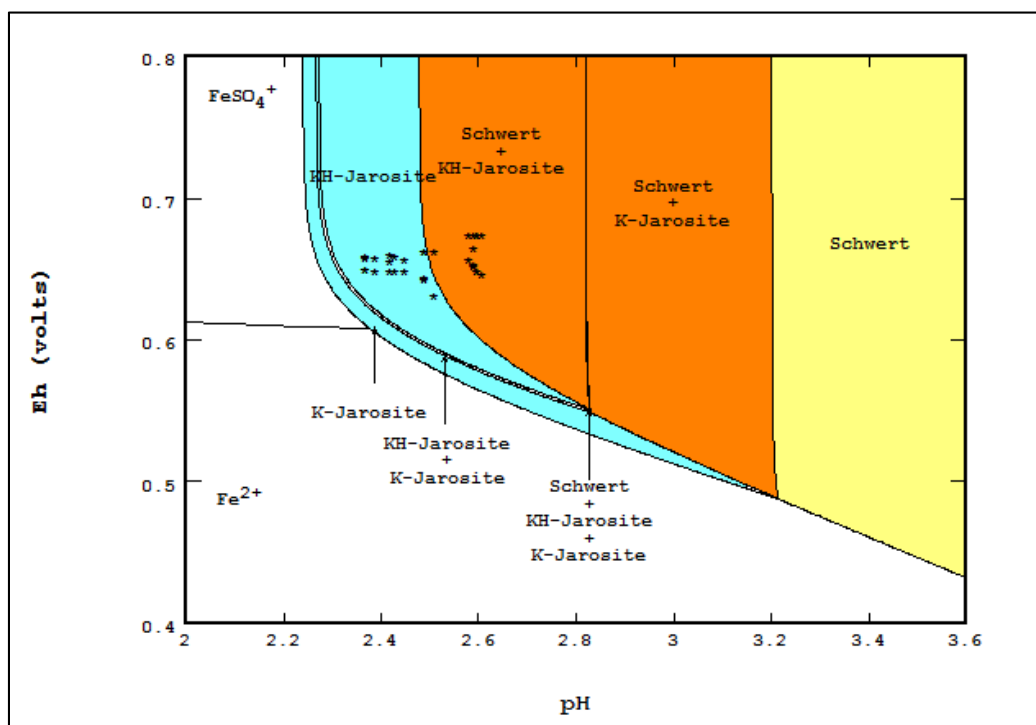


Figure 7: Eh-pH Diagram at 4°C showing Schwertmannite and Various Jarosite Species

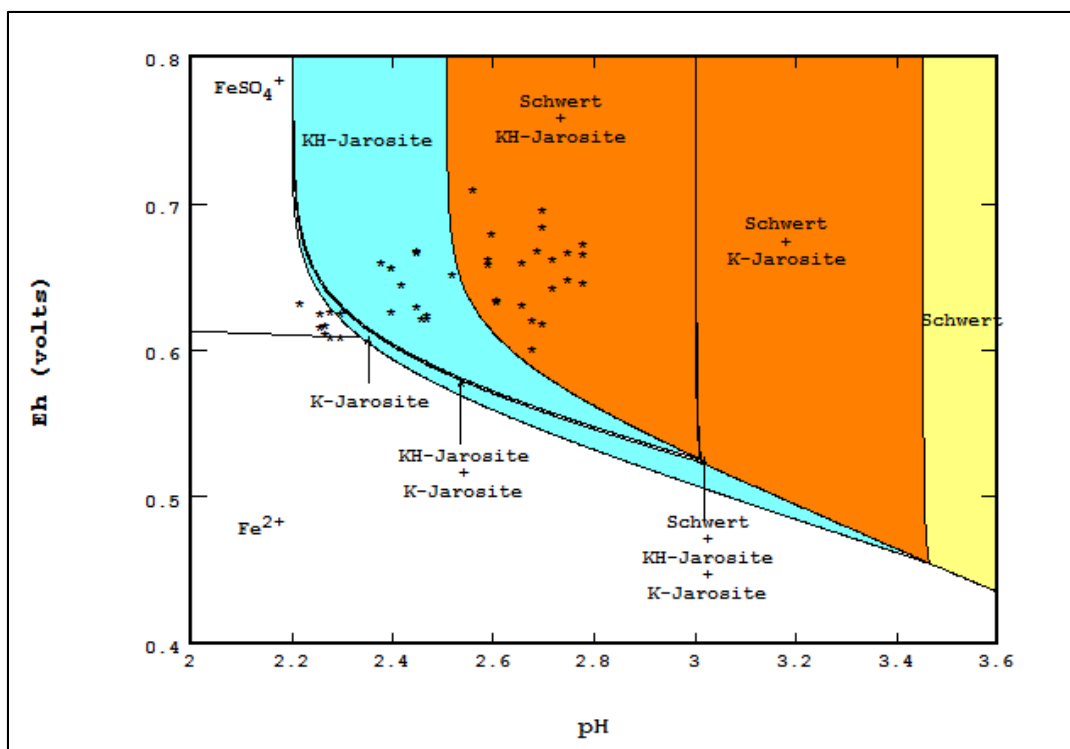


Figure 8: Eh-pH Diagram at 6°C showing Schwertmannite and Various Jarosite Species

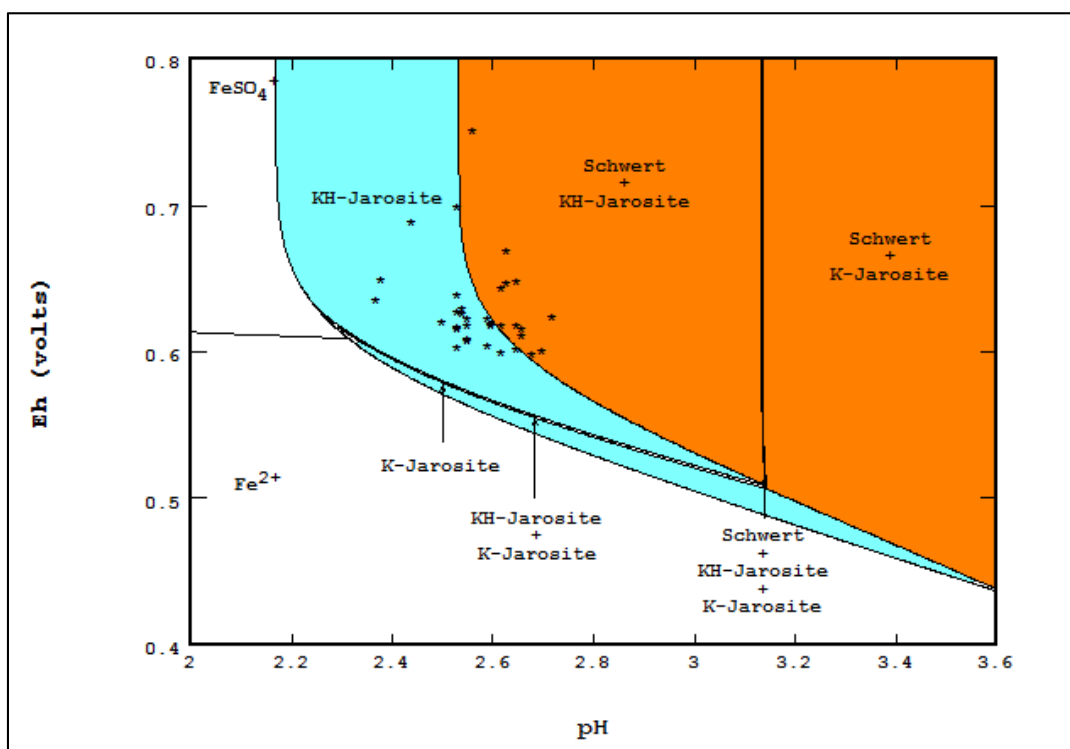


Figure 9: Eh-pH Diagram at 7°C showing Schwertmannite and Various Jarosite Species

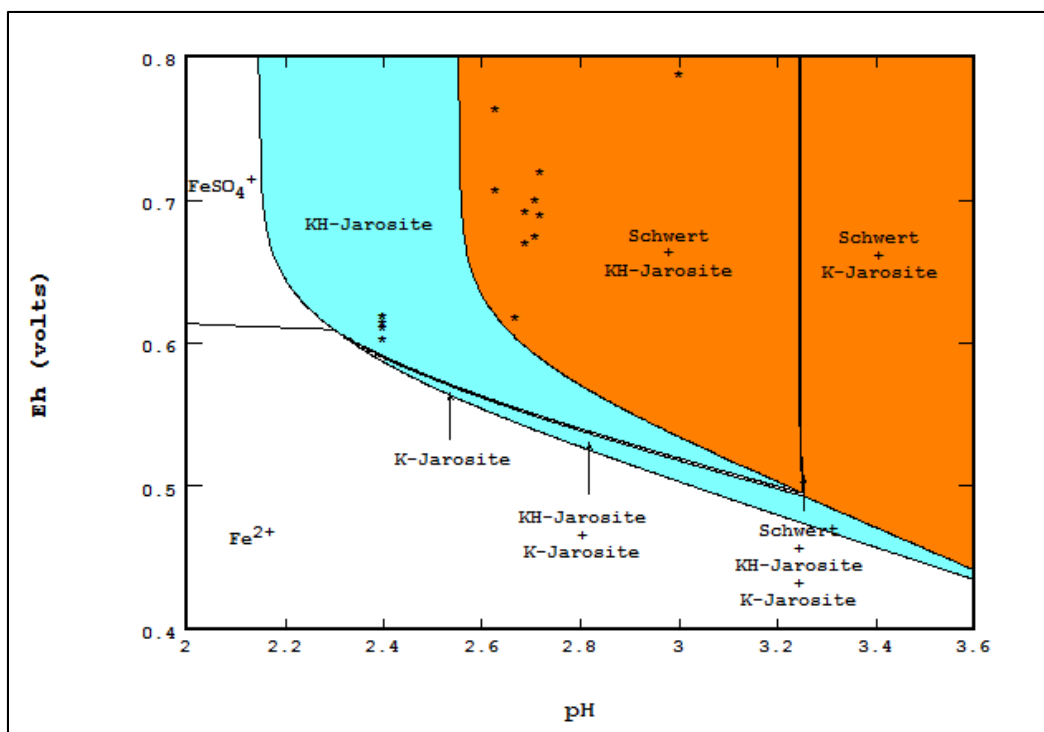


Figure 10: Eh-pH Diagram at 8°C showing Schwertmannite and Various Jarosite Species

3.4.5. Acidity of the Berkeley pit water

The best way to estimate the acidity of acid mine drainage is to laboratory titrate the solution with caustic until pH 8.3 is reached. The Standard Methods for the Examination of Water and Wastewater (Eaton—1995)⁴² gives a calculation method shown in Equation 22.

Equation 22: Standard Equation to Calculate Acidity

$$\text{Acidity, as mg } \frac{\text{CaCO}_3}{\text{L}} = \frac{[(A \times B) - (C \times D)] \times 50,000}{\text{ml sample}}$$

Where:

A = ml NaOH titrant used

B = normality of NaOH

C = ml H₂SO₄ used

D = normality of H₂SO₄

A rough method for calculating the acidity can be simulated based on the titration from an equilibrium calculation. This is performed in the Stabcal program.

As an example, three samples at different dates listed in Table VIII from Part II (Speciation of the Berkeley pit water, and log Q of Investigated Solids) were tested. Table XXVIII shows the important variables, and Table XXIX shows the results of the acidity calculations in section 3.4.5.1.

Table XXVIII: MBMG Sample Data Before, During, and After Cu Cementation Process

Sample ID	Date	Depth (ft)	pH	Temp (C)	ORP (mv)	Remark
98	11/19/1999	200	2.20	4.90	637	Prior to the initial pumping of water at depth to recover Cu (08/98 to 7/00)
195/502	05/04/05	100	2.45	5.56	667	Right after the second time to recover Cu (from 11/ 2003)
291	06/14/12	250	2.58	2.67	679	Before 2012 landslide that damaged boating area

Similar to the equilibrium calculation for log Q of the mineral species, the NBS database was used. The NBS database included 177 aqueous species but excluded all metal-Fe₂O₃ and Metal-FeO compounds. There were also 323 additional species plus newly estimated Schwertmannite, KH and K-Jarosit. Truncated temperatures to zero decimal places were also used.

3.4.5.1. Conditions for titration simulation

One normality NaOH (1N) was used for titrating 1L of water sample. The volume of titrant used was to ensure the pH was greater than 8.3. The titration did not consider oxidation of Fe(2) to Fe(3). The effect of this oxidation reaction would have been to increase the pH due to the presence of additional [H⁺] from reaction [1] shown in section 3.5. The equilibrium results from Sample ID 195 is shown on the following Stabcal screenshots in Figures 11 & 12.

Work Speciation

File/copy Clear View/Edit species Import species, dG, conc Save then (Calculate Exit to..) Quit w/o Save Help

Number of components: include no H(1) or O(-2). Enter number to change. Change Unit of Conc

System Information		Component Information									
	System data	Elm	Val	Gas	Redox	Unit	Mass or pressure	#Sp	M-AQ	Cmpt	
# Components	27	Ca	2			P	466	4		1	
Temperature oC	6	Mg	2			P	471	5		2	
System pH	2.45	Na	1			P	78.3	10		3	
System Eh	0.667	K	1			P	10.57	4		4	
Disslvd. O2	1.34380E-05	Fe	2			P	499	6		5	
dG(kcal) OH-	-38.638	Mn	2			P	233	7		6	
dG(kcal) H2O	-57.421	Si	4			P	48.1462532953426	33		7	
dG(kcal)O2(a)	3.451	Cl	-1			P	1	25		8	
Dielectric C.	78.38442	S	6			P	3007.41024509273	38	2	9	
O2 (atm)		F	-1			P	17	18		10	
Calc Accuracy	1.0E-8	Al	3			B	230138	57		11	
# Compt-Gas Ext	0	As	5			B	88	9	4	12	
# Compt-gas Totl	0	B	3			B	1	29	2	13	
delta Eh(V)	0.2	Cd	2			B	1676	30		14	
dG data source	P	Co	2			B	1105	21		15	
Adsorbent		Cu	2			B	67712	25		16	
Surface Area		Li	1			B	321	23		17	
Const I. Strngth?	N	Ni	2			B	1189	24		18	
Activity Model	1	Sr	2			B	1551	14		19	
		U	6			B	563	23		20	
		Zn	2			B	527315	28		21	
		Ce	3			B	1	8		22	
		La	3			B	1	6		23	
		Nd	3			B	1	5		24	
		Pr	3			B	1	7		25	
		Th	4			B	1	21		26	
		Fe	3		S	P		21		27	

If possible, Delete most of Solids that will not form, or Omit components having extremely small Masses Total # Species 501

k:\ra\acidity\195allsolids Win-STABCAL 2013 Brief Information

Figure 11: Stabcal Initial Titration Screen for ID#195

Read n-Redox Titr (January-15)

Tabulated Results-Current Stage View (Species Solids Orig. solutions) Branch solution Exit To or Quit Help

Stage1: solution before titr/mix: To change stage #: a. Use scroll bar, or b. <pg keys>, or Enter the stage # directly W32-STABCAL

Total Stages: 51 Current stage 39 Enter stage 39 OK

System Information		Component Information					
	System data	Elm	Val	Un-dissolved m/L	Aqueous Moles/L	Gas log10(atm)	
# Components	27	Ca	2	6.537292E-3	4.268234E-3		
Temperature oC	6	Mg	2	3.260876E-4	0.0176787		
pH of System	8.2529354095459	Na	1		0.07379727		
Original Eh(V)	0.667	K	1		2.512255E-4		
Eh (not calculated)		Fe	2	2.495508E-3	6.653732E-8		
Stage Number	39	Mn	2		3.941584E-3		
Calc Accuracy	1.0E-8	Si	4	1.593157E-3	6.155234E-9		
# Gas Compts.	0	Cl	-1		2.621409E-5		
Name of Titrant	NaOH 0 A	S	6	6.547081E-3	0.08062205		
Max Amnt Titrant	0.1	F	-1	6.521752E-4	1.794347E-4		
Conc if AQ titr	1	Al	3	7.927016E-3	4.854139E-9		
Total # Stage	51	As	5		1.0916E-6		
Total solid g/L	3.00531665154908	B	3	8.580397E-8	1.610708E-10		
Vol sol L/L host	1.076	Cd	2		1.385784E-5		
		Co	2		1.868729E-5		
How titrant add	AQ solution	Cu	2	9.903898E-4	3.353124E-22		
Lits added/L host	0.076	Li	1		4.299281E-5		
Mols added/L host	0.076	Ni	2	4.290198E-8	1.877874E-5		
Grms added/L host	3.03978492	Sr	2	9.788451E-6	6.6627E-6		
Ionic Strength	0.133790607714141	U	6	2.198094E-6	9.170854E-11		
Activity Model	Davies	Zn	2	6.524106E-3	9.72753E-4		
		Ce	3		6.632658E-9		
		La	3		6.690433E-9		
		Nd	3		6.443206E-9		
		Pr	3		6.595613E-9		
		Th	4	4.005241E-9	2.14473E-21		
		Fe	3	5.808446E-3	1.933645E-13		

Click Command Button to change from Current Settings Digits Accuracy (7) Concentration (Mols/L) Redox (Help?)

Filename: k:\ra\acidity\195allsolids

Figure 12: Stabcal Final Titration Screen for ID#195

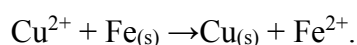
Using Equation 22, the calculated results are as follows. The A & B values are plugged into Equation 22, but C and D values are not used. As an example, the A value (ml of NaOH titrant used from Equation 22) for sample ID 195 is shown in Figure 12. In column 2 next to “Lits added/L host” is the value of 0.076L. Multiplying by 1000 ml/L gives 76 ml of NaOH titrant added which gives A. The B value is 1N NaOH and is consistent for all samples. The results are tabulated in Table XXIX.

Table XXIX: Cu Cementation Acidity Calculation Results for Berkeley Pit

ID Number	Date	A	B	Acidity
98	11/19/1999	1	1	5100
195	05/04/05	7	1	3800
291	06/14/12	7	1	3600

3.4.6. Simulation of water chemistry due to the copper recovery process

The copper recovery cementation process changed the chemistry of the Berkeley pit water drastically, and particularly water at depth (see Figure 13, Duime & Tucci; 2011).⁴³ Montana Resources started pumping water from depth beginning in 8/98 for approximately two years then stopped. Cementation recommenced in January 2002 until February 2013. The total volume of water pumped was approximately 1.3 times greater than the volume of the Berkeley pit (Gammons and Tucci)⁴⁴. As mentioned earlier, the copper cementation process involved pumping the copper rich pit water to “laundries” filled with scrap iron. These “laundries” reduced the copper by the gain of electrons from the scrap iron which precipitated out the native copper and produced ferrous iron according to the Cu cementation reaction which was presented in section 1.2, but is repeated for convenience as,



After the copper had precipitated out, the ferrous iron rich water was returned to the surface of the pit lake as illustrated in Figure 1.

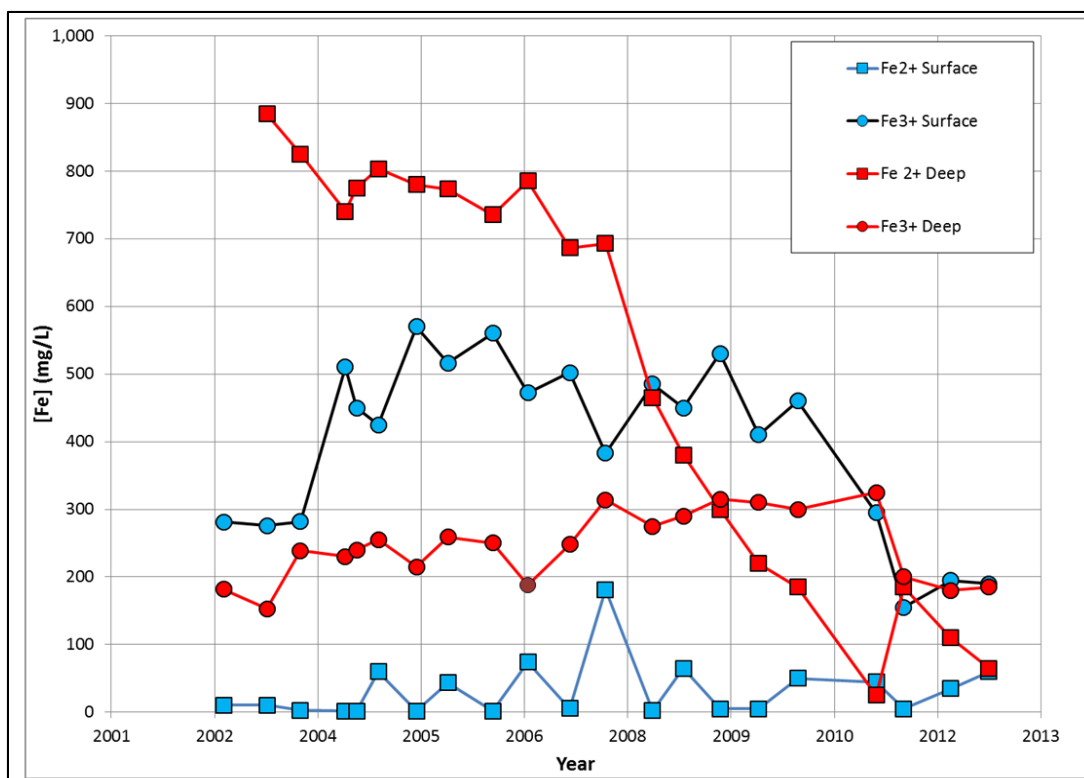


Figure 13: Concentration of Fe²⁺ and Fe³⁺ during Cementation Process 2002-2012 (Duaime & Tucci 2012)

3.5. Analysis of Iron Species Concentration over Time

Taking a look at Figure 13 reveals that the concentration of Fe²⁺ in the deep pit waters decreased from a concentration of approximately 800 mg/L to 200 mg/L, but the concentration of Fe³⁺ remained relatively constant at 200 mg/L. This is an indication that Fe²⁺ was oxidized to Fe³⁺ which then precipitated out as the iron oxy(hydroxysulfate) compounds such as Schwertmannite and Jarosite. Because the Fe³⁺ concentration was relatively constant, it is likely that the ferric ion equilibrated with the solid compounds over time.

This can be seen from the MBMG analytical report excerpt shown in Table XXX. These samples represent the water quality values before, during, and towards the end of the copper cementation process.

Table XXX: Selected Water Quality Info Adapted from MBMG Analytical Report Related to Cu Cementation

ID #	Date	Depth	pH	Temp	ORP	Fe Total	Fe ²⁺	Fe ³⁺
	mm/dd/yy	(Feet)		C	mV	mg/l	mg/l	mg/l
Near the Beginning of Copper Recovery								
492	05/27/04	200	3.01	7.01	472	1062	790	272
498	11/03/04	200	2.65	6.99	602	1046	802	244
504	05/04/05	200	2.40	7.50	620	995	780	215
During the recovery process when concentrations of Fe(2) began to drop								
528	10/27/06	250	2.55	7.26	608	970	750	220
534	05/17/07	300	2.72	7.22	668	938	681	257
Near the End of Copper Recovery								
565	11/16/09	250	2.45	4.10	649	520	220	300
566	11/16/09	500	2.43	4.05	649	510	205	305

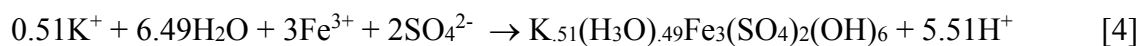
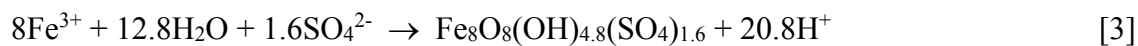
Near the end of the copper cementation process, the Eh potential of the water was higher than at the beginning of copper recovery. The higher Eh potential can be explained by the following oxidation reaction [1].



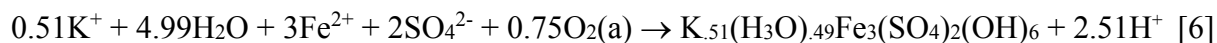
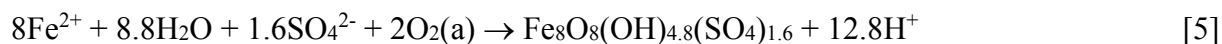
Since the ferrous solution being pumped back into the pit had plenty of time to contact air, the most likely source of oxidant would be the dissolved oxygen according to the following oxidation reaction [2].



Precipitation of iron oxy(hydroxysulfate) compounds from Fe³⁺ ions in solution also produced additional H⁺ ions that decreased the pH value. The following two reactions for Schwertmannite [3] and KH-Jarosite [4] show the molar quantity of excess hydrogen ion produced from ferric iron as follows.



Combining with the oxidation reaction for dissolved oxygen, the net quantity of H⁺ ion produced from the ferrous iron is given by reactions [5] and [6].



3.6. Computer Simulation & Fe²⁺/Fe³⁺ Results

The simulation was performed by using the samples at the beginning of cementation which were (ID #492, 498 and 504 that had reportable Fe²⁺ and Fe³⁺) used to titrate with aqueous O₂ to an Eh potential close to what was reported from the samples at the end of copper cementation, i.e. 649 mV (representing sample ID #565, 566). Equations [3] to [6] represent the oxidation reactions. The assumption was that in addition to using aqueous O₂ as the titrant, no species were added or removed from the system. All 27 components plus zero valence oxygen were included in the simulation calculations and the final temperature was 4°C.

Table XXXI shows the results of the aqueous O₂ titration from the water samples which had measured Fe²⁺ and Fe³⁺ values. It shows good agreement with the average values from the sample near the end of the copper recovery process. The simulated titration indicated that since the ferrous water had more time to contact the air on return to the Berkeley Pit, Fe²⁺ would be readily oxidized to Fe³⁺, and the oxidized Fe³⁺ would then precipitate out the iron oxy(hydroxysulfate) compounds. The precipitated amounts of these compounds are listed for Schwertmannite and KH-Jarosite in Table XXXI.

Table XXXI: Titration Simulation of Samples with Aqueous O₂ for Cu Recovery Process

ID Number	Date	O ₂ Used	Eh End Period	pH End Period	Fe ²⁺	Fe ³⁺	Schwertmannite	KH-Jarosite
		mole/L	V		mg/L	mg/L	mg/L ppt	mg/L ppt
Fe²⁺ & Fe³⁺ Concentrations near the Beginning of Copper Recovery								
492	05/27/04	0.00228	0.6497	2.495	280.68	435.27	557.6	113.00
498	11/03/04	0.0020	0.6500	2.464	355.22	447.57	390.3	81.91
504	05/04/05	0.00192	0.6498	2.458	351.10	507.96	171.9	120.06
Fe²⁺ & Fe³⁺ Concentrations during the recovery process when [Fe²⁺] began to drop								
528	10/27/06	0.00180	0.6496	2.464	347.92	429.68	287.3	99.61
534	05/17/07	0.00168	0.6499	2.482	305.71	401.42	354.1	104.3
Comparison of average concentration of Fe²⁺ & Fe³⁺ near the End of Cu Recovery Process								
258-259,565-566	11/16/09		0.6490	2.440	222.10	265.65		

3.6.1. Titration diagram

Figure 13 indicates that the concentration of Fe²⁺ started to drop almost linearly from 2006 to 2010. Using Sample ID #534 in Table XXXI, the titration response as a function of O₂ addition was plotted on the following diagram labeled Figure 14 which was created in Stabcal. The vertical dashed line indicates when the Eh (0.6496V) is the closest to the Eh of the water near the end of the copper recovery process. As shown in the diagram, concentration of Fe²⁺ dropped almost linearly, and fell below the concentration of Fe³⁺ as shown in Figure 13. The pH line shown in blue also decreased because of excess hydrogen ions generated as a result of reactions [3] and [4] shown in Section 3.5.

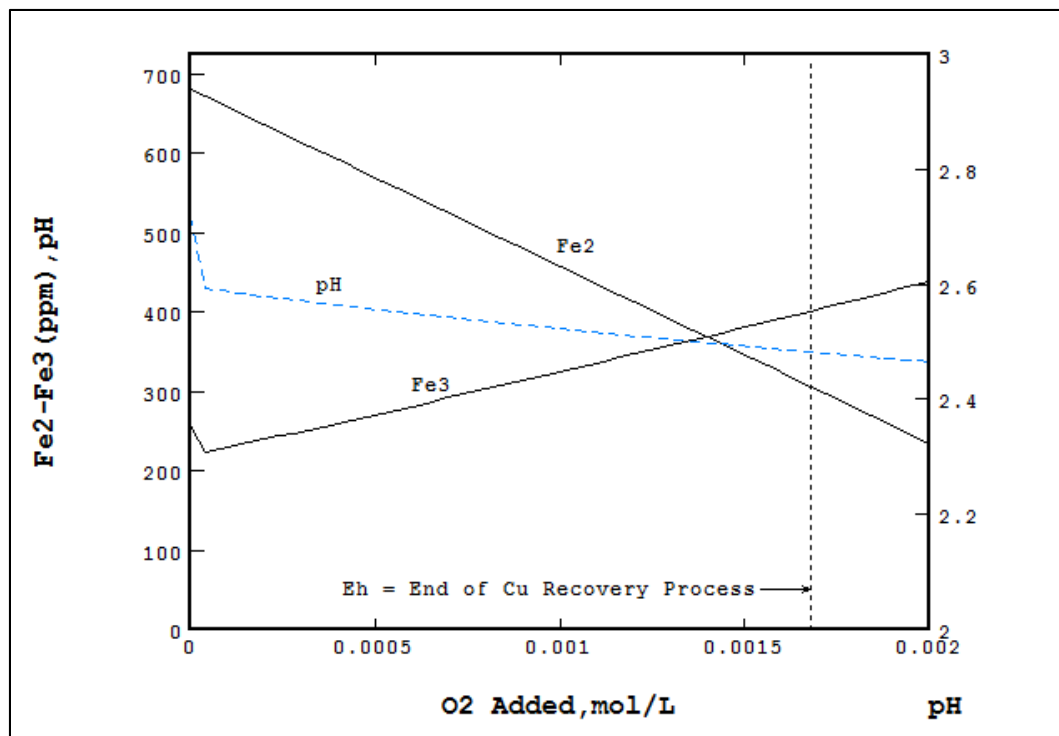


Figure 14: Aqueous Titration Simulation with O₂ for Fe²⁺/Fe³⁺ during Cementation Process

4. Results

4.1. Matlab Output (3D Stem Plot)

Section 4 shows log Q Matlab output versus Eh and pH for Schwertmannite, Potassium Hydronium Jarosite, Potassium Jarosite, Ferrihydrite, and Goethite between 4°C and 8°C. The purpose of the diagrams is to show how log Q varies as a function of Eh and pH. The type of Matlab graph shown in this section is called a 3D stem plot. The 3D stem plot shows each data point marked as a blue diamond for each Eh, pH, and log Q value. The stem represented as a blue line shows the magnitude of the log Q value for a given Eh and pH. For ease of visual interpretation, a continuous response surface was added to illustrate the change in magnitude of the log Q value for each Eh and pH value.

4.1.1. Stem Plot Range of Values & Summary Tables

The temperature range of 4°C to 8°C covered approximately 2/3 of the analyzed records and was deemed to be the most reliable because of the high frequencies of occurrence in this interval. Eh, pH, and Log Q values were graphed. However, Hydronium jarosite was not graphed because it did not form a separate species according to the Eh-pH diagrams from Stabcal shown in section 3.4.4 (figures 7 to 10). Although the Matlab output only covered the temperature range of 4°C to 8°C, a complete summary table for the temperature range of 2°C to 14°C is shown at the end of each section (Tables XXXII to XXXVI). Each table includes the Average Log Q values and basic statistics for each solid iron species that was modeled.

4.2. Log Q Matlab Output for Schwertmannite

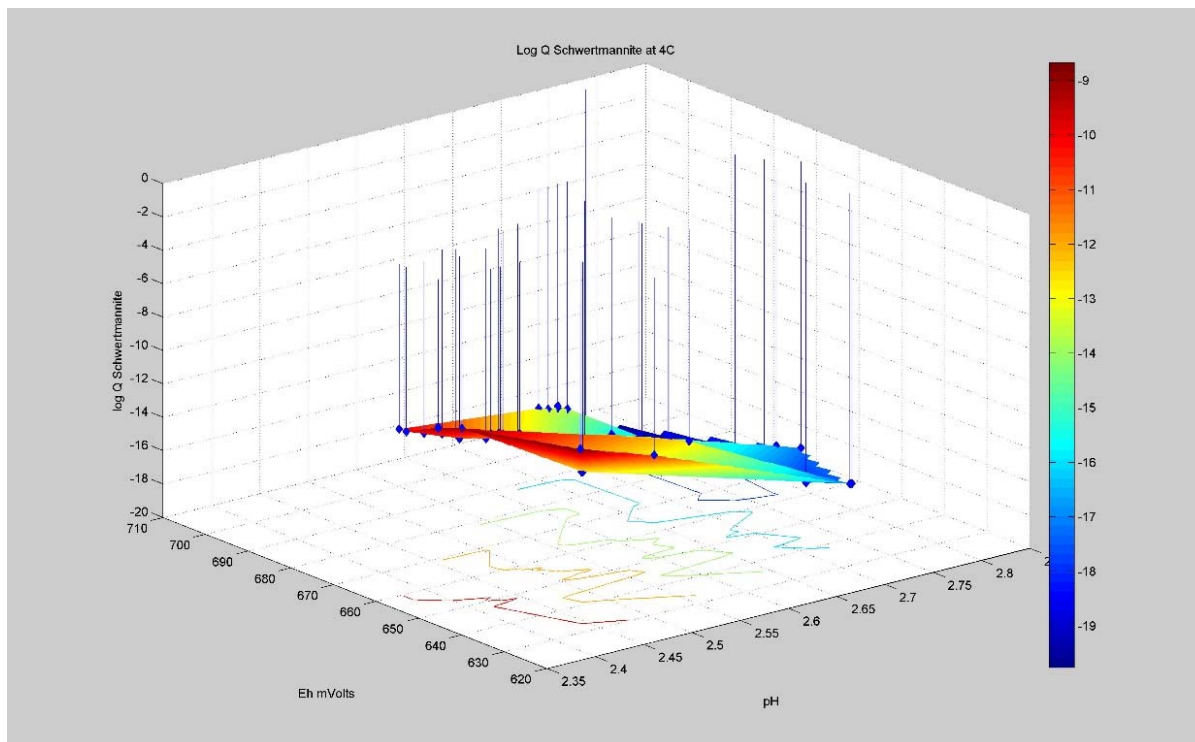


Figure 15: Schwertmannite 4° C Matlab Output

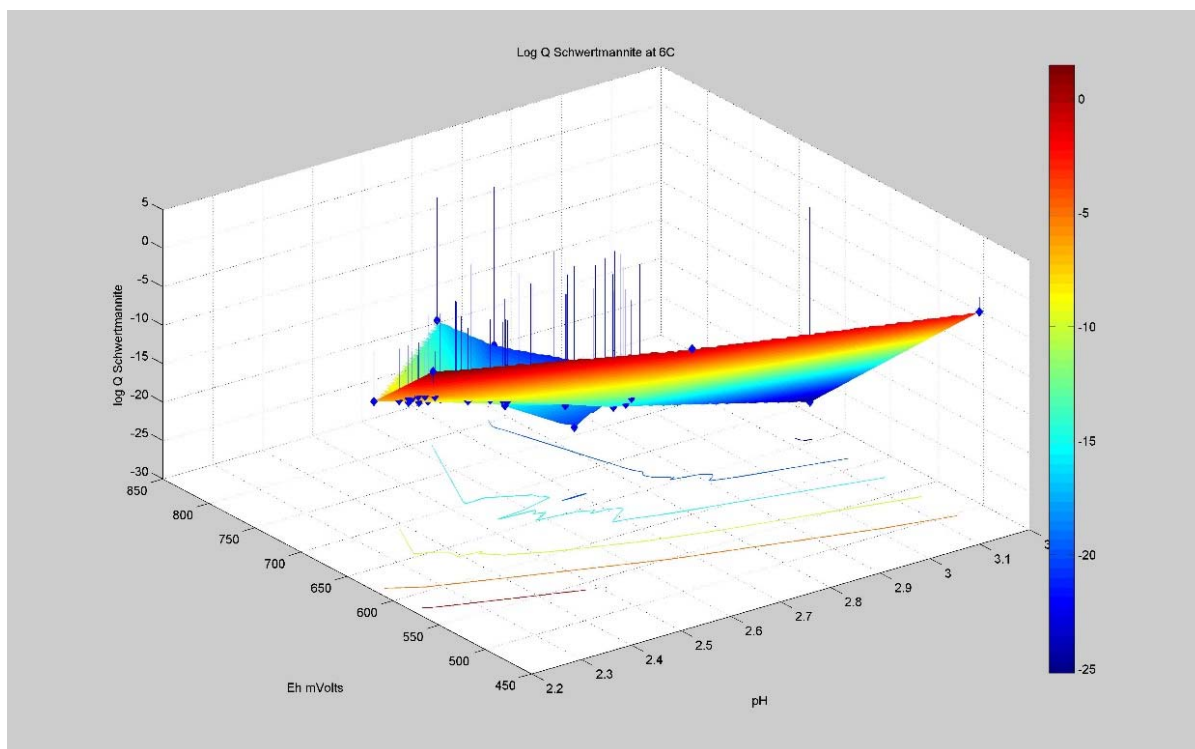


Figure 16: Schwertmannite 6° C Matlab Output

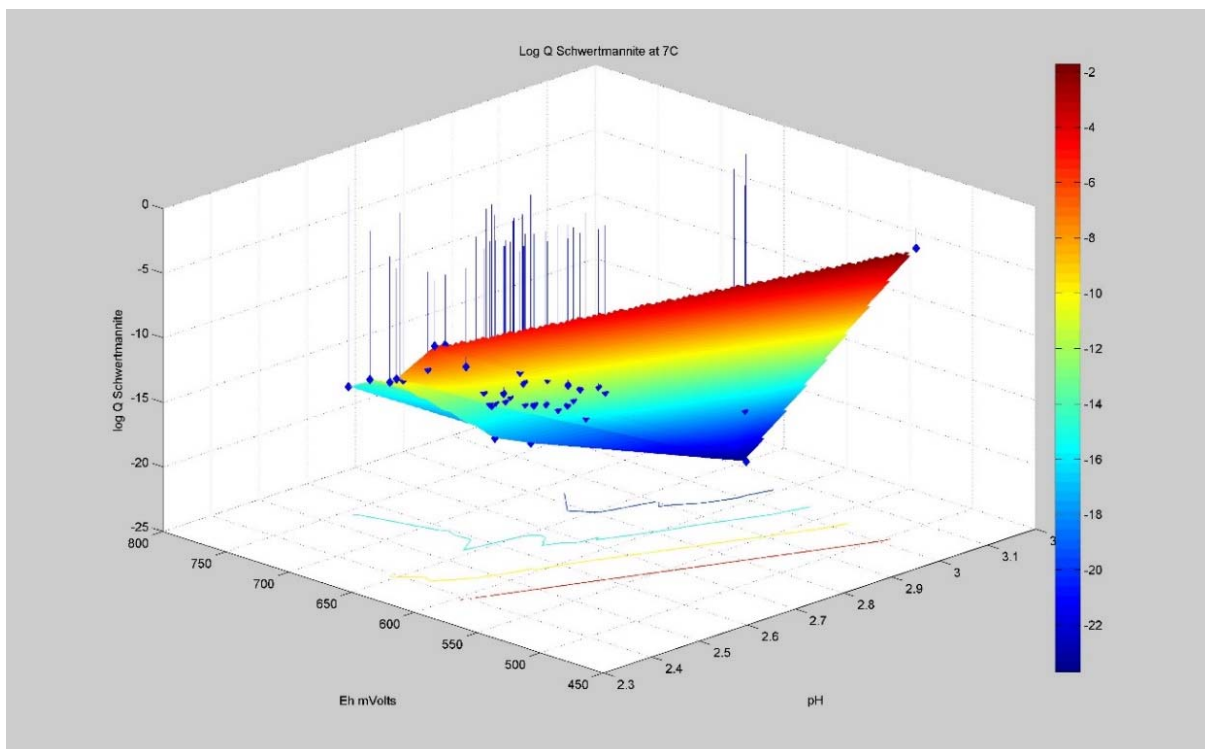


Figure 17: Schwertmannite 7°C Matlab Output

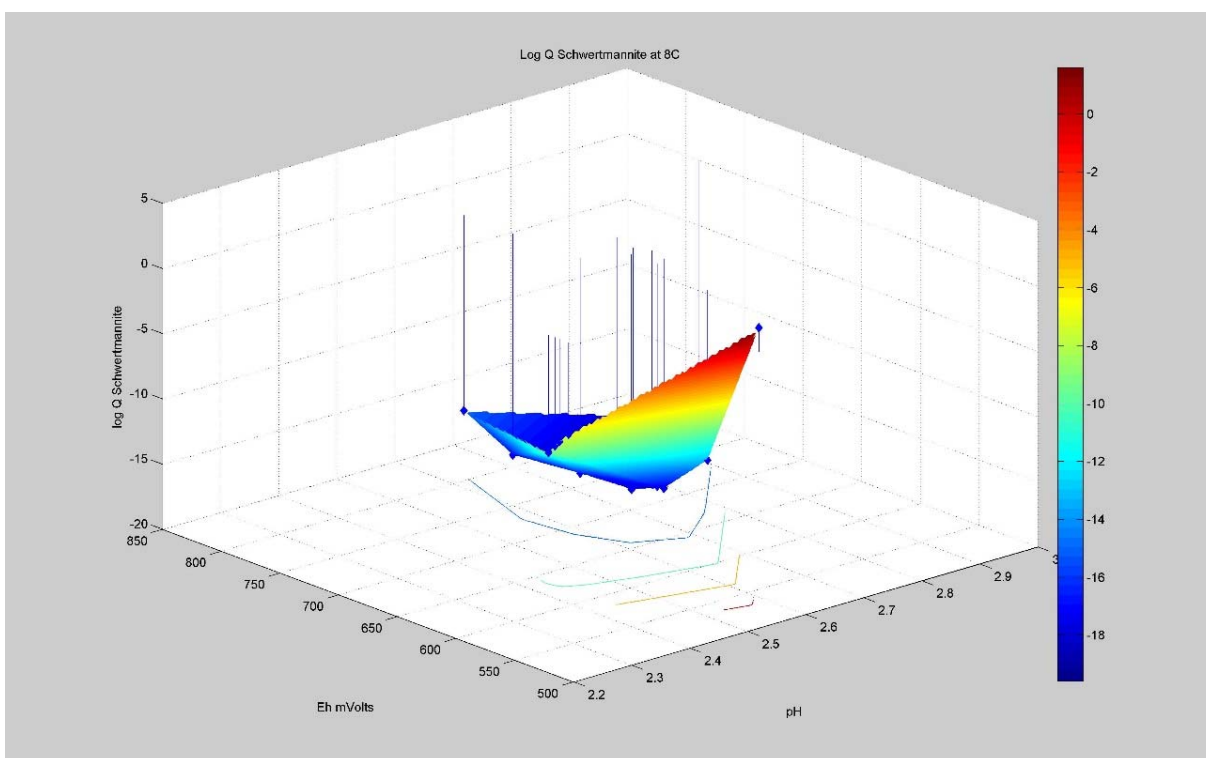


Figure 18: Schwertmannite 8°C Matlab Output

4.2.1. Stabcal Output Summary by Temperature—Schwertmannite

Table XXXII: Avg Log Q for Schwertmannite by Temperature

Summary Table Schwertmannite					
Temp °C	Frequency	Avg. Log Q	Std. Dev	Variance	
2	3	-14.921900	4.524	20.463	
3	5	-12.352999	0.489	0.239	
4	41	-12.999202	3.023	9.140	
5	19	-10.457849	4.169	17.382	
6	48	-12.291827	5.547	30.771	
7	46	-12.525301	3.976	15.812	
8	17	-13.282105	5.802	33.659	
9	11	-7.830338	11.108	123.379	
10	8	-6.415385	19.222	369.478	
11	7	8.619220	10.524	110.750	
12	10	-16.542251	3.902	15.224	
13	8	-14.770709	10.219	104.425	
14	9	-12.708048	14.426	208.098	

4.3. Log Q Matlab Output for Potassium Hydronium Jarosite

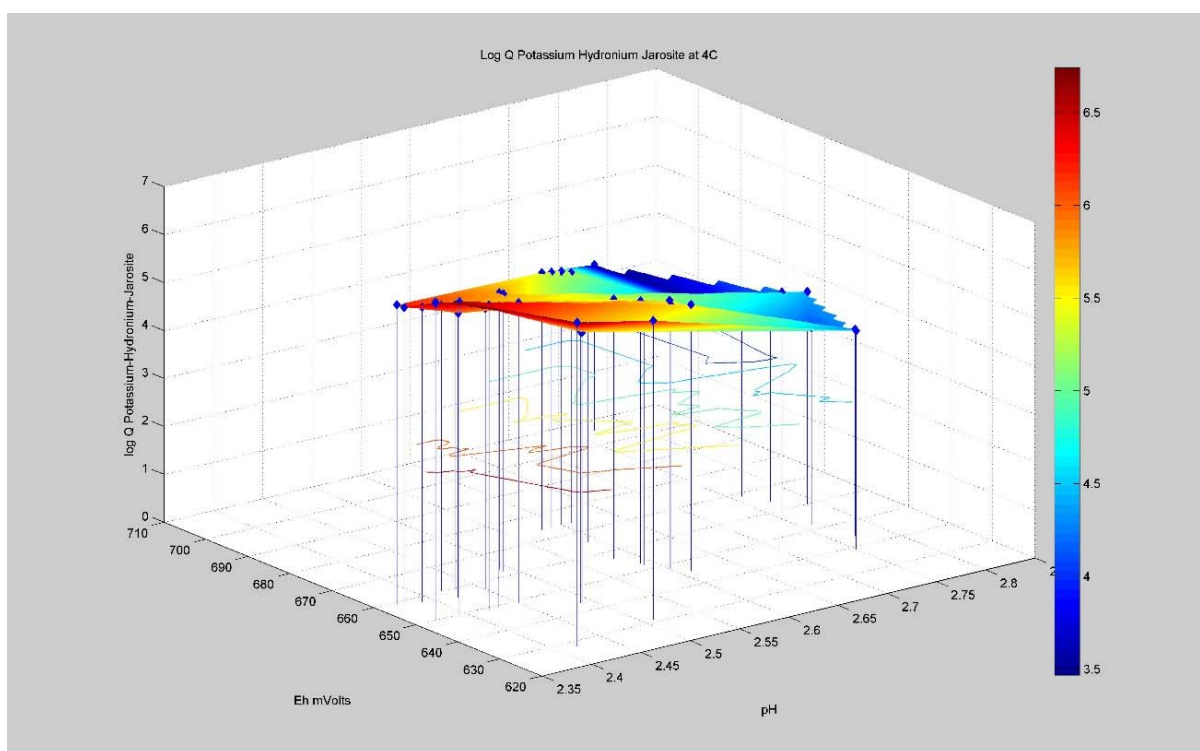


Figure 19: Potassium Hydronium Jarosite 4°C Matlab Output

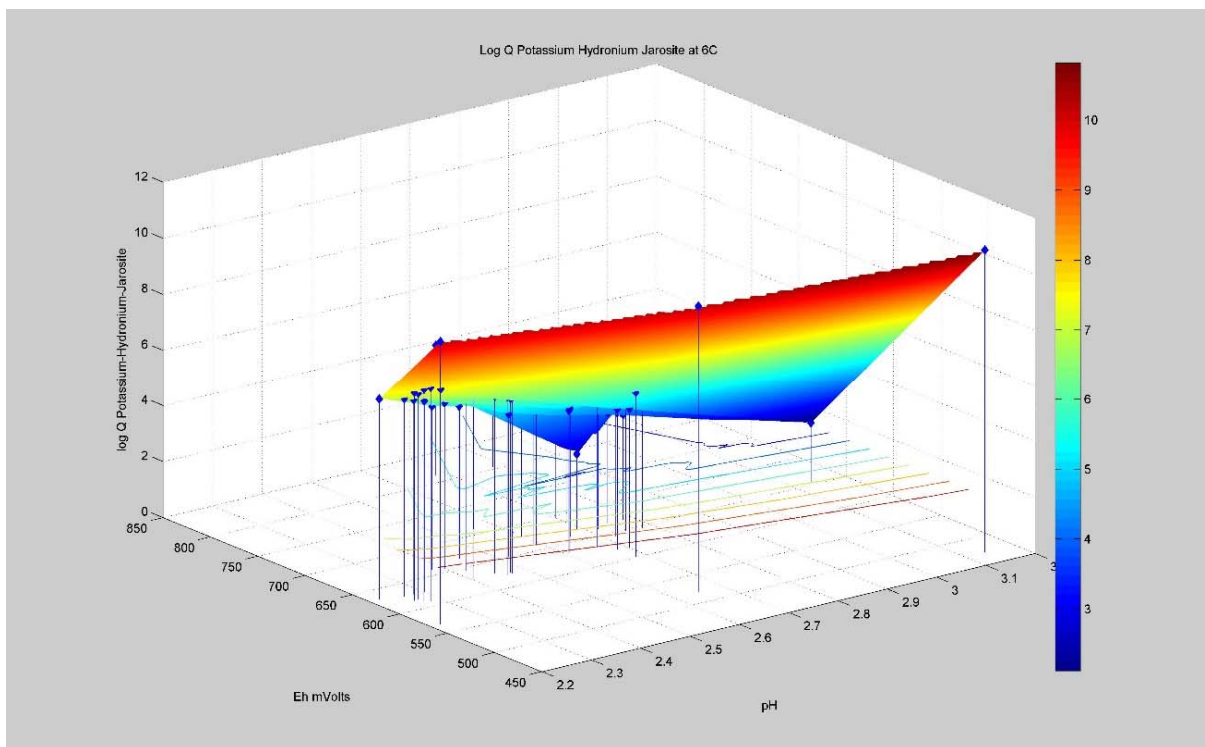


Figure 20: Potassium Hydronium Jarosite 6°C Matlab Output

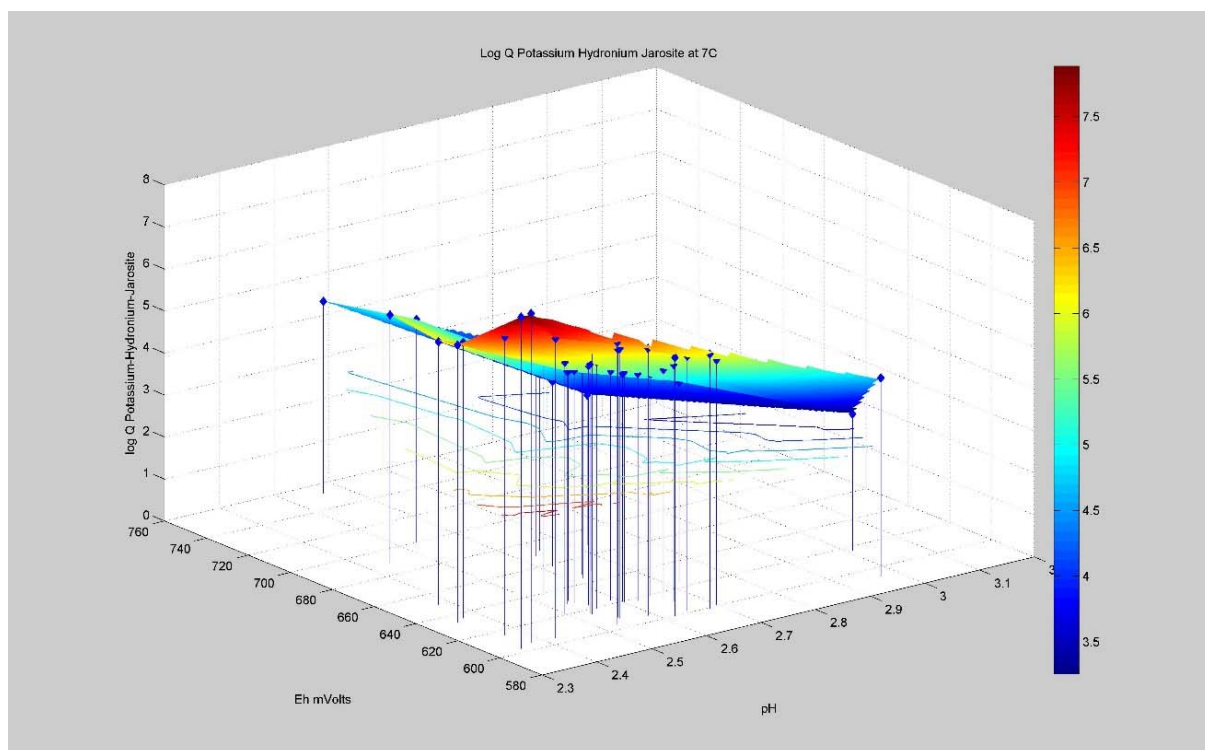


Figure 21: Potassium Hydronium Jarosite 7°C Matlab Output

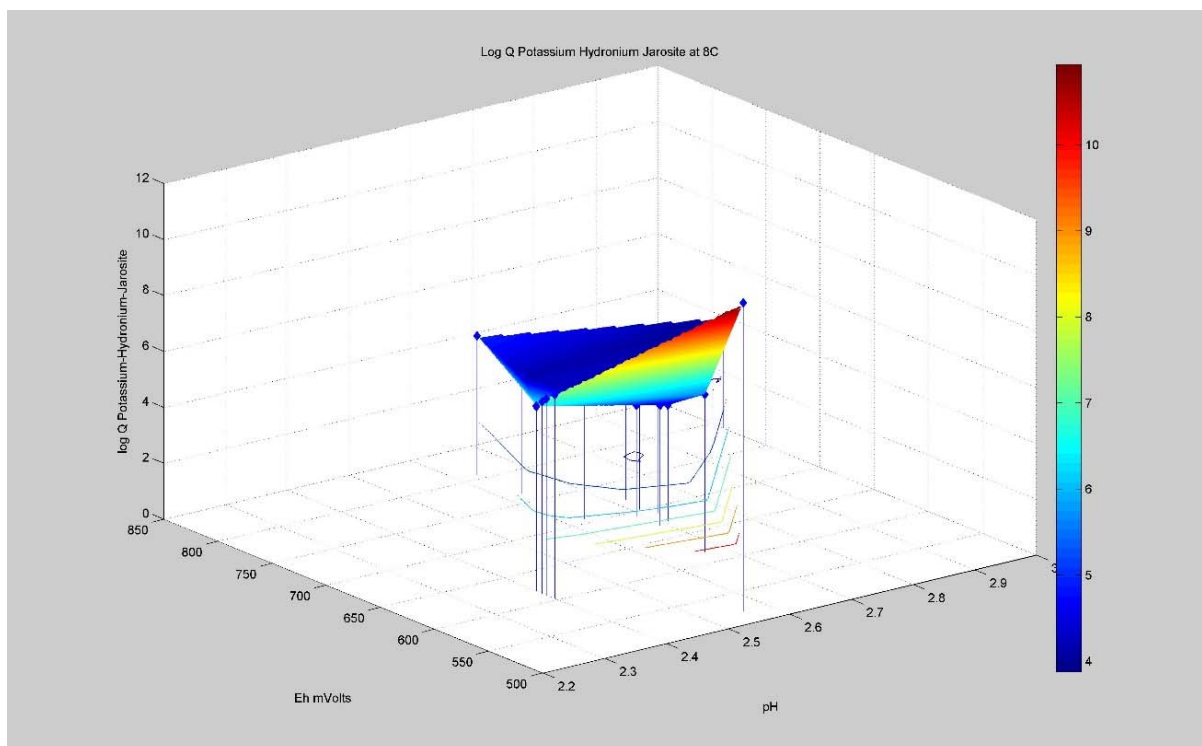


Figure 22: Potassium Hydronium Jarosite 8°C Matlab Output

4.3.1. Stabcal Output Summary by Temperature—KH Jarosite

Table XXXIII: Avg. Log Q for KH-Jarosite by Temperature

Summary Table KH-Jarosite					
Temp °C	Frequency	Avg. Log Q	Std. Dev	Variance	
2	3	4.875628	1.264	1.597	
3	5	6.863312	2.627	6.899	
4	41	5.461176	0.839	0.704	
5	19	6.097924	1.107	1.225	
6	48	5.739292	1.780	3.168	
7	44	5.702778	0.955	0.912	
8	17	5.503175	1.881	3.539	
9	11	7.339860	3.971	15.767	
10	8	8.011057	6.747	45.528	
11	7	13.732385	4.026	16.210	
12	10	4.608647	1.224	1.497	
13	8	5.289237	3.141	9.867	
14	9	6.500763	5.231	27.363	

4.4. Log Q Matlab Output for Potassium Jarosite

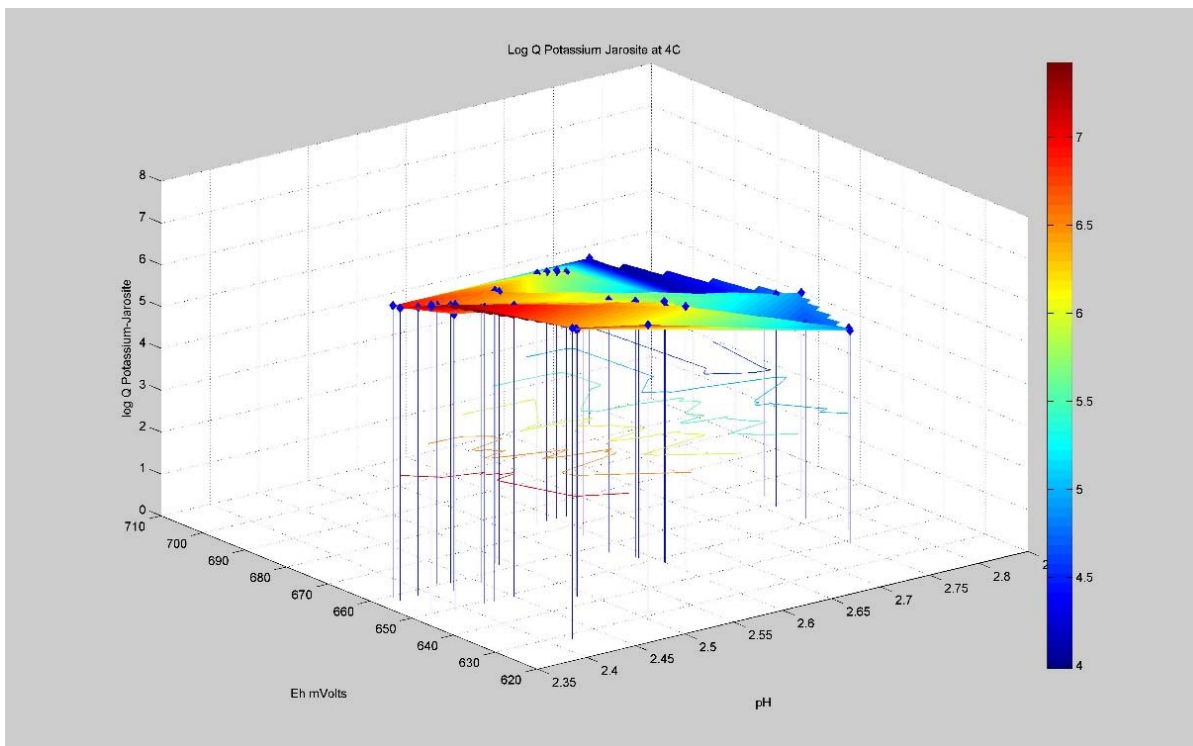


Figure 23: Potassium Jarosite 4°C Matlab Output

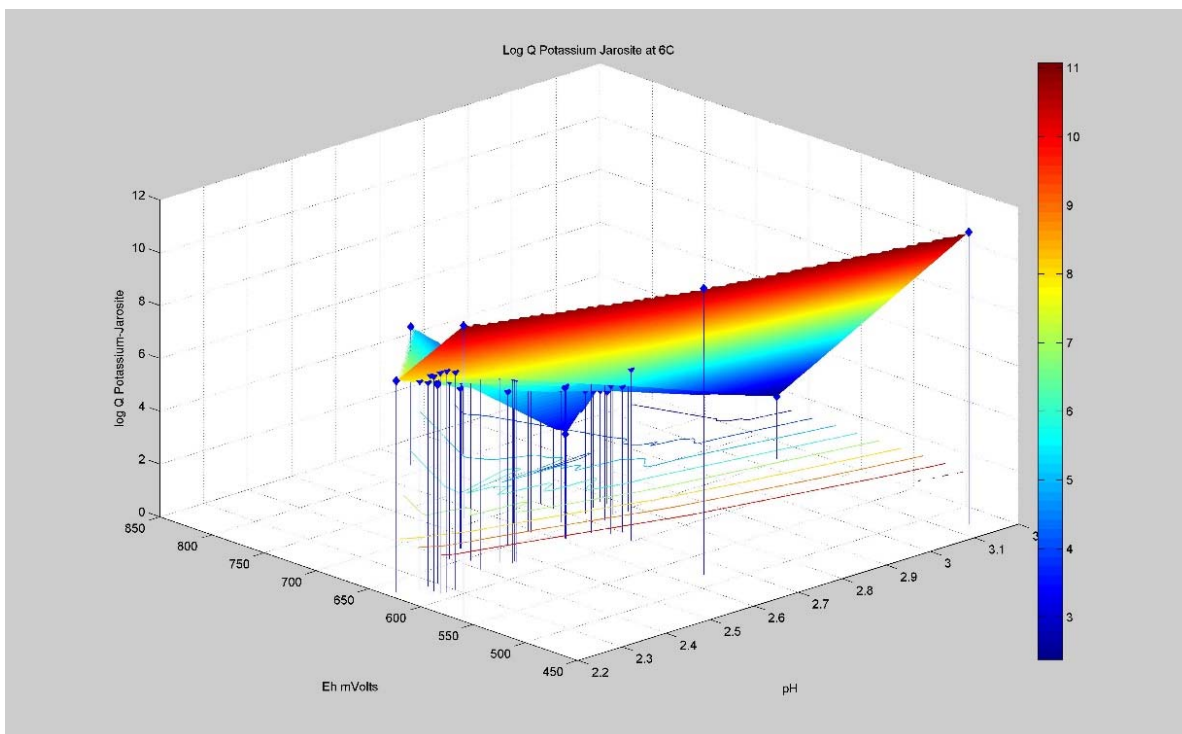


Figure 24: Potassium Jarosite 6°C Matlab Output

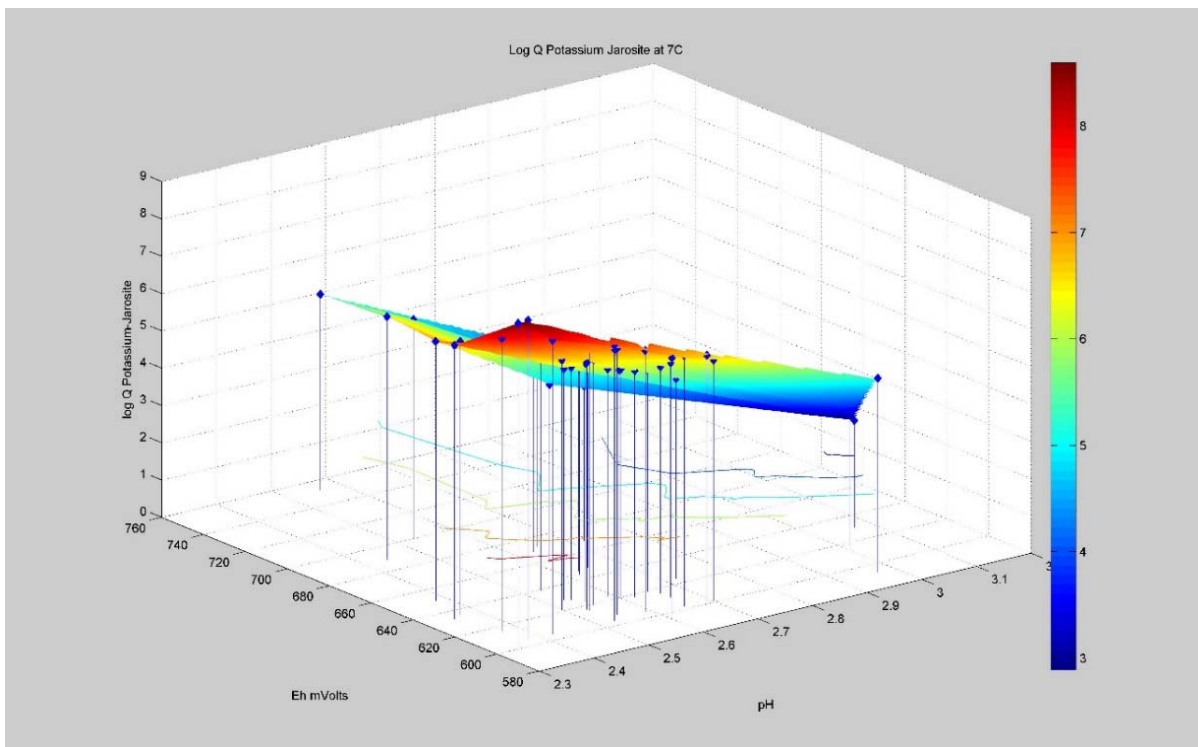


Figure 25: Potassium Jarosite 7°C Matlab Output

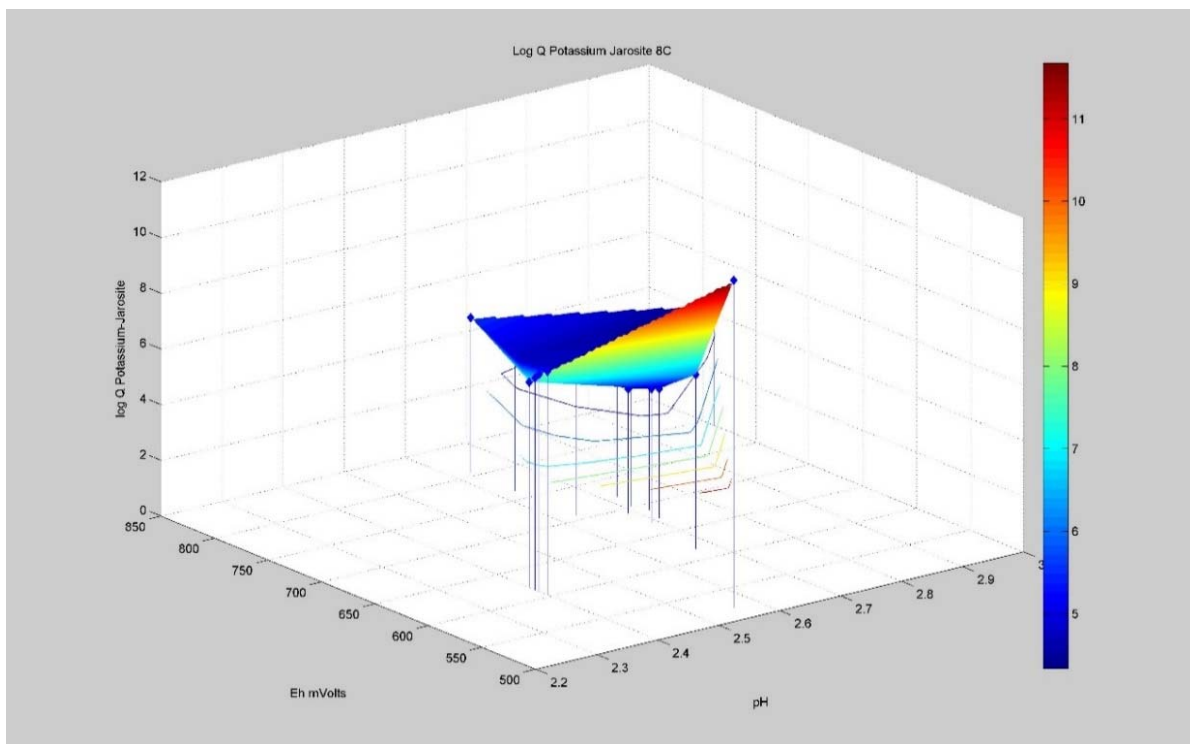


Figure 26: Potassium Jarosite 8°C Matlab Output

4.4.1. Stabcal Output Summary by Temperature—Potassium Jarosite

Table XXXIV: Avg. Log Q for Potassium Jarosite by Temperature

Summary Table K-Jarosite					
Temp °C	Frequency	Avg. Log Q	Std. Dev	Variance	
2	3	5.428657	1.319	1.739	
3	5	7.457053	2.608	6.801	
4	41	6.097962	0.918	0.843	
5	19	6.823945	1.213	1.471	
6	48	6.401671	1.859	3.455	
7	45	6.273918	1.126	1.268	
8	17	6.093357	1.997	3.989	
9	11	7.941639	3.948	15.586	
10	8	8.553780	6.791	46.121	
11	7	14.259953	3.948	15.584	
12	10	5.028544	1.283	1.647	
13	8	5.611350	3.238	10.485	
14	9	6.683190	5.262	27.684	

4.5. Log Q Matlab Output for Ferrihydrite

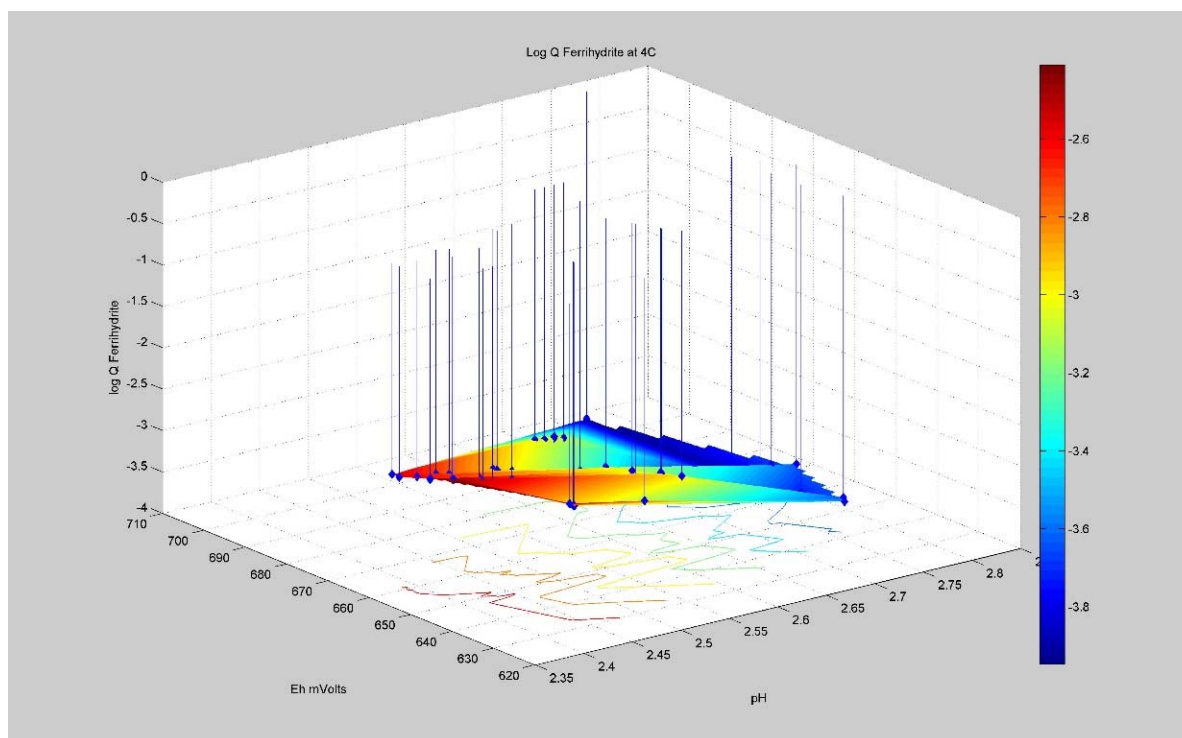


Figure 27: Ferrihydrite 4°C Matlab Output

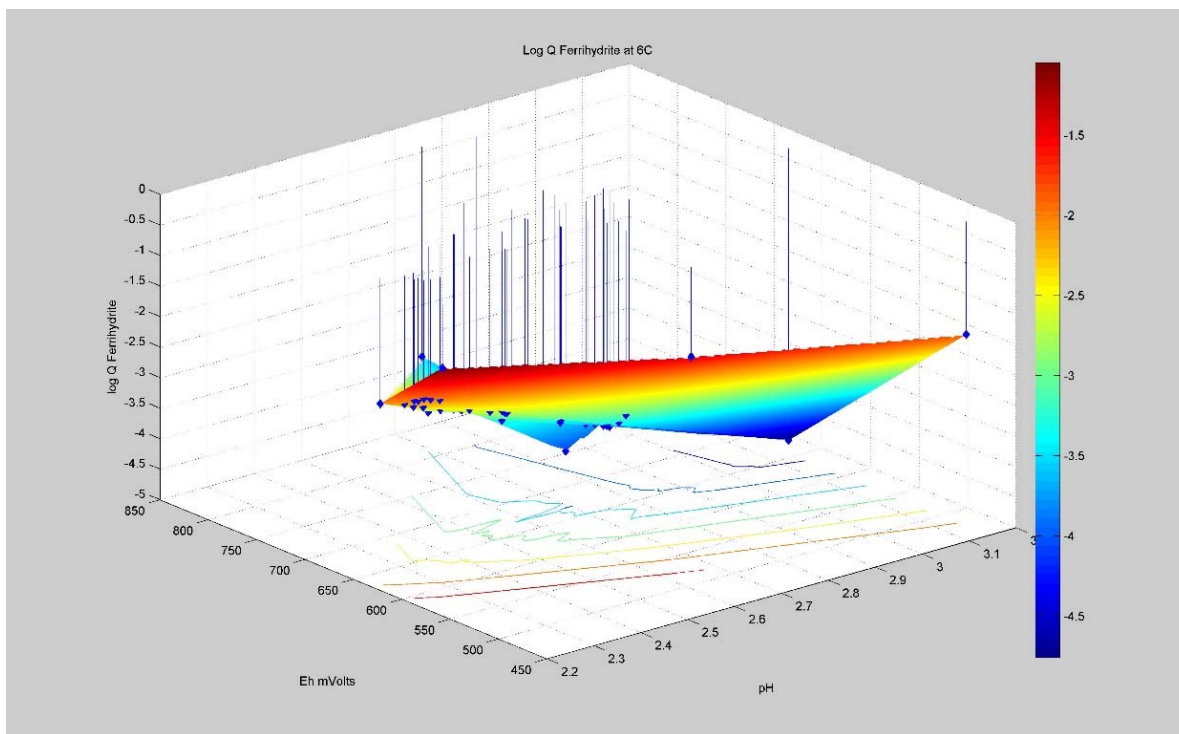


Figure 28: Ferrihydrate 6°C Matlab Output

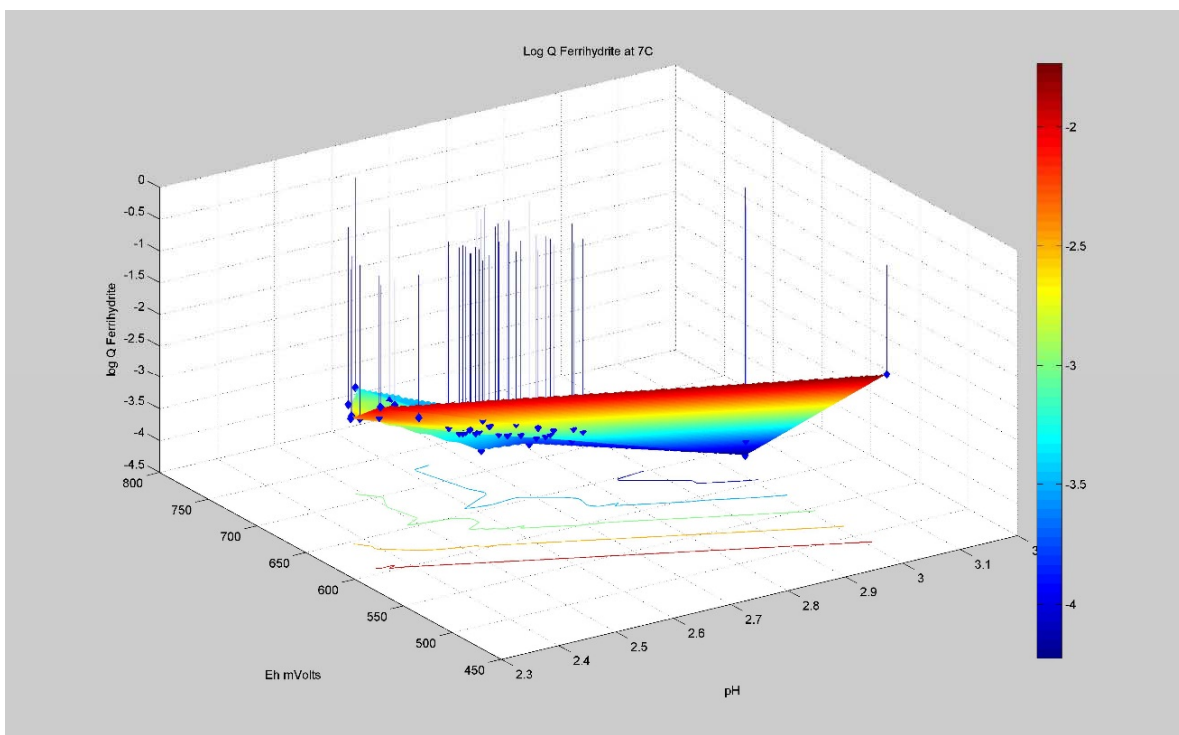


Figure 29: Ferrihydrate 7°C Matlab Output

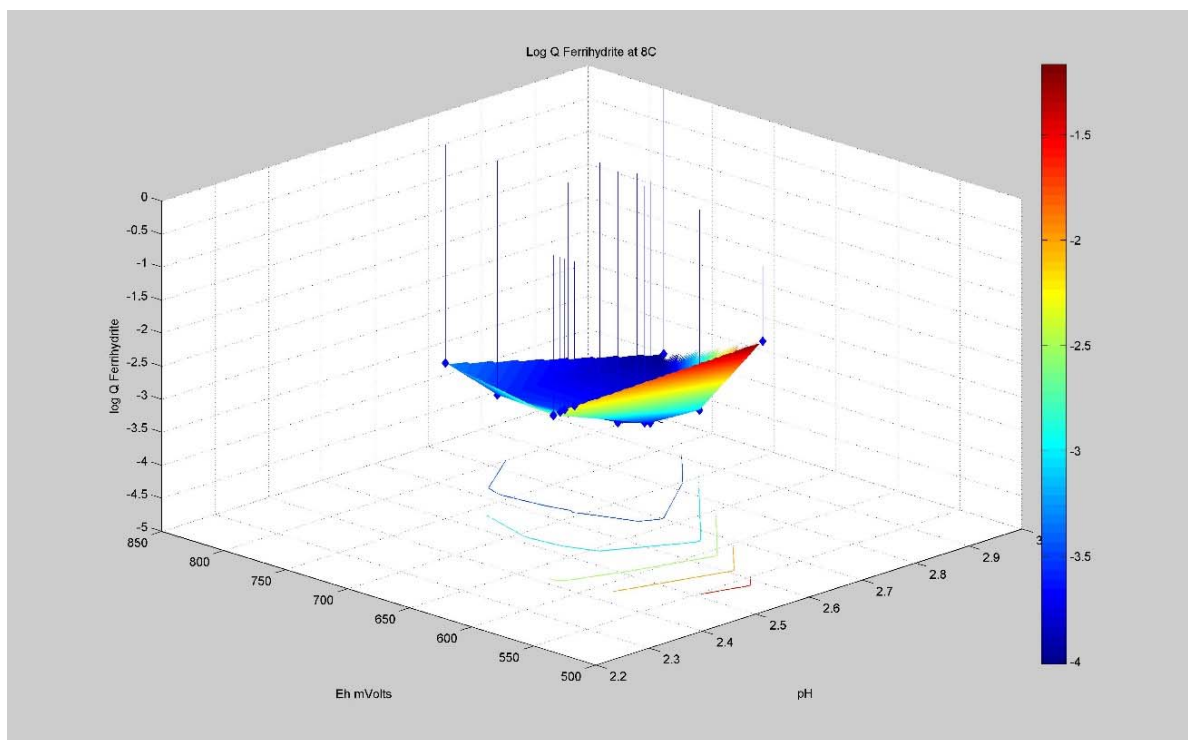


Figure 30: Ferrihydrite 8°C Matlab Output

4.5.1. Stabcal Output Summary by Temperature—Ferrihydrite

Table XXXV: Avg. Log Q for Ferrihydrite by Temperature

Summary Table Ferrihydrite					
Temp °C	Frequency	Avg. Log Q	Std. Dev	Variance	
2	3	-3.278914	0.635	0.404	
3	5	-3.098084	0.324	0.105	
4	41	-3.006772	0.432	0.187	
5	19	-2.630654	0.603	0.363	
6	48	-2.916380	0.758	0.575	
7	45	-2.926531	0.491	0.241	
8	17	-3.070219	0.790	0.624	
9	11	-2.357349	1.414	1.999	
10	8	-2.209345	2.476	6.131	
11	7	-0.344180	1.295	1.676	
12	10	-3.549918	0.539	0.291	
13	8	-3.345338	1.421	2.019	
14	9	-3.170850	1.837	3.374	

4.6. Log Q Matlab Output for Goethite

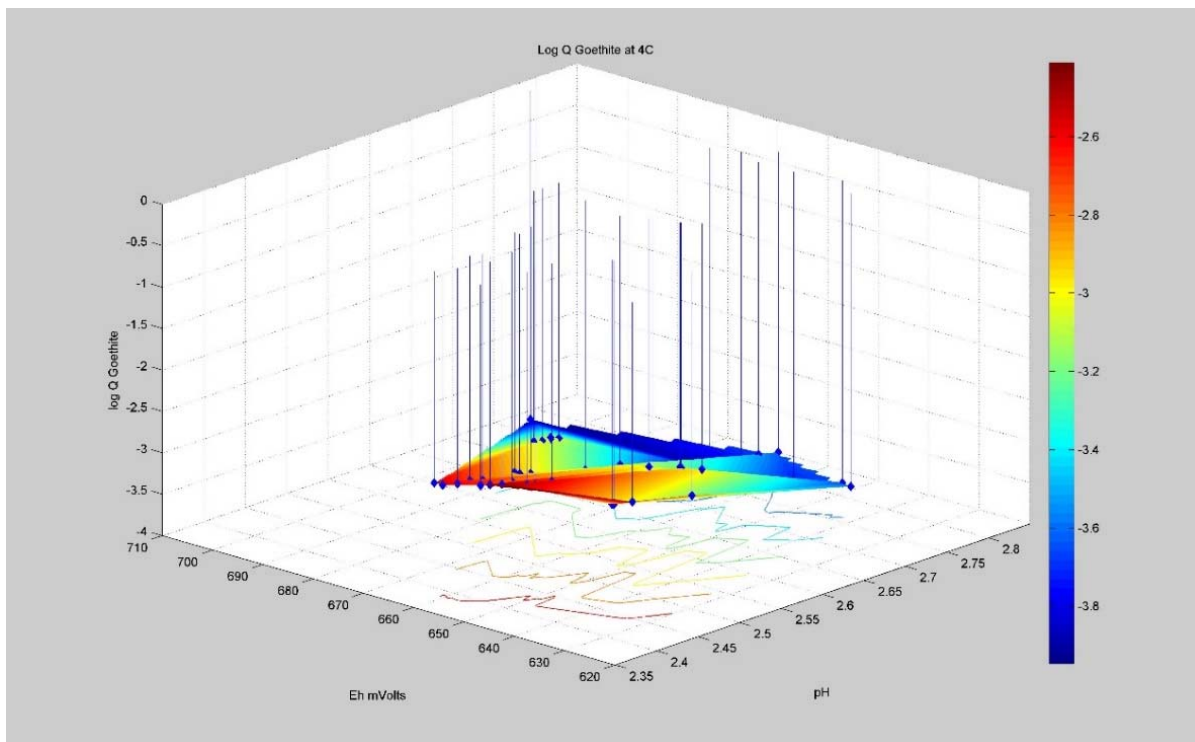


Figure 31: Goethite 4°C Matlab Output

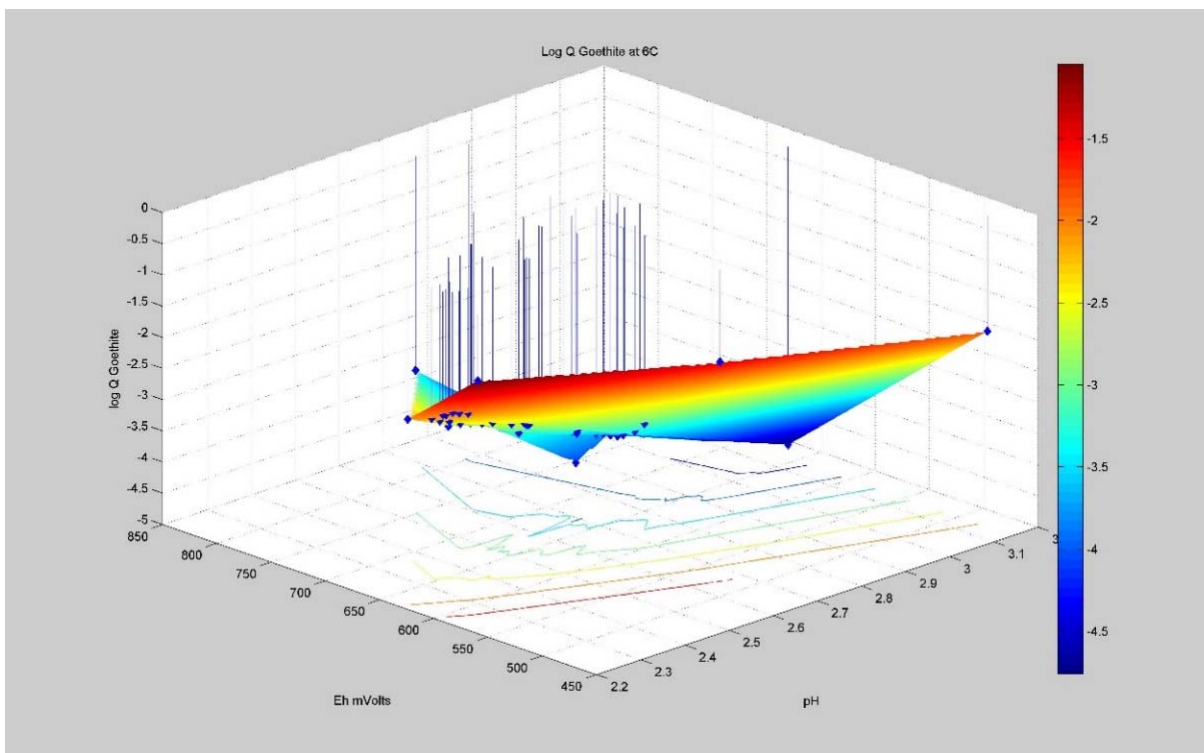


Figure 32: Goethite 6°C Matlab Output

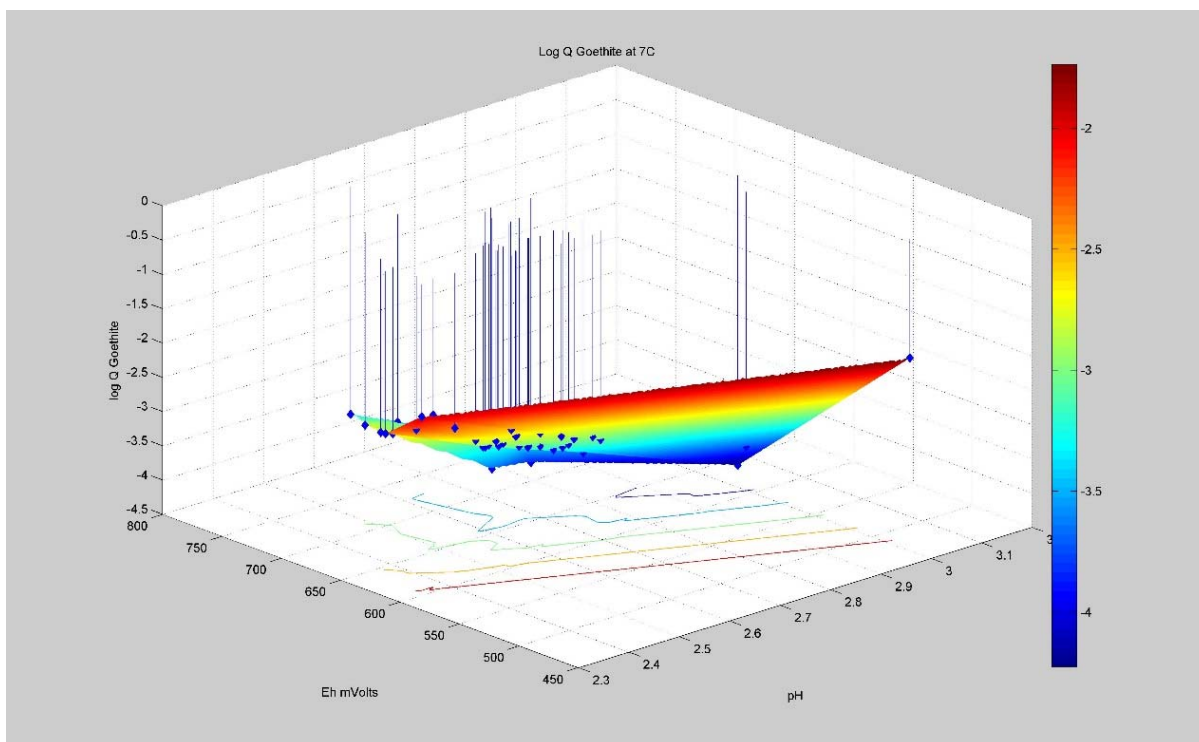


Figure 33: Goethite 7°C Matlab Output

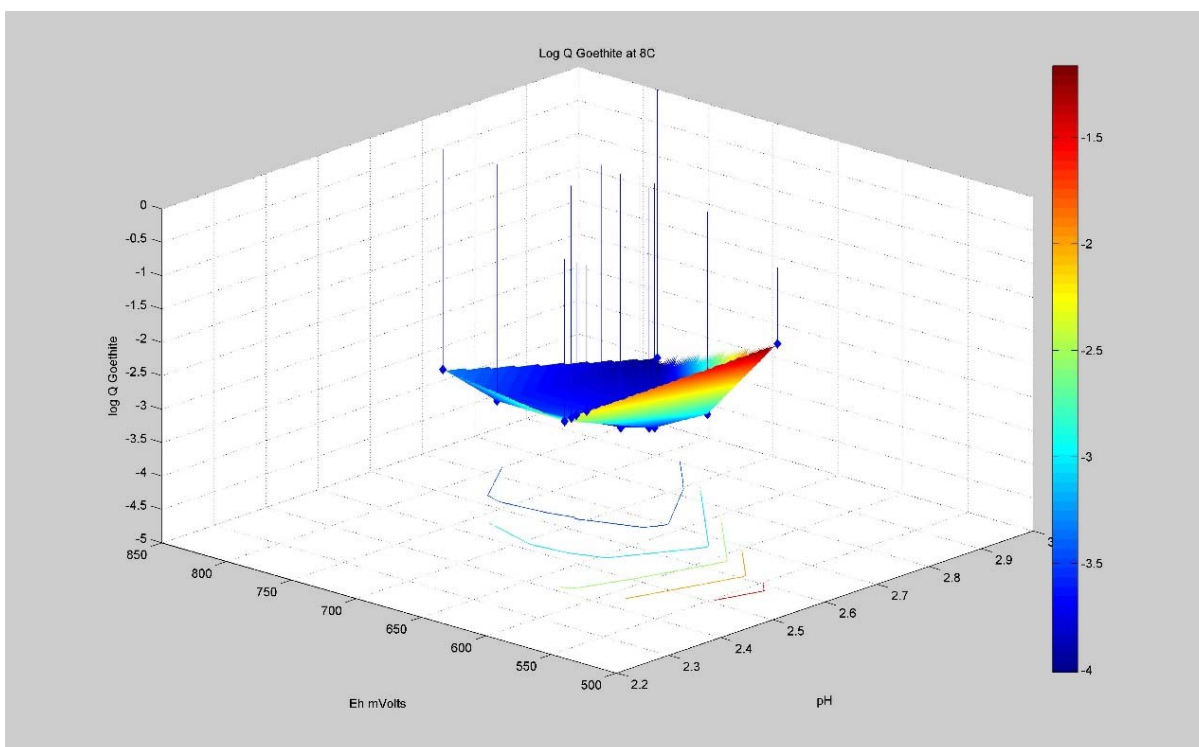


Figure 34: Goethite 8°C Matlab Output

4.6.1. Stabcal Output Summary by Temperature—Goethite

Table XXXVI: Avg. Log Q for Goethite by Temperature

Summary Table Goethite					
Temp °C	Frequency		Avg. Log Q	Std. Dev	Variance
2	3		-3.278914	0.635	0.404
3	5		-3.098084	0.324	0.105
4	41		-3.006772	0.432	0.187
5	19		-2.630654	0.603	0.363
6	48		-2.916380	0.758	0.575
7	45		-2.926531	0.491	0.241
8	17		-3.070219	0.790	0.624
9	11		-2.357349	1.414	1.999
10	8		-2.209345	2.476	6.131
11	7		-0.344180	1.295	1.676
12	10		-3.549918	0.539	0.291
13	8		-3.345338	1.421	2.019
14	9		-3.170850	1.837	3.374

5. Discussion

5.1. Ferrihydrite, Goethite & K-Jarosite Saturation Indices

Based on the results presented in Section 3.2.2 and shown in Table XI, the number of sample records used to compute the saturation indices totalled 226. The average saturation index for Goethite between 2°C and 14°C was 1.932 and -1.361 for Ferrihydrite. Since a positive saturation index value indicates oversaturation, Goethite was determined to be oversaturated while Ferrihydrite was undersaturated. These results were expected because Ferrihydrite is known to be five to six times more soluble⁴⁵ in acid mine waters compared to Goethite. This observation confirms the analytical finding that Goethite precipitates out of solution whereas Ferrihydrite does not. The saturation index value for Potassium Jarosite was determined to be 1.362. Figure 35 is a scatter plot of temperature versus saturation index for the three species using the data from Table XI. Goethite and Ferrihydrite had trendlines that appeared identical. The reason was that Goethite and Ferrihydrite had identical log Q values which were used to compute the saturation index. However the vertical shift from a positive to negative saturation index for Goethite and Ferrihydrite respectively was due to a difference in log K values. The green line of K-Jarosite had a positive saturation index at 2°C but became negative at 3°C before becoming positive from 4°C to 8°C. The saturation index then dropped off significantly again at 9°C and 10°C before turning positive again from 11°C to 14°C. It was unclear why the saturation index was negative at 3°C, 9°C and 10°C. However, examination of the statistical data in Table XXXIV revealed that at 3°C, 9°C, 10°C, 11°C, 13°C and 14°C, the variance was quite high, suggesting a widely dispersed group of log Q values. Since 2/3 of the sampling data fell within the range of 4°C to 8°C, it was concluded by Dr. Huang that this temperature interval

gave the best results. The saturation index for K-Jarosite within this temperature was found to be 1.384 which was close to the overall average of 1.362.

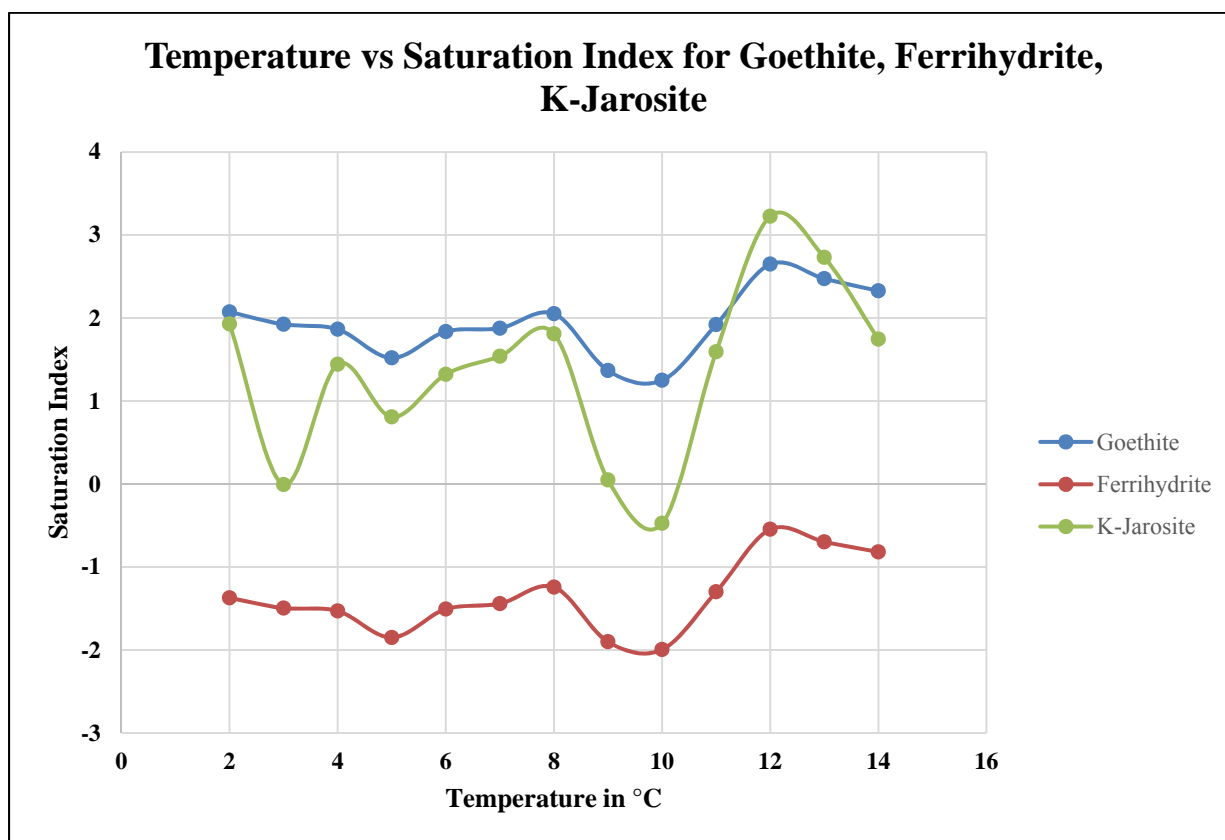


Figure 35: Temperature vs Saturation Index for Goethite, Ferrihydrite, K-Jarosite

5.2. Thermodynamic Output for Schwertmannite

Based on the results shown in Table XXXII from Section 4.2, temperature versus average log Q was plotted for Schwertmannite and is shown in Figure 36. As mentioned earlier, the data range between 4°C and 8°C had a lower amount of variance compared to the other temperature intervals and also contained the bulk of the data upon which the thermodynamic calculations were performed. Combining Equations 5 and 6 along with data in Tables XX and XXI gave the Maier-Kelley regression coefficients resulting in the updated equations for enthalpy and entropy

determination of Schwertmannite between 4°C and 8°C. The equation for enthalpy is shown in Equation 23 and for Enthalpy in equation 24.

Equation 23: Enthalpy Equation for Schwertmannite between 4°C and 8°C based on Multiple Linear Regression Model

$$H_T = H_{rm} + \int_{298.15}^T C_p dT$$

Where $H_{rm} = -2964.030$ kcal, $C_p = a + b \times 10^{-3}T + c \times 10^5T^{-2}$, and $a = 161273488$, $b = -378690560$,
 $c = -43316576$

Equation 24: Entropy Equation for Schwertmannite between 4°C and 8°C based on Multiple Linear Regression Model

$$S_T = S_{rm} + \int_{298.15}^T C_p dT$$

Where $S_{rm} = -6049.433$ cal, $C_p = a + b \times 10^{-3}T + c \times 10^5T^{-2}$, and $a = 161273488$, $b = -378690560$,
 $c = -43316576$

These equations were used to predict the G and dG values between 4°C and 8°C for Schwertmannite as a function of temperature. The results are plotted in figure 37. A second order polynomial trendline was added for fitting purposes. However, these equations cannot be used for predicting any thermodynamic properties. They were only added for illustration.

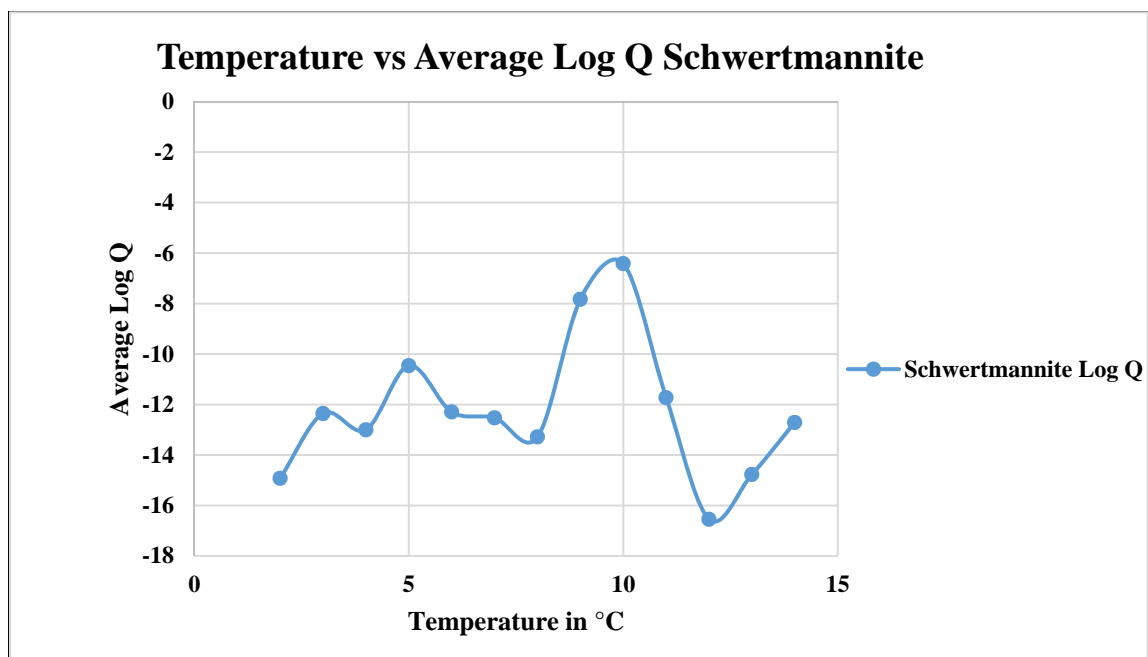


Figure 36: Temperature vs Log Q Schwertmannite

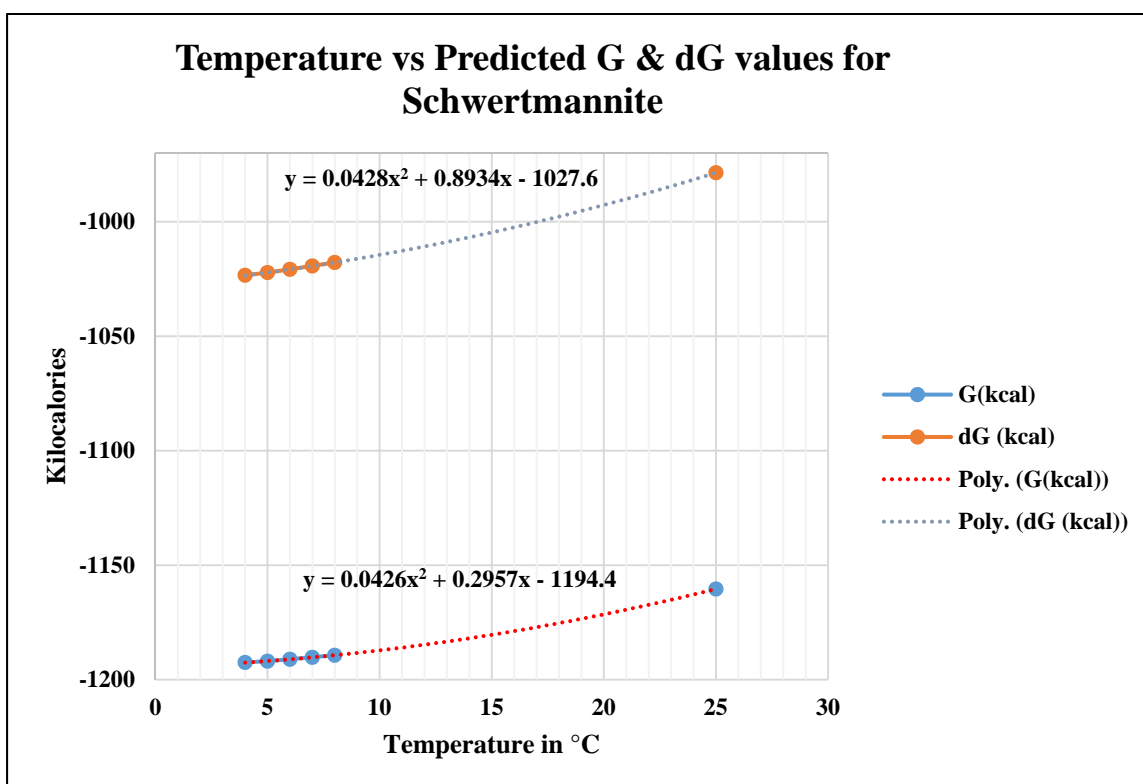


Figure 37: Temperature vs G & dG values for Schwertmannite

5.3. Thermodynamic Output for KH-Jarosite & K-Jarosite

Based on the results shown in Section 4.3 Table XXXIII, and Section 4.4 Table XXXIV, temperature versus average log Q was plotted for KH-Jarosite and K-Jarosite as Figure 38. The temperature range of 4°C to 8°C from Tables XXXIII & XXXIV minimized the variance and gave reliable results since a majority of the calculated log Q values was within that temperature interval. Examination of the trendlines in Figure 38 clearly shows that KH and K Jarosite species have similar log Q values as a function of temperature. Using the same procedure that was outlined for Schwertmannite in Section 5.2, regression coefficients, enthalpy and entropy values were calculated along with G and dG values from the predicted enthalpy and entropy equations within the temperature range of 4°C to 8°C. Equations 25 to 28 show the enthalpy and entropy equations created from the multiple linear regression model. Figures 39 and 40 shows graphs of temperature versus predicted G values for KH and K Jarosite based on Equations 25 to 28 and were plotted from the numbers calculated in Tables XXIII and XXV.

Equation 25: Enthalpy Equation for KH-Jarosite between 4°C and 8°C based on Multiple Linear Regression Model

$$H_T = H_{rm} + \int_{298.15}^T C_p dT$$

Where $H_{rm} = 586.546$ kcal, $C_p = a + b \times 10^{-3}T + c \times 10^5T^{-2}$, and $a = -145717088$, $b = 342660160$,
 $c = 39022976$

Equation 26: Entropy Equation for KH-Jarosite between 4°C and 8°C based on Multiple Linear Regression Model

$$S_T = S_{rm} + \int_{298.15}^T C_p dT$$

Where $S_{rm} = 5118.474$ cal, $C_p = a + b \times 10^{-3}T + c \times 10^5T^{-2}$, and $a = -145717088$, $b = 342660160$,
 $c = 39022976$

Equation 27: Enthalpy Equation for K-Jarosite between 4°C and 8°C based on Multiple Linear Regression Model

$$H_T = H_{rm} + \int_{298.15}^T C_p dT$$

Where $H_{rm} = -1249.793$ kcal, $C_p = a + b \times 10^{-3}T + c \times 10^5T^{-2}$, and $a = -46482960$, $b = 107543872$,
 $c = 112836016$

Equation 28: Entropy Equation for K-Jarosite between 4°C and 8°C based on Multiple Linear Regression Model

$$S_T = S_{rm} + \int_{298.15}^T C_p dT$$

Where $S_{rm} = -1138.889$ cal, $C_p = a + b \times 10^{-3}T + c \times 10^5T^{-2}$, and $a = -46482960$, $b = 107543872$,
 $c = 112836016$

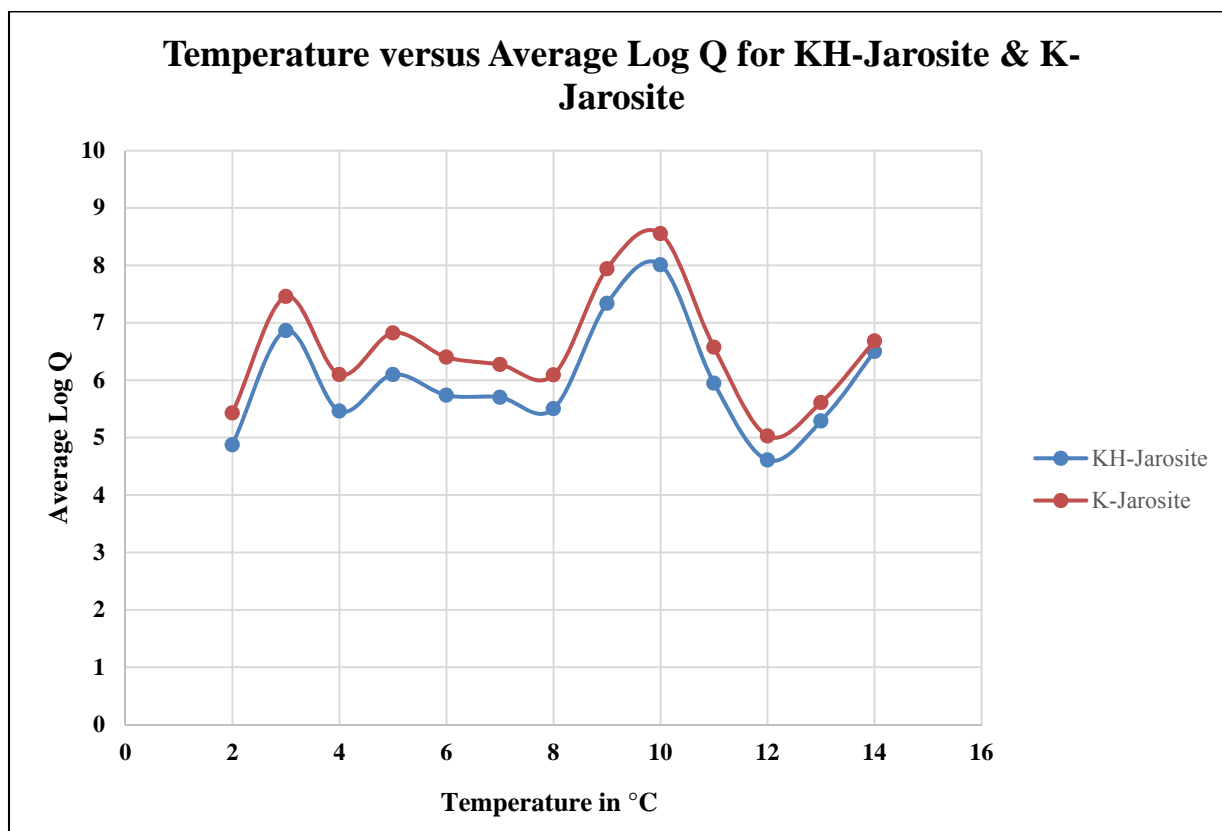


Figure 38: Temperature vs Average Log Q for KH-Jarosite & K-Jarosite

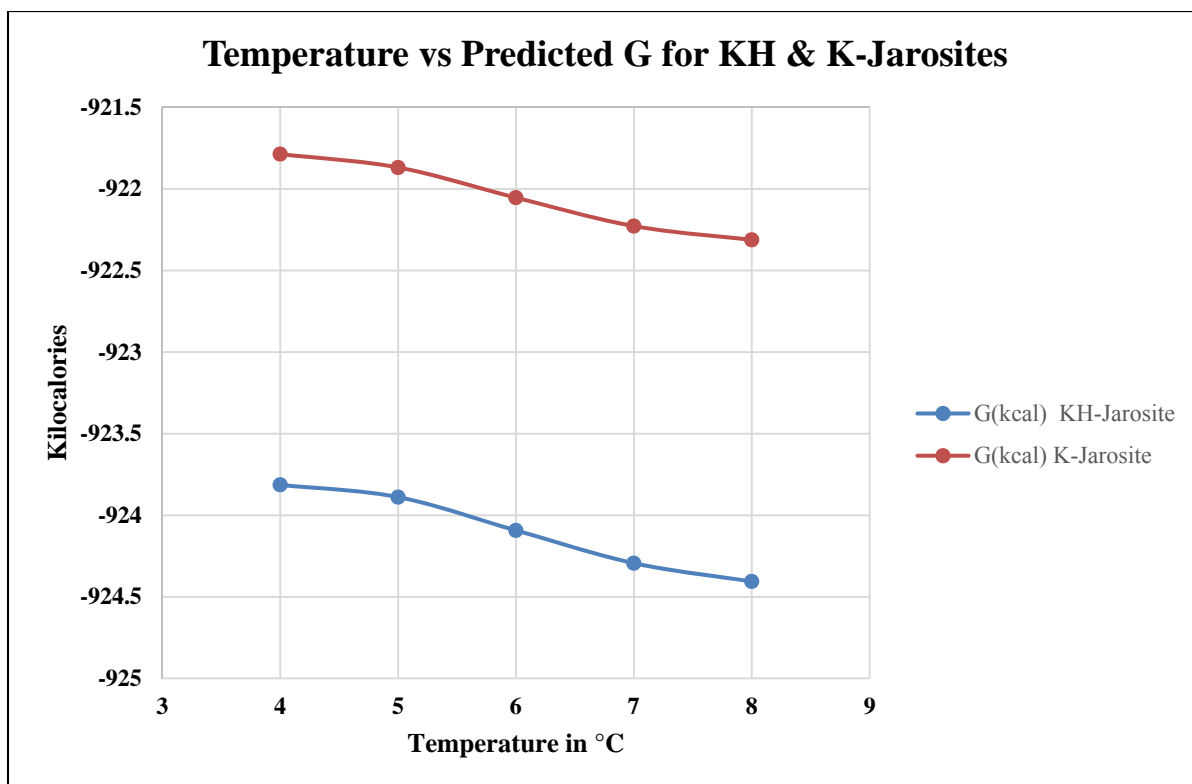


Figure 39: Temperature vs Predicted G(kcal) for KH & K Jarosite

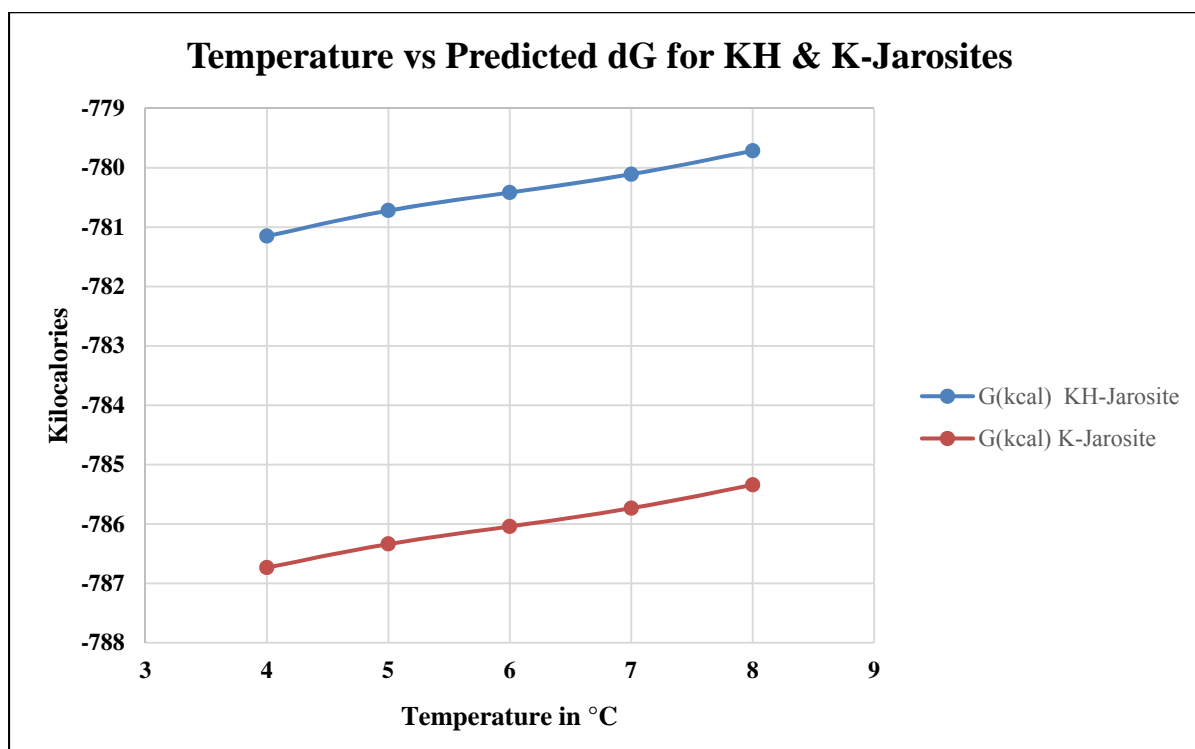


Figure 40: Temperature vs Predicted dG for KH & K-Jarosites

5.4. Copper Cementation Effect on Solid Iron Species Formation

As shown in figures 37 and 40, the predicted dG values for Schwertmannite KH and K-Jarosites were quite negative ranging from approximately -1000 kcal to -775 kcal. Moore⁴⁶ points out that when the dG value is <60 kJ/mol, the equilibrium position indicates effective completion of the reaction. Since 1 kcal = 4.184 kJ, the converted dG values which are much less than 60 kJ/mol indicate that production of Schwertmannite, KH-Jarosite and K-Jarosite is undoubtedly taking place in the Berkeley Pit. Figure 13 revealed that during the copper cementation period from 2002 to 2012, Fe²⁺ ion concentration dropped dramatically while Fe³⁺ ion concentration stayed fairly constant. The explanation is that the Fe²⁺ was converted into Fe³⁺ ions in the presence of oxygen which then formed Schwertmannite and different Jarosites in the pit water. This accounts for the Fe²⁺ ion concentration decreasing while the Fe³⁺ ions stayed fairly constant. The Fe³⁺ ions also formed supersaturated Goethite along with the other solid iron species which are now at the bottom of the Berkeley pit.

6. Conclusion

The Berkeley pit water was analyzed for the presence of solid iron species due to copper cementation over a nine year period. Log Q values and saturation indices were computed for Ferrihydrite, Goethite, and K-Jarosite. Ferrihydrite had a negative saturation index and was undersaturated. Goethite had a positive saturation index and was oversaturated. K-Jarosite had a positive saturation index and was slightly oversaturated.

The results from the estimation of the free energy and entropy for Schwertmannite within a temperature range of 4°C to 8°C were found using Stabcal and a multiple regression model in Excel. Regression coefficients [a, b, c] of the Maier-Kelley equation were further determined. Enthalpy values at room temperature H_{rm} were determined indirectly using $G_{rm} = H_{rm} - TS_{rm}$. Schwertmannite was found to have a dG of -978 kcal/mol, S_{rm} of -6049.433 cal, and a H_{rm} of -2964.030 kcal/mol. Maier-Kelley regression coefficients for Schwertmannite were determined to be [a = 161273488, b = -378690560, c = -43316576]. Free energy, entropy and Maier-Kelley regression coefficients were calculated for KH-Jarosite and K-Jarosite. KH-Jarosite had a dG of -786 kcal/mol, an S_{rm} of 5118 cal, and an H_{rm} of 586.486 kcal/mol. Maier-Kelley regression coefficients for KH-Jarosite were determined to be [a = -145717088, b = 342660160, c = 39022976]. K-Jarosite had a dG of -765 kcal/mol, an S_{rm} of -1139 cal, and an H_{rm} of -1249.793 kcal/mol. Maier-Kelley regression coefficients for K-Jarosite were determined to be [a = -46482960, b = 107543872, c = 112836016].

Eh-pH diagrams were constructed for Schwertmannite, KH & K-Jarosite. It was concluded that Schwertmannite does not form below a pH of 2.4. It was also concluded that formation of Schwertmannite was temperature dependent. At a temperature of 4°C and a pH greater than 2.4, approximately equal amounts of mixed Schwertmannite—KH-Jarosite, mixed

Schwertmannite—K-Jarosite, and pure Schwertmannite were found to coexist. As temperature increased to 6°C, larger amounts of mixed Schwertmannite—KH-Jarosite and mixed Schwertmannite—K-Jarosite with smaller amounts of pure Schwertmannite coexisted. At temperatures of 7°C and 8°C, only mixed Schwertmannite—KH-Jarosite and mixed Schwertmannite—K-Jarosite were found to coexist. Below a pH of 2.4, various combinations of KH-Jarosite and K-Jarosite were found to exist between 4°C and 8°C through a range of Eh values.

A titration simulation was performed using Stabcal with three water quality records which were taken near the beginning, middle and end of the copper cementation process. In agreement with recorded data, it was found that Fe^{2+} concentrations decreased four fold over time while Fe^{3+} concentrations stayed fairly constant. This was explained by ferrous ion to ferric ion conversion in the presence of O_2 which subsequently formed various iron oxide and oxyhydroxysulfate species which precipitated out of solution.

6.1. Recommendations

Berkeley pit water quality monitoring has not been conducted since 2012 when a pit wall failure occurred. In addition, copper cementation had also ceased at the beginning of 2013. Since that time, water quality samples have not been recorded, so it is unclear what changes may have occurred to the pit water chemistry.

One recommendation would be to restart a collection of water quality samples to analyze if there have been any water quality changes over the last two years. Water quality sampling at depth using Imhoff cones would also allow for sedimentation sampling to occur and further chemical analysis. The result may provide some insight into solid iron species formation in the Berkeley pit.

7. References

- 1.) Montana Bureau of Mines and Geology, Butte Mine Flooding Summary, Updated March 2014. (Updated February 2015—Ted Duaiame Personal Conversation)
- 2.) Montana Bureau of Mines and Geology Website, GWIC
- 3.) Personal Conversation with Duaiame, Terence. Senior Research Hydrologist, Montana Bureau of Mines and Geology, 2014.
- 4.) Tucci, Nicholas J., Gammons, Christopher H. “Influence of Copper Recovery on the Water Quality of the Acidic Berkeley Pit Lake, Montana, U.S.A.” *Environmental Science & Technology* 2015
- 5.) Tucci, Nicholas J., Gammons, Christopher H. “Influence of Copper Recovery on the Water Quality of the Acidic Berkeley Pit Lake, Montana, U.S.A.” *Environmental Science & Technology* 2015
- 6.) Tucci, Nicholas J., Gammons, Christopher H. “Influence of Copper Recovery on the Water Quality of the Acidic Berkeley Pit Lake, Montana, U.S.A.” *Environmental Science & Technology* 2015
- 7.) Huang, Hsin H. Stabcal Speciation Program, Thesis Research Class, Spring 2014, Montana Tech.
- 8.) The International Network for Acid Prevention (INAP), 2009. Global Acid Rock Drainage Guide (GARD Guide). <http://www.gardguide.com>
- 9.) Stumm, Werner. Morgan, James J. Aquatic chemistry: an introduction emphasizing chemical equilibria in natural waters. *Environmental Science and Technology: A Wiley-Interscience Series of Texts and Monographs*, Wiley-Interscience Publication, 1981.
- 10.) The International Network for Acid Prevention (INAP), 2009. Global Acid Rock Drainage Guide (GARD Guide). <http://www.gardguide.com>
- 11.) The International Network for Acid Prevention (INAP), 2009. Global Acid Rock Drainage Guide (GARD Guide). <http://www.gardguide.com>
- 12.) The International Network for Acid Prevention (INAP), 2009. Global Acid Rock Drainage Guide (GARD Guide). <http://www.gardguide.com>
- 13.) D. Paktunc, J. Dutrizac, V. Gertsman, *Geochimica et Cosmochimica Acta*, 72, 2649-2672
- 14.) Gammons, Christopher H. Lecture on Ferrous/Ferric Iron Chemistry, Acid Rock Drainage 531 Class Fall 2014, Montana Tech.
- 15.) Gammons, Christopher H. Lecture on Ferrous/Ferric Iron Chemistry, Acid Rock Drainage 531 Class Fall 2014, Montana Tech.

- 16.) Gammons, Christopher H. Lecture on Ferrous/Ferric Iron Chemistry, Acid Rock Drainage 531 Class Fall 2014, Montana Tech.
- 17.) Gammons, Christopher H. Lecture on Ferrous/Ferric Iron Chemistry, Acid Rock Drainage 531 Class Fall 2014, Montana Tech.
- 18.) Huang, Hsin H. Stabcal Speciation Program, Thesis Research Class, Spring 2014, Montana Tech.
- 19.) Duaiame, Terence. Senior Research Hydrologist, Montana Bureau of Mines and Geology, 2014.
- 20.) Huang, Hsin H. Stabcal Speciation Program, Thesis Research Class, Spring 2015, Montana Tech.
- 21.) <http://en.wikipedia.org/wiki/Schwertmannite>
- 22.) Bigham, J.M. et al. "Schwertmannite and the chemical modeling of iron in acid sulfate waters." *Geochimica et Cosmochimica Acta*, Vol. 60, No. 12, pp. 2111-2121, 1996.
- 23.) <http://scu.edu.au/geoscience/index.php/69>
- 24.) Caraballo, Manuel A. et al. "Metastability, nanocrystallinity and pseudo-solid solution effects on the understanding of Schwertmannite solubility." *Chemical Geology* 360-361 (2013) pp. 22-31
- 25.) Dutrizac, J.E. (1983) Factors affecting alkali Jarosite precipitation. *Metallurgical Transactions*, 14B, 531-539.
- 26.) Tucci, Nicholas J., Gammons, Christopher H. "Influence of Copper Recovery on the Water Quality of the Acidic Berkeley Pit Lake, Montana, U.S.A." *Environmental Science & Technology* 2015
- 27.) NBS – D.D. Wagman, et. Al. "The NBS Tables of chemical thermodynamic properties", *J. of Physical and Chemical References Data*, Vol. 11, Sup. 2 (1982), and Errata. Vol. 18 (1989)
- 28.) Sverjensky, D.A., Shock, E.L., Helgeson, H. C. "Prediction of the thermodynamic properties of aqueous metal complexes to 1000°C and 5kb." *Geochimica et Cosmochimica Acta*, Vol. 61, No. 7, pp. 1359-1412. 1997
- 29.) G. B. Naumov, et. Al. "Handbook of thermodynamic data", translated by G.H. Soleimani, USGS, NTIS PB 226-722 (1974)
- 30.) CRITICAL – R. M. Smith and A.E. Martell, "Critical Stability Constants," Plenum Press (1974-1985) for Inorganic and NIST Software for inorganic (1995)

- 31.) Johnson, James W., Oelkers, Eric H., Helgeson, Harold C. "SUPCRT92: A SOFTWARE PACKAGE FOR CALCULATING THE STANDARD MOLAL THERMODYNAMIC PROPERTIES OF MINERALS, GASES, AQUEOUS SPECIES AND REACTIONS FROM 1 TO 5000 BAR AND 0 TO 1000°C.", Computers & Geosciences, Vol. 18, No. 7, pp. 899-947, 1992
- 32.) MINTEQA2 Database – J.D. Allison, et al. "MINTEQA2/PRODEFA2, A Geochemical Assessment Model for Environmental Systems", Window Version. The data were converted to dG_{rm} , S_{rm} , and $C_p(T)$ by H.H. Huang using Stabcal
- 33.) LLNL Database – Originally created by Jim Johnson at Lawrence Livermore National Laboratory, converted to Phreeqc format by Greg Anderson then converted to dG_{rm} , S_{rm} , $C_p(T)$ format by H. H. Huang
- 34.) WATEQ4F Database – Originally created by Archer and Nordstrom at Lawrence Livermore National Laboratory, converted to Phreeqc format by Greg Anderson then converted to dG_{rm} , S_{rm} , $C_p(T)$ format by H. H. Huang
- 35.) http://wwwbr.cr.usgs.gov/projects/GWC_coupled/phreeqc/mail/msg00046.html
- 36.) http://en.wikipedia.org/wiki/Van_%27t_Hoff_equation
- 37.) http://www.eqi.ethz.ch/fmi/xsl/eqi/eqi_property_details_en.xsl?node_id=1457
- 38.) <http://www.science.uwaterloo.ca/~cchieh/cact/c123/massacti.html>
- 39.) Brown, Theodore L., Lemay Jr. Eugene H., Bursten, Bruce E. Chemistry—The Central Science. 6th edtn. Prentice Hall, 1994.
- 40.) <http://mathworld.wolfram.com/NewtonsMethod.html>
- 41.) Himmelblau, David M., Process Analysis by Statistical Method, 1st edtn. John Wiley & Sons, 1970.
- 42.) A.Eaton, L.S. Clesceri and A.E. Greenberg, Standard Method for Examination of water and Wastewater, Part 2310, Acidity, American Public Health Association, 19th edition 1995.
- 43.) Duaiame, Terence E., Tucci, Nicholas J. Butte Mine Flooding Operable Unit Water-Level Monitoring and Water-Quality Sampling 2012 Consent Decree Update Butte, MT 1982-2011, pgs.171, Montana Bureau of Mines and Geology Open File Report 641
- 44.) Tucci, Nicholas J., Gammons, Christopher H. "Influence of Copper Recovery on the Water Quality of the Acidic Berkeley Pit Lake, Montana, U.S.A." Environmental Science & Technology 2015
- 45.) Gammons, Christopher H. Lecture on Ferrous/Ferric Iron Chemistry, Acid Rock Drainage 531 Class Fall 2014, Montana Tech.

46.) Moore, J.J. Chemical Metallurgy, 2nd edtn. Butterworths Ltd. Publishing Co. 1990

Appendix

1. Computer Speciation Procedure in Stabcal

1.1. Data Source

The Montana Bureau of Mines and Geology water-quality dataset from 1987 to 2012 was created in Excel format and maintained by Ted Duaime, Associate Research Hydrogeologist at the MBMG over the last several decades. In order to calculate the thermodynamic properties for Schwertmannite, Potassium Jarosite, Potassium Hydronium Jarosite, etc. It was necessary to extract data from the spreadsheet for the Excel fields and variables that the thermodynamic modeling was calculated from and subsequently input the data into Stabcal for modeling. Stabcal is a computer speciation and geochemical calculation program developed by Dr. Hsin H. Huang of Montana Tech. It is analogous to PHREEQC developed by the USGS. However, Stabcal is more powerful because it allows the user to access all of the thermodynamic databases used currently. It uses a mass-balanced approach for calculating thermodynamic quantities, which is considered the most accurate and also uses Newton's Method for carrying out iterative calculations. This section will describe the modeling procedures that were utilized.

1.1.1. Data Population from MBMG

A total of 127 water quality records from independent samples were used in the evaluation for the time period from October 1987 to June 2012. A sample "record" is shown in Table VIII which contains 27 elemental components that were exported from Excel to process in the Stabcal program. From this "record", a total iron speciation was performed. Iron speciation refers to the formation of different inorganic species (especially of ions) as the environment changes.²¹ The 127 sample records were duplicated in Excel and copied to a separate spreadsheet. Then, water-quality data for Fe³⁺ from a different spreadsheet was inserted into the

original spreadsheet corresponding to the identical records. From the modified spreadsheet, 99 samples were separately analyzed using recorded Fe^{3+} values (total of 226 samples). These values were then used to calculate Fe^{2+} values. The Nernst Equation was used to calculate the $\text{Fe}^{2+}/\text{Fe}^{3+}$ couple as follows:

$$\mathbf{Eh \text{ for } \text{Fe}^{2+}/\text{Fe}^{3+} = 0.77\text{V}}$$

$$\mathbf{E = (E_0 - 0.059/n) * \log Q = 0.77 - 0.059 * \log(\text{Fe}^{2+}/\text{Fe}^{3+})}$$

$$\mathbf{Q = [\text{Fe}^{2+}] / [\text{Fe}^{3+}]}$$

$$\mathbf{1/(1+Q) = \text{Fraction of solution as } \text{Fe}^{3+}}$$

$$\mathbf{1 - \text{Fraction of solution as } \text{Fe}^{3+} = \text{Fraction as } \text{Fe}^{2+}}$$

Since 28 of the original 127 water quality records did not contain accurate Eh values to calculate Fe^{2+} concentrations, these sample records could not be used.

Tables XXXVII and XXXVIII shows selected variables from the water quality records that were used for computer modeling in Stabcal. Based on published thermodynamic data, activity coefficients and reaction quotients were calculated as explained in Section 3. These water quality records correspond to the original numbers from the MBMG record file.

Table XXXVII: MBMG Water Quality Records for Total Iron Speciation

RECORD	DATE (mm/dd/yy)	DEPTH (Feet)	pH	Temp (C)	ORP (MV)	Fe total (mg/l)
21	10/14/87	Surface	2.76	11.5	817	183
22	10/14/87	3	2.72	8.2	720	231
23	10/14/87	10	2.84	11.5	643	376
24	10/14/87	50	2.95	12.1	570	711
25	10/14/87	100	3.08	13.3	501	982
26	10/14/87	200	3.15	13.5	457	983
27	10/14/87	300	3.15	13.5	468	984
28	10/14/87	400	3.14	13.7	463	1,010
30	05/21/91	3.4	2.47	13.0	610	666
33	05/21/91	3.4	2.48	13.1	613	593
35	05/21/91	3.4DUP	2.48	13.1	613	567
41	05/22/91	225	2.84	13.5	410	1,088
74	04/19/94	150	2.44	9.0	446	1,160
75	04/19/94	200	2.45	9.0	445	1,107
79	10/25/95	200	2.45	9.5	379	1,116
80	11/08/95	200	2.31	9.8	384	1,138
96	11/19/99	60	2.17	4.9	638	938
97	11/19/99	100	2.18	4.8	637	940
98	11/19/99	200	2.20	4.9	637	942
119	11/06/01	1	2.68	5.9	812	269
121	11/06/01	25	2.56	5.7	710	641
122	11/06/01	50	2.61	5.7	635	876
124	11/06/01	100	2.65	5.8	519	961
125	11/05/01	700	2.70	5.9	618	971
127	11/07/01	1	2.63	7.8	806	270
129	11/07/01	25	2.56	6.8	752	560
130	11/07/01	50	2.61	5.7	634	821
140	07/02/02	25	2.17	4.8	684	505
141	07/02/02	50	2.22	5.8	632	975
142	07/02/02	75	2.26	6.0	616	1,020
143	07/02/02	100	2.27	6.1	611	1,030
144	07/02/02	200	2.28	6.2	609	1,050
145	07/02/02	240	2.30	6.2	609	1,050
160	11/07/02	Surface	2.42	2.3	831	286
161	11/07/02	10	2.44	2.3	828	288
162	11/07/02	25	2.44	6.9	689	317
163	11/07/02	50	2.42	6.0	645	638
164	11/07/02	75	2.45	6.2	630	786
165	11/07/02	100	2.47	6.3	624	883
166	11/07/02	200	2.47	6.4	622	913
167	11/07/02	300	2.46	6.5	622	891
170	02/24/03	10	2.40	5.94	627	899
172	05/14/03	1	2.71	14.0	631	245
177	10/22/03	1	2.47	11.9	815	258
178	10/22/03	50	2.40	6.3	657	697
179	10/22/03	200	2.60	6.8	619	1,032
182	04/27/04	~125	2.56	7.7	520	800
183	05/27/04	1	3.48	12.9	514	481
184	05/27/04	50	3.14	5.76	472	536

RECORD	DATE (mm/dd/yy)	DEPTH (Feet)	pH	Temp (C)	ORP (MV)	Fe total (mg/l)
185	05/27/04	200	3.01	7.01	472	1,035
189	11/03/04	1	2.71	7.91	675	514
190	11/03/04	50	2.69	8.00	671	518
191	11/03/04	200	2.65	6.99	602	1,032
192	11/03/04	700	2.68	6.23	601	1,042
194	05/04/05	1	2.53	8.90	782	469
195	05/04/05	100	2.45	5.56	667	499
196	05/04/05	150	2.40	7.50	620	1,030
197	05/04/05	200	2.40	7.50	620	997
203	10/05/05	1	2.71	9.74	686	564
204	10/05/05	50	2.66	8.72	646	573
205	10/05/05	200	2.62	7.28	600	1,048
207	01/25/06	1	2.80	1.97	671	587
208	01/25/06	150	2.76	4.01	652	582
209	01/25/06	200	2.66	7.30	611	979
211	05/10/06	1	2.86	10.22	762	576
212	05/10/06	100	2.77	3.76	644	571
213	05/10/06	170	2.75	4.26	639	573
214	05/10/06	200	2.70	7.18	601	974
215	05/10/06	700	2.68	7.20	599	955
217	10/26/06	>700	2.97	6.99	593	949
218	10/27/06	1	2.78	6.22	673	538
219	10/27/06	150	2.65	6.55	648	516
220	10/27/06	200	2.63	6.56	647	537
221	10/27/06	250	2.55	7.26	608	917
222	10/27/06	700	2.55	7.26	609	924
226	05/17/07	250	2.77	4.17	706	526
227	05/17/07	300	2.72	7.22	668	912
230	11/06/07	1	2.75	6.10	648	484
231	11/06/07	100	2.78	5.84	646	482
232	11/06/07	250	2.72	5.94	643	495
233	11/06/07	300	2.66	6.10	631	511
234	11/06/07	350	2.59	7.18	605	862
235	11/06/07	700	2.53	7.24	604	873
236	11/01/07	>700	2.54	9.16	611	879
240	06/17/08	350	2.59	4.14	652	547
241	06/17/08	450	2.53	7.31	616	631
242	06/17/08	700	2.37	7.42	616	883
244	11/18/08	1	2.70	6.35	684	516
245	11/18/08	250	2.71	4.98	680	482
246	11/18/08	500	2.59	6.22	659	533
247	11/18/08	700	2.62	6.80	644	534
249	05/14/09	1	2.63	7.50	707	512
250	05/14/09	300	2.51	3.87	631	543
251	05/14/09	600	2.42	4.01	628	439
252	05/14/09	650	2.35	6.62	603	768
253	05/14/09	700	2.38	6.63	606	642
255	11/16/09	1	2.57	4.50	719	360
256	11/16/09	50	2.48	4.65	653	405

RECORD	DATE (mm/dd/yy)	DEPTH (Feet)	pH	Temp (C)	ORP (MV)	Fe total (mg/l)
257	11/16/09	100	2.47	4.66	651	439
258	11/16/09	250	2.45	4.10	649	445
259	11/16/09	500	2.43	4.05	649	476
260	11/16/09	650	2.42	4.05	649	470
261	11/16/09	675	2.37	4.06	650	469
262	11/16/09	700	2.37	4.06	650	460
263	11/16/09	780	2.39	4.06	649	452
265	05/26/10	1	2.63	11.80	805	428
266	05/25/10	50	2.49	4.28	662	452
267	05/25/10	250	2.49	4.28	663	448
268	05/26/10	750	2.44	9.34	663	444
273	06/10/11	50	2.61	4.47	674	362
274	06/10/11	100	2.60	4.46	674	361
275	06/10/11	200	2.60	4.47	674	361
276	06/10/11	400	2.59	4.48	674	362
277	06/10/11	600	2.58	4.49	674	360
278	06/10/11	790	2.54	4.50	674	296
282	10/19/11	1	3.00	8.42	789	136
283	10/19/11	50	2.79	4.20	660	339
284	10/19/11	250	2.79	4.12	660	343
285	10/19/11	500	2.76	4.14	659	341
286	10/19/11	790	2.71	4.72	660	339
288	12/04/12	0	2.61	3.34	686	204
289	12/04/12	0	2.61	3.34	686	232
290	06/14/12	50	2.56	2.67	680	246
291	06/14/12	250	2.58	2.67	679	260
292	06/14/12	500	2.59	2.68	679	264
293	06/14/12	725	2.60	6	680	260
294	06/14/12	0	2.55	10.59	809	211

Table XXXVIII: MBMG Water Quality Records for Fe²⁺/Fe³⁺ Speciation

RECORD	DATE (mm/dd/yy)	DEPTH (Feet)	pH	Temp (C)	ORP (MV)	Fe ²⁺ (mg/l)	Fe ³⁺ (mg/l)
328	10/14/87	Surface	2.76	11.5	817	0	196
329	10/14/87	3	2.72	8.2	720	60	202
330	10/14/87	10	2.84	11.5	643	262	276
331	10/14/87	50	2.95	12.1	570	622	650
332	10/14/87	100	3.08	13.3	501	900	910
333	10/14/87	200	3.15	13.5	457	938	854
334	10/14/87	300	3.15	13.5	468	944	958
335	10/14/87	400	3.14	13.7	463	962	986
337	05/21/91	3.4	2.47	13.0	610	13	630
338	05/21/91	400	2.69	6.1	416	570	1050
403	11/19/99	60	2.17	4.9	638	500	395
404	11/19/99	100	2.18	4.8	637	635	285
405	11/19/99	200	2.20	4.9	637	660	260
447	07/02/02	25	2.17	4.8	684	91.9	427
448	07/02/02	50	2.22	5.8	632	921	36.3
449	07/02/02	75	2.26	6.0	616	682	309
450	07/02/02	100	2.27	6.1	611	762	243
451	07/02/02	200	2.28	6.2	609	711	305
452	07/02/02	240	2.30	6.2	609	714	312
456	10/16/02	Surface	2.66	10.4	61	10.4	281
457	10/16/02	15	2.63	8.6	16	12.3	265
458	10/16/02	20	2.64	9.6	23	10.4	277
459	10/16/02	25	2.53	6.9	80	41.7	307
460	10/16/02	50	2.52	6.3	433	396	487
461	10/16/02	75	2.54	6.5	505	641	338
462	10/16/02	100	2.54	6.7	610	661	325
463	10/16/02	200	2.53	6.8	740	777	250
464	10/16/02	300	2.50	6.8	840	722	272
465	10/17/02	725	2.67	7.6	1000	518	182
479	05/14/03	1	2.71	14.0	631	10.4	276
480	05/14/03	50	2.38	6.1	480	298	486
481	05/14/03	200	2.42	6.6	450	847	156
482	05/14/03	710	2.40	8.3	451	884	153
484	10/22/03	1	2.47	11.9	815	2.7	282
485	10/22/03	50	2.40	6.3	657	283	431
486	10/22/03	200	2.60	6.8	619	783	276
487	10/22/03	710	2.50	9.6	na	825	239
490	05/27/04	1	3.48	12.9	514	3.2	478
491	05/27/04	50	3.14	5.76	472	216	305
492	05/27/04	200	3.01	7.01	472	790	272
496	11/03/04	1	2.71	7.91	675	64.8	449
497	11/03/04	50	2.69	8.00	671	92.2	448
498	11/03/04	200	2.65	6.99	602	802	244
499	11/03/04	700	2.68	6.23	601	803	255
501	05/04/05	1	2.53	8.90	782	<5	570
502	05/04/05	100	2.45	5.56	667	185	435
503	05/04/05	150	2.40	7.50	620	800	195
504	05/04/05	200	2.40	7.50	620	780	215
510	10/05/05	1	2.71	9.74	686	43.8	516
511	10/05/05	50	2.66	8.72	646	196	379

RECORD	DATE (mm/dd/yy)	DEPTH (Feet)	pH	Temp (C)	ORP (MV)	Fe ²⁺ (mg/l)	Fe ³⁺ (mg/l)
512	10/05/05	200	2.62	7.28	600	773	259
515	01/25/06	150	2.76	4.01	652	195	395
516	01/25/06	200	2.66	7.30	611	775	205
525	10/27/06	1	2.78	6.22	673	<5	560
526	10/27/06	150	2.65	6.55	648	170	400
527	10/27/06	200	2.63	6.56	647	190	385
528	10/27/06	250	2.55	7.26	608	750	220
529	10/27/06	700	2.55	7.26	609	735	250
531	05/18/07	>700	3.07	6.98	664	629	317
533	05/17/07	250	2.77	4.17	706	191	344
534	05/17/07	300	2.72	7.22	668	681	257
537	11/06/07	1	2.75	6.10	648	181	383
538	11/06/07	100	2.78	5.84	646	193	386
539	11/06/07	250	2.72	5.94	643	221	360
540	11/06/07	300	2.66	6.10	631	233	354
541	11/06/07	350	2.59	7.18	605	708	260
542	11/06/07	700	2.53	7.24	604	693	314
543	11/01/07	>700	2.54	9.16	611	929	50.4
547	06/17/08	400	2.59	4.14	652	180	355
548	06/17/08	450	2.53	7.31	616	360	250
549	06/17/08	700	2.37	7.42	616	465	275
551	11/18/08	1	2.70	6.35	684	65	450
552	11/18/08	250	2.71	4.98	680	205	335
553	11/18/08	500	2.59	6.22	659	220	335
554	11/18/08	700	2.62	6.80	644	200	290
556	05/14/09	1	2.63	7.50	707	5	530
557	05/14/09	300	2.51	3.87	631	185	335
558	05/14/09	600	2.42	4.01	628	235	320
559	05/14/09	650	2.35	6.62	603	515	280
560	05/14/09	700	2.38	6.63	606	300	315
562	11/16/09	1	2.57	4.50	719	<5	410
563	11/16/09	50	2.48	4.65	653	130	340
564	11/16/09	100	2.47	4.66	651	180	315
565	11/16/09	250	2.45	4.10	649	220	300
566	11/16/09	500	2.43	4.05	649	205	305
567	11/16/09	650	2.42	4.05	649	205	315
568	11/16/09	675	2.37	4.06	650	210	310
569	11/16/09	700	2.37	4.06	650	225	310
570	11/16/09	780	2.39	4.06	649	220	310
572	05/26/10	1	2.63	11.80	805	428	460
573	05/25/10	50	2.49	4.28	662	452	300
574	05/25/10	250	2.49	4.28	663	448	300
575	05/26/10	750	2.44	9.34	663	444	300
580	06/10/11	50	2.61	4.47	674	195	220
581	06/10/11	100	2.60	4.46	674	180	225
582	06/10/11	200	2.60	4.47	674	185	240
583	06/10/11	400	2.59	4.48	674	175	250
584	06/10/11	600	2.58	4.49	674	160	265
585	06/10/11	790	2.54	4.50	674	25	325

1.1.2. General Speciation Procedure in Stabcal

The speciation procedure involved using Microsoft Excel and Stabcal developed by Dr. H.H. Huang of Montana Tech. Total iron and the $\text{Fe}^{2+}/\text{Fe}^{3+}$ couple were evaluated separately. The following sections describe each procedure in greater detail.

1.1.2.1. Total Iron Speciation

Data was exported from Excel using a “copy data by list #” button created in Visual Basic. The purpose in using this button was to eliminate any possible user error in selecting the appropriate record. Once the copy button was clicked, a screen popped up which allowed the user to enter the desired record number for further Stabcal processing. After entering the required record number, the data was transferred to the computer’s clipboard memory. The Stabcal program was opened, and the speciation and titration menu was clicked. The record was saved as a Stabcal file, and then the “Work1” button on the speciation interface in Stabcal was clicked. From the main menu, “import species—paste Eh, pH components, Conc—from MT Bureau Analytical Report. Next, click “Save then calculate—start calculation”. Once the calculation is completed, click “results to clipboard—copy only selected species—copy results now to clipboard.” The next step involves transferring the data back to Excel and is common to both the total and separate iron speciations, so it will be described following the next section.

1.1.2.2. $\text{Fe}^{2+}/\text{Fe}^{3+}$ Iron Speciation

The identical procedure was used for separate iron speciation, except that after “start calculation” in Stabcal is completed, the user must click “View other situation—specification menu”, then click Column B1—item B4 “Eh of Fe”—Finish selection before selecting “results to clipboard—copy only selected species—copy results now to clipboard.”

1.1.2.3. Creation of Speciation File and Reimportation into Stabcal

For both types of speciation, after the results are copied to the clipboard, then the data needs to be transferred back to Excel before sending back to Stabcal for calculation of dG values. The first step is to create a speciation results excel file and then paste the clipboard values into the excel spreadsheet. Assuming that the data is pasted into column A initially, column C should be formatted for scientific notation and 6 decimal places, so that when the data is re-exported into Stabcal, the speciation results are accurate. The next step is to highlight Column C “Activities from row H + A down to Fe 3+ A” and copy to clipboard. Also check that the activity of H₂O is 1. The next step is to send the clipboard information to Stabcal. Reopen Stabcal and click on—“A3 Aqueous Utility and dbase” followed by “Convert dG<>logK listed in Group D Utility for AQ and Special Project.” On the convert menu click—“Worksheet File—Retrieve (desired template) from saved—Choose Sh (for Schwertmannite). The next step is to change the temperature in the Stabcal interface to the desired temperature that is to be analyzed. When the temperature is changed, Stabcal will automatically change the imported dG values for that temperature. Next, place the cursor under the column activity of balance species and row H and then click—CTRL+V to paste activity values from the speciation results worksheet. Next click button D on the Stabcal interface—“Activity to dG nonRedox under Category “Convert a Group of Specie”—then click—Yes to skip reading file. Next click —“OK to popup screen” and Stabcal will calculate the log K_o values and dG values and load the data into the clipboard. The final step is to paste the clipboard data back into the speciation spreadsheet and save the data.

1.1.2.4. Speciation Flowsheet Summary

Figure 41 is a condensed flowsheet showing the steps in performing a total Fe speciation or Fe²⁺/Fe³⁺ speciation.

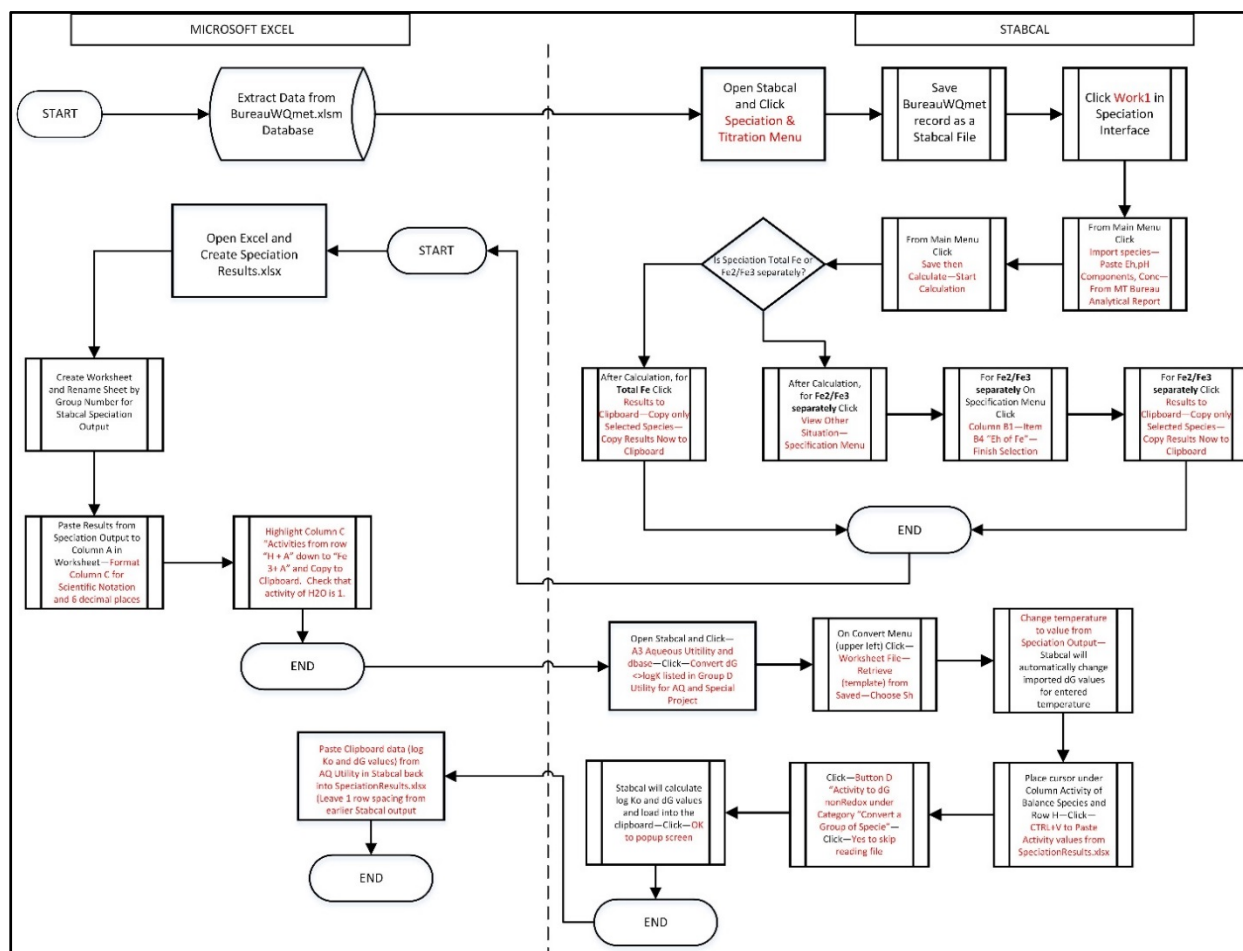


Figure 41: Fe Speciation Flowsheet Summary

1.1.2.5. Matlab Graph Output Procedure

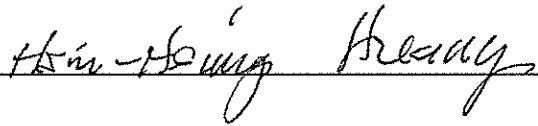
Section 4 contains Matlab graphs of pH, Eh and log Q values for Schwertmannite, Hydronium-Jarosite, Potassium Hydronium-Jarosite, etc. In order to generate the Matlab output, results were initially compiled in Excel. Values for log Q were taken from Stabcalf and organized by record from the original MBMG data files. Records were sorted by temperature, and the average value along with frequency was compiled into Stabcalf output summary Tables by temperature. Tables XXXII to XXXVI in Section 4 show the average log Q for each temperature and some related statistics for all of the minerals of interest. Matlab text files were generated using temperature data from Stabcalf to plot log Q, pH, and Eh values. Those text files

were run in Matlab to generate 3D stem plots for each temperature. The graphs show the deviation from the average Log Q value on the Z axis. The Matlab 3D stem plots were generated for 4°C to 8°C.

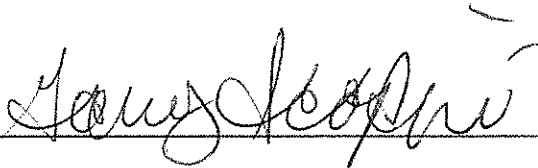
SIGNATURE PAGE

This is to certify that the thesis prepared by Rajesh Srivastava entitled "Estimation and Thermodynamic Modelling for Solid Iron Species in the Berkeley Pit Water" has been examined and approved for acceptance by the Department of Metallurgical and Materials Engineering, Montana Tech of The University of Montana, on this 29th day of April, 2015.

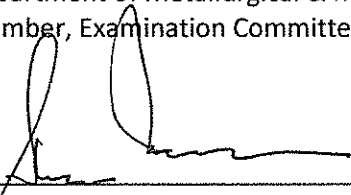
Hsin H. Huang, PhD, Professor
Department of Metallurgical & Materials Engineering
Chair, Examination Committee

x 

Gary Icopini, PhD, Research Professor
Montana Bureau of Mines & Geology
Member, Examination Committee

x 

Steve McGrath, MS, Metallurgical Engineer
Department of Metallurgical & Materials Engineering
Member, Examination Committee

x 

Larry G. Twidwell, PhD, Professor Emeritus
Department of Metallurgical & Materials Engineering
Member, Examination Committee

x 